UNIVERSITEIT VAN PRETORIA
UNIVERSITY OF PRETORIA
YUNIBESITHI YA PRETORIA

Electrochemical behaviour of boron-doped diamond electrodes

by

Kaveshini Naidoo

Submitted in partial fulfilment of the requirements for the degree

MAGISTER SCIENTIAE

in the Faculty of Natural & Agricultural Science

University of Pretoria

Pretoria

October 2001

© University of Pretoria

Electrochemical behaviour of boron-doped diamond electrodes

by

Kaveshini Naidoo

Supervisor: Dr Raluca I Stefan

Co-Supervisor: Professor Jacobus F. van Staden

Department of Chemistry

University of Pretoria

Degree: Magister Scientiae

SYNOPSIS

Conducting diamond electrodes provide unique advantages for electrochemistry such as a wide potential window, low baseline current, chemical inertness and resistance to fouling. De Beers boron-doped diamond electrodes, manufactured by chemical vapour deposition and containing varying amounts of boron, were therefore investigated in order to determine their suitability for future electrochemical applications. These electrodes were initially characterised using techniques such as SEM, LA-ICP-MS, Raman spectroscopy and XPS. The electrochemical behaviour of these electrodes was investigated in two redox systems (potassium iron (III) cyanide and cerium (III) sulphate) and two biological systems (dopamine and ascorbic acid). These results were compared against that of the conventional glassy carbon electrode. Porous boron-doped diamond, a novel electrode material, was used for the electrochemical detection of thyroid hormones (L-T_3 and L-T_4).

These hormones have never previously been investigated using a boron-doped diamond electrode.

The De Beers boron-doped diamond electrode was found to outperform the conventional glassy carbon electrode, which fouled very easily, in the detection of dopamine. Peak separation between dopamine and the interfering ascorbic acid was attained at a pretreated boron-doped diamond electrode. The feasibility of detecting thyroid hormones using a porous boron-doped diamond electrode was demonstrated, and the electrode material was patented.

Elektrochemiese gedrag van boorbevattende diamantelektrodes

deur

Kaveshini Naidoo

Leier: Dr Raluca I. Stefan

Medeleier: Professor Jacobus F. van Staden

Departement Chemie

Universiteit van Pretoria

Graad: Magister Scientiae

SAMEVATTING

Geleidende diamantelektrodes lewer unieke voordele in elektrochemie, soos 'n wye potensiaalgebied, 'n lae basislyn, onreaktiewe chemiese eienskappe, en 'n weerstand teen die vorming van 'n neerslag op die oppervlakte, wat die elektrodewerking belemmer. De Beers se boorhoudende diamantelektrodes, wat verskeie hoeveelhede boor bevat, is ondersoek met die doel om hul geskiktheid vir toekomstige elektrochemiese toepassings te bepaal. Hierdie elektrodes is berei deur die neerslag van koolstof in die dampfase in die teenwoordigheid van boor. Dit is aanvanklik gekarakteriseer deur gebruik te maak van tegnieke soos SEM, Raman spektroskopie en XPS. Hierdie elektrodes is getoets in twee redokssisteme (kalium yster(III)sianied en serium(III)sulfaat) en twee biologiese sisteme (dopamien en askorbiensuur). Die verkreë resultate is vergelyk met dié van konvensionele glasagtige koolstofelektrodes. Porieuse boorbevattende diamant, 'n unieke

elektrodemateriaal, is aangewend vir die elektrochemiese bepaling van skildklierhormone (L-T_3 en L-T_4). Hierdie hormone is nog nie voorheen bepaal deur gebruik te maak van hierdie tipe elektrode nie.

De Beers se boorhoudende diamantelektrode het die werking van die gewone glasagtige koolstofelektrode oorskry; by laasgenoemde vorm 'n aanpaksel op die elektrodeoppervlakte baie geredelik in die bepaling van dopamien. Die skeiding van dopamien en belemmerende askorbiensuur, is bewerkstellig deur gebruik te maak van hierdie elektrodes. Die moontlikheid om skildklierhormone te bepaal d.m.v. 'n porieuse boorhoudende diamantelektrode is aangetoon, en hierdie elektrodemateriaal is gepatenteer.

Acknowledgments

I would like to thank the De Beers Research Laboratory (DRL) for financially supporting my studies, and giving me the opportunity to further my formal qualifications. I would also like to thank my supervisor at the DRL, Anine Ras, for her guidance and support in this endeavour. My thanks also to my supervisor and co-supervisor at the University of Pretoria, Dr R I Stefan and Professor van Staden, for their role in making this thesis possible.

I would like to thank Brett Lancaster (DRL) for his help in the TGA analysis of the CVD diamond samples. I would also like to thank Hester Burks (DRL) for her help in the SEM analysis of the samples, and Amanda Quadling at the De Beers GeoScience Centre for her help in the LA-ICP-MS analysis of the diamond samples. I would like to thank Brett Lancaster and Johan Myburgh (DRL) for their input and support.

And finally, I would like to express my sincere love and gratitude to my family and friends, for their encouragement, love and support in this undertaking.

To Jesus, my closest friend,

In all things, you do so righteously tend,

Unlike, the billowing sand,

Which may lead to a barren land,

I have no fear, 'cause you have my life in the palm of your hand

And so, in you I will forever love and trust.

Table of Contents

CHAPTER 1

Introduction

Diamond together with a few other materials can be used as a gem stone and as an industrial tool [1]. One of the most remarkable features of diamond is that it is pre-eminent in both of these fields, i.e. it is the most beautiful of all gem stones and the most powerful of all cutting materials. Natural diamond is predominantly used as gem stones, whilst synthetic diamond is used in industrial applications.

The two vital properties which make diamond so important as an industrial material are its combination of extreme hardness and high thermal conductivity [1]. Diamond possesses other technologically important properties such as high electrical resistance, chemical inertness, high electron and hole mobilities and optical transparency [2,3]. Diamond is chemically inert in a variety of environments including strong acids, bases, fluoride and chloride environments [4].

One of the techniques of manufacturing synthetic diamond is high pressure, high temperature synthesis, and the other is chemical vapour deposition (CVD) of diamond onto a substrate. The high pressure, high temperature route gives rise to single diamond crystals, whilst the CVD route produces diamond thin films. These films are deposited via two methods : hot filament chemical vapour deposition (HF-CVD) and microwave

assisted chemical vapour deposition (MA-CVD) (refer to Chapter 2). The as-grown diamond films are non-conductive, i.e. they are insulators. In order to enhance their conductivity, these synthetic diamond films are doped with boron.

There are many applications for boron-doped CVD diamond [5], such as :

- Electrosynthesis
- Corrosion protection
- Energy storage devices
- Electrochemical-based toxic waste remediation
- Detection of sodium azide in groundwater
- Anodic stripping voltammetry of heavy-metal ions in aqueous media

Another potential use for boron-doped CVD diamond is as a biosensor in biological systems. At present, there is a worldwide interest in the use of diamond thin films in electroanalysis [5-11]. Conducting diamond electrodes provide unique advantages for electrochemistry :

- Wide potential window of water stability
- Low background current density (low baseline current)
- Exceptional chemical and structural stability
- Resistance to fouling

The wide potential range of water stability at diamond electrodes permits reactants with large positive or negative standard potentials to be investigated on diamond without

interference from water electrolysis [12]. The low background current density also enables diamond to have a lower detection limit (higher signal/noise ratio) than most other materials.

In recent years, several groups have made progress understanding the factors that influence the electrochemical response of diamond thin film electrodes, including those of Fujishima and Yagi (Japan) [10], Pleskov (Russia) [13], Angus and Miller (USA) [11], Swain (USA) [8] and Compton (England) [14]. However, there can be significant variability in the response of the diamond electrodes, as reported in results from different laboratories. According to Swain et. al. [15], this variability can be ascribed to two sets of factors :

a) The solution condition, surface cleanliness, the redox analyte and the electrolyte composition
b) Diamond film quality issues

The factors that can influence the film quality are :

- Presence of non-diamond carbon
- The surface state of the diamond film, i.e. oxygen or hydrogen terminated surface
- Type of dopant, doping level and the distribution of the dopant in the diamond film
- Grain boundaries and other morphological defects
- The primary crystallographic orientation

1.1 Aim of investigation

The aim of this investigation was to study the electrochemical behaviour of boron-doped CVD diamond electrodes, in order to establish its potential use as a biosensor. Part of the study entailed a thorough literature survey on diamond electrodes, their properties and applications. Research work was carried out to characterise the diamond electrode in terms of its microstructure, quantity of non-diamond carbon present, boron concentration and surface chemistry. The techniques used were scanning electron microscopy (SEM), energy dispersive spectroscopy (EDS), Raman spectroscopy, laser ablation inductively coupled plasma mass spectroscopy (LA-ICP-MS) and X-ray photoelectron spectroscopy (XPS).

The surface of the electrode is deemed to be extremely important in determining the electrochemical behaviour of the diamond electrode in certain systems. The redox systems investigated were potassium iron (III) cyanide and cerium (III) sulphate, whilst the biological systems were dopamine and ascorbic acid. The electrode surface was therefore modified to become either oxygen terminated or hydrogen terminated, and the effect on the various systems was investigated.

Potassium iron (III) cyanide is a standard electrochemical system that is often used to determine the electrochemical behaviour of electrodes. The cerium redox couple is not very well resolved using a glassy carbon electrode. However, a fairly well resolved cerium redox couple is obtained using a boron-doped diamond electrode because of its

wide potential window. Dopamine is found in the brain fluid in conjunction with ascorbic acid (an interfering species). Literature reports that dopamine can be separated from ascorbic acid using an anodically pretreated boron-doped diamond electrode.

A voltammetric comparison of the diamond electrode with the glassy carbon electrode was also undertaken in these electrochemical systems, as the glassy carbon electrode is the most widely used commercial electrode with which diamond would have to compete. Lastly, the ability of the diamond electrode to detect the presence of thyroid hormones (L-T_3 and L-T_4) in synthetic samples was investigated in order to assess the feasibility of using diamond electrodes as immunosensors.

1.2 References

[1] R Berman, **Physical Properties of Diamond;** Clarendon Press, Oxford (1965).

[2] T D Moustakas, **In Synthetic Diamond : Emerging Science and Technology,** John Wiley and Sons, New York (1994) 145.

[3] C J Hartley and H L Shergold, **Chemistry and Industry**, (1980) 224.

[4] R Ramesham and M F Rose, **Journal of High Temperature and Materials Science, 38** (1997) 1.

[5] J Xu, M C Granger, Q Chen, J W Strojek, T E Lister and G M Swain, **Analytical Chemistry News & Features, 69** (1997) 591A.

[6] S Alehashem, F Chamber, J W Strojek, G M Swain and R Ramesham, **Anal. Chem., 67** (1995) 2812.

[7] S Jolley, M D Koppang, T Jackson and G M Swain, **Anal. Chem., 69** (1997) 4041.

[8] J Xu and G M Swain, **Anal. Chem., 70** (1998) 1502.

[9] M D Koppang, M Witek, J Blau and G M Swain, **Anal. Chem., 71** (1999) 1188.

[10] T N Rao, I Yagi, T Miwa, D A Tryk and A Fujishima, **Anal. Chem., 71** (1999) 2506.

[11] J C Angus, H B Martin, U Landau, Y E Evstefeeva, B Miller and N Vinokur, **New Diamond and Frontier Carbon Technology, 9** (1999) 175.

[12] A Argoitia, H B Martin, E J Rozak, U Landau and J L Angus, **Mater. Res. Soc. Proc., 416** (1996) 349.

[13] Y V Pleskov, **Russian Chemical Reviews, 68** (1999) 381.

[14] C H Goeting, F Marken, A Gutierrez-Sosa, R G Compton and J S Foord, **New Diamond and Frontier Carbon Technology, 9** (1999) 207.

[15] M C Granger, M Witek, J Xu, J Wang, M Hupert, A Hanks, M D Koppang, J E Butler, G Lucazeau, M Mermoux, J W Strojek and G M Swain, **Anal. Chem., 72** (2000) 3793.

CHAPTER 2

Manufacture of boron-doped CVD diamond

2.1 Introduction

The low pressure synthesis of diamond thin films by chemical vapour deposition (CVD) methods began about two decades ago. Chemical vapour deposition involves a gas-phase chemical reaction occurring above a solid surface, which causes deposition onto that surface [1]. The process gas usually used for the production of CVD diamond is a hydrocarbon gas, typically methane, in an excess of hydrogen.

In order to produce diamond films, the gas-phase carbon molecules need to be activated. This generally involves plasma (for example microwave) or thermal (for example hot filament) activation, or use of a combustion flame (oxyacetylene or plasma torches) [1]. The two most common low pressure CVD techniques are hot filament CVD and microwave plasma CVD. The grown CVD diamond can show mechanical and even electronic properties comparable to those of natural and high pressure, high temperature synthetic diamond.

2.2 Hot filament CVD and microwave plasma CVD techniques

One of the most commonly used substrates for the deposition of diamond film is the p-type (100) silicon wafer [2-5]. This substrate is usually scratched with diamond paste before deposition to increase the nucleation density of the diamond particles which make up the film. Typical growth conditions for the hot filament and microwave plasma CVD techniques are carbon/hydrogen volume ratios of 0.5 - 2%, pressures of 10 – 100 torr, substrate temperatures of 800 – 1000°C, and microwave powers of 1000 – 1300 W, or filament temperatures of approximately 2100°C, depending on the method used [6].

The most common method of incorporating boron into the diamond film is during the process of its growth. Since the boron atoms are almost the same magnitude as the carbon atoms, they are easily incorporated into the diamond lattice by substitution of a carbon atom. Boron doping of the diamond film can be accomplished by either supplementing the gas phase with a volatile boron compound, for example trimethyl borate, or by introducing the boron into the diamond film from the solid state by, for example, gasifying a piece of hexagonal – boron nitride (h-BN) or boron trioxide powder [7,8].

Figure 2.1 illustrates a schematic diagram of a hot filament CVD apparatus. A mixture of hydrogen and methane is introduced into the reaction chamber, while the rotary pump displaces the mixed gas in the chamber to balance the inside pressure. The bond of the gas molecules is broken by the thermal energy of a tungsten (W) filament and carbon atoms are deposited on the substrate located just below the filament. Boron trioxide

(B_2O_3) powder is placed in a quartz boat in the branch tube of the deposition chamber and heated electrically to the required temperature.

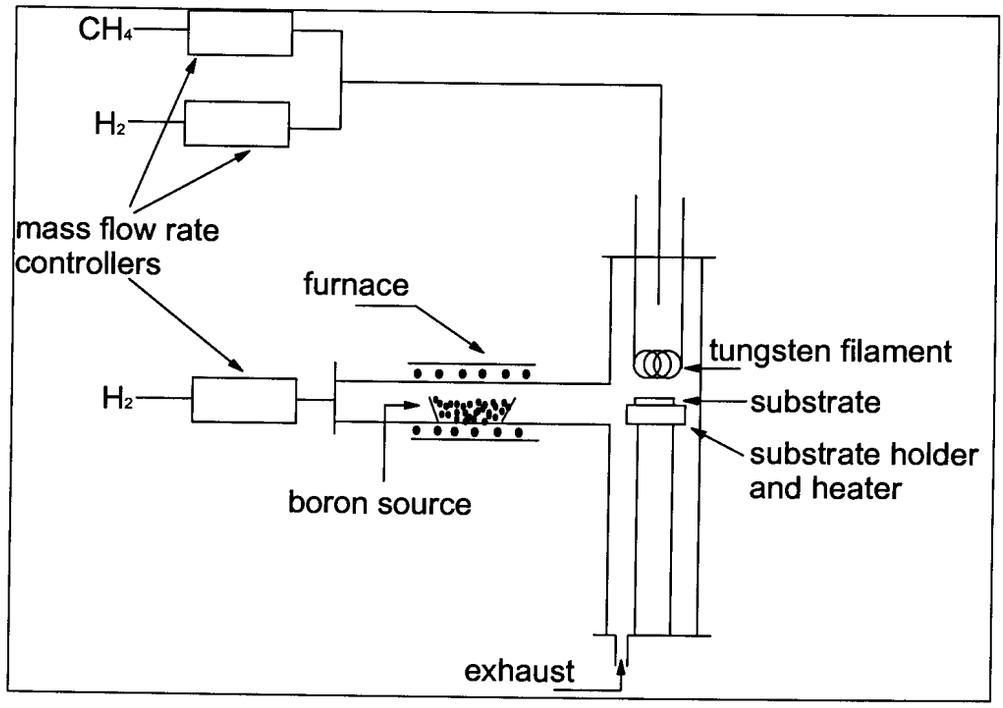

Figure 2.1 : Schematic diagram of a hot filament CVD apparatus [2]

Figure 2.2 represents a schematic diagram of a microwave plasma enhanced CVD reactor. The volatile boron compound is introduced with the reactant gas. This reactant gas is activated via microwaves that are generated by the microwave generator.

The morphology of the polycrystalline diamond films is sensitive to the precise growth conditions. Growth rates for the various deposition processes vary considerably, and it is usually found that the higher the growth rate of the film, the lower the quality [1]. The term "quality" refers to factors such as the ratio of sp^3 (diamond) to sp^2-bonded (graphite) carbon in the sample and the crystallinity of the film. The average growth rate of the hot

filament and plasma methods is 0.1 – 10 μm/h. One of the great challenges facing researchers in CVD diamond technology is to increase the growth rates to economically viable rates, that is hundreds of μm/h or even to mm/h, without compromising film quality.

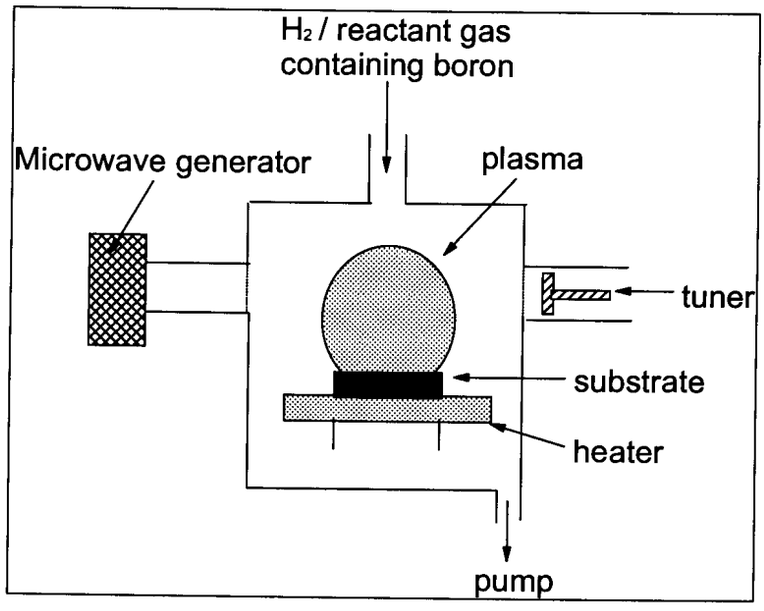

Figure 2.2 : Schematic diagram of a microwave plasma enhanced CVD reactor [1]

Graphite is the thermodynamically stable form of solid carbon at ambient pressures and temperatures. The fact that diamond films can be formed by CVD techniques is most probably linked to the presence of hydrogen atoms, which are generated by the activation of the gas molecules. These hydrogen atoms are believed to play a number of crucial roles in the CVD process [1] :

(a) They undergo hydrogen abstraction reactions with stable gas-phase hydrocarbon molecules, producing highly reactive carbon-containing radical species. This is

important, since stable hydrocarbon molecules do not react to cause diamond growth. The reactive radicals, for example methyl ($\cdot CH_3$), can thus diffuse to the substrate surface and react, forming the C-C bond necessary to propagate the diamond lattice.

(b) Hydrogen atoms prevent the reconstruction of the 'dangling' carbon bonds to a graphite-like surface by terminating these carbon bonds with hydrogen atoms on the growing diamond surface, thus hindering them from cross-linking.

(c) Atomic hydrogen is known to etch both diamond and graphite. Under typical CVD conditions, the rate of diamond growth exceeds its etch rate, whilst the converse is true for other forms of carbon, for example graphite. Thus, the atomic hydrogen, even though it is very short lived, is effective in etching out non-diamond particles. This is believed to be the basis for the preferential deposition of diamond rather than graphite.

2.3 Effect of varying deposition conditions on the morphology of CVD diamond

The surface morphology of CVD diamond was found to be dependent on the concentration of methane in the feed gas [9]. **Figure 2.3** shows typical examples of the morphology of as-grown surfaces as the concentration of methane in the feed gas is increased from 0.5% to 5.0%. Low methane concentrations, for example 0.5%, were found to yield (111) faces, whereas methane concentrations greater than 1.5% yielded (100) faces. The (100) faces occurred as square or rectangular forms. For the films grown at a 5% methane concentration, the crystalline morphology was entirely lost.

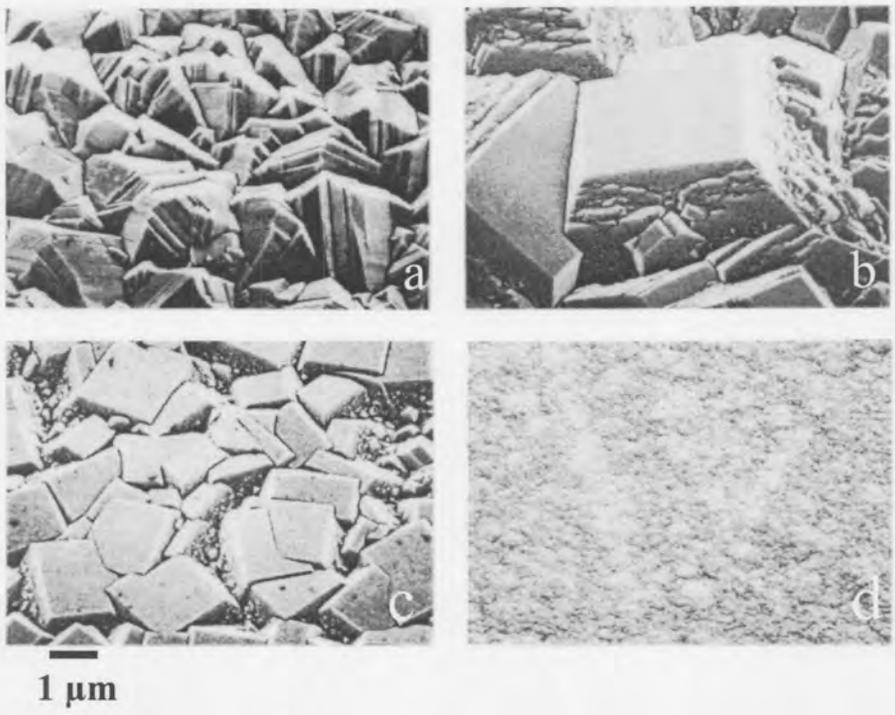

Figure 2.3 : Morphology of as-grown surfaces as the concentration of methane in the feed gas is increased from 0.5% to 5.0%, (a) 0.5%, (b) 2%, (c) 4%, (d) 5% [9]

Figure 2.4 represents the fractured cross-sections of as-grown films grown at methane concentrations of 0.5 – 5.0%. The texture of the films deposited at methane concentrations of 0.5 – 4.0% seems to be columnar or better described as diamond 'whiskers'. Sato and Kamo also found that the growth rate increased with increasing methane concentration. However, a methane concentration of approximately 5.0% or more resulted in the production of inferior quality diamond films. This was evidenced by the reduction of the diamond peak (1332 cm^{-1}) and the occurrence of a broad non-diamond carbon peak (approx. 1550 cm^{-1}) in the Raman spectrum.

UNIVERSITEIT VAN PRETORIA
UNIVERSITY OF PRETORIA
YUNIBESITHI YA PRETORIA

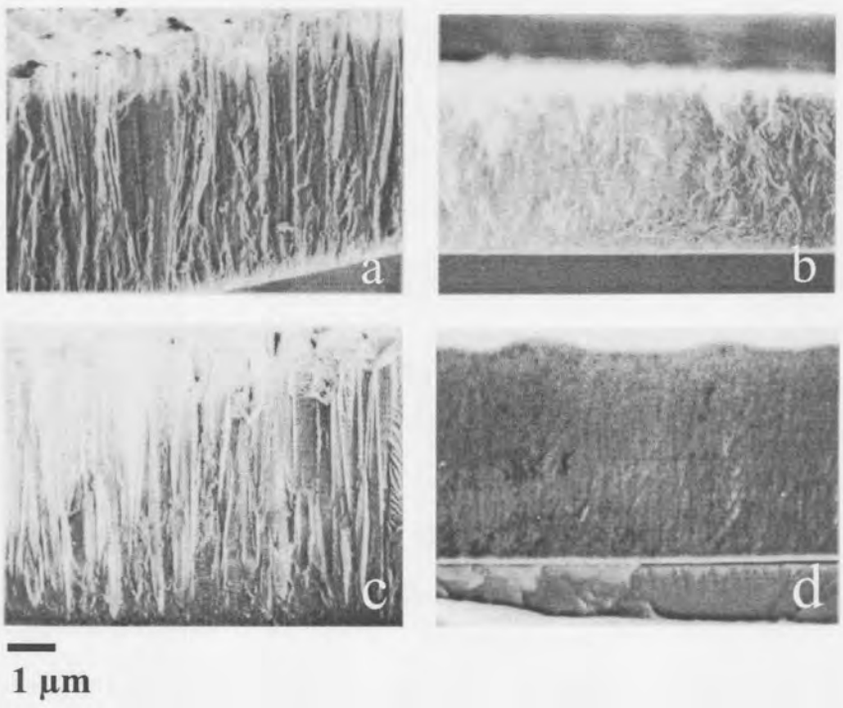

Figure 2.4 : Fractured cross-sections of as-grown films grown at methane concentrations of 0.5 – 5.0%, (a) 0.5%, (b) 2%, (c) 4%, (d) 5% [9]

According to the work undertaken by Hussain et. al. [10], the quality of the diamond thin film was found to be further dependent on the system pressure and the substrate temperature. It was found that, as the reaction chamber pressure decreased from 60 torr to 5 torr, the nucleation density of the diamond crystals on the substrate surface increased. This reduced the crystal size of the diamond film and increased the film coverage. Furthermore, the substrate temperature was found to play a very important role in determining the diamond crystal size. As the substrate temperature decreased from 920°C to 860°C, the crystal size of the diamond film also decreased.

Figure 2.5 illustrates the dependence of the morphology of the diamond film on the methane concentration and the substrate temperature. The growth conditions may be divided into regions A-F : in region A, no or little deposition of either diamond or graphite takes place; in B, the (111) face predominates; in C, (111) and (100) faces occur with comparable frequency; in D, (100) predominates; in D*, the (100) face predominates and diamond grains grow preferentially along the <100> axis; and in E, the surface is smooth and the crystalline morphology is lost. As the methane concentration or substrate temperature increases, the content of diamond in the CVD film decreases.

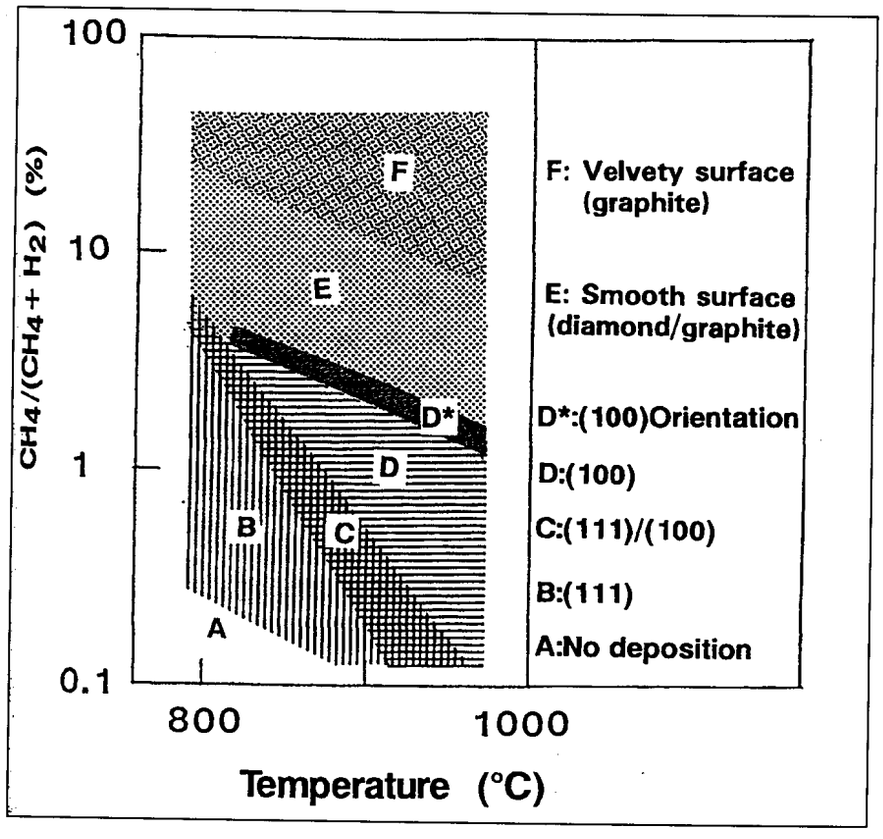

Figure 2.5 : Diagram illustrating the dependence of the morphology of the diamond film on the methane concentration and the substrate temperature [9]

2.4 Effect of boron on CVD diamond

Diamond is a wide band gap semiconductor and its bonding orbitals (valence band) are filled, while its anti-bonding orbitals (conduction band) are much higher in energy. The energy gap is therefore too great for diamond to be conductive or for diamond to absorb visible light. Therefore pure diamond is termed an insulator and appears colourless. However, the presence of trace amounts of boron in diamond leads to a blue colouration. It appears that the more boron present in the diamond, the deeper the blue colour observed.

Carbon contains four valence electrons, whilst boron contains only three valence electrons. When the diamond lattice is doped with boron, the boron atom substitutes a carbon atom in the crystal lattice, thereby forming a B-C bond. Since boron contains only three valence electrons, one of the B-C bonds must be deficient by one electron. Using band theory [11], it is found that the energy level associated with each single-electron B-C bond does not form part of the valence band of diamond. Instead, it forms a discreet level or atomic orbital just above the top of the valence band (refer to **Figure 2.6** [12]). This level is known as an acceptor level because it is capable of accepting an electron, thereby creating a positive hole in the valence band.

Positive holes move when an electron enters them, leaving its own position vacant as a fresh positive hole. This transfer of charge under an applied potential is what makes boron-doped diamond conductive.

In addition, the relatively small gap (0.1 eV) between the valence band and this acceptor level means that the electrons situated at various energy levels in the valence band, may be excited into the acceptor level by light in the lower energy wavelengths of the visible spectrum, so that mostly red, but also some orange, yellow and green light is absorbed. Blue light is not absorbed and that is the colour that is observed.

The investigation carried out by Kanda et. al. [4] entailed a detailed study based on the uptake of nitrogen and boron in the various growth sectors : (111), (001), (011) and (113). Denoting the concentrations of nitrogen atoms by N_D, it was found that N_D (111) > N_D (001) > N_D (113) > N_D (011).

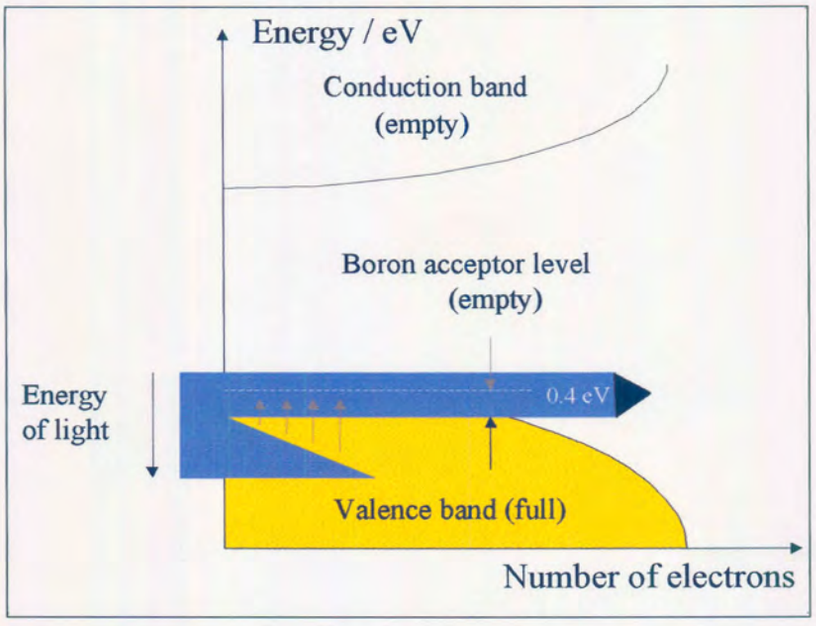

Figure 2.6 : Energy level diagram for boron [11]

The semiconducting property of diamond depends on the uncompensated boron concentration present in the diamond film. Denoting the total boron concentrations by N_A, the uncompensated boron acceptor concentrations will be $(N_A - N_D)$. **Figure 2.7** illustrates a schematic diagram (Kanda diagram) depicting the behaviour of the relative uncompensated boron acceptor concentrations, $(N_A - N_D)$, in the various growth sectors when moving from low (B_L) to high (B_H) levels of boron doping. It is important to note that semiconducting behaviour begins in each sector as N_A exceeds N_D for that sector. For a lightly doped diamond sample, it was found that the uncompensated boron acceptor concentrations for the various facets decreased in the following order: (011) > (113) > (001) > (111), whereas for a more heavily boron doped sample, it decreased as follows: (111) > (011) > (113) > (001).

In a boron-doped CVD diamond film, the specific resistance of diamond depends on the boron content of the film [13]. It can vary from 10^4 Ω.cm (at a content of boron atoms in diamond of approx. $10^{18}cm^{-3}$) to tenth and even thousandth fractions of Ω.cm (at a content of boron atoms in diamond of approx. $10^{21}cm^{-3}$). As the resistivity of the diamond decreases, the diamond acquires successively the properties of a semiconductor, a degenerate semiconductor and then of a semimetal.

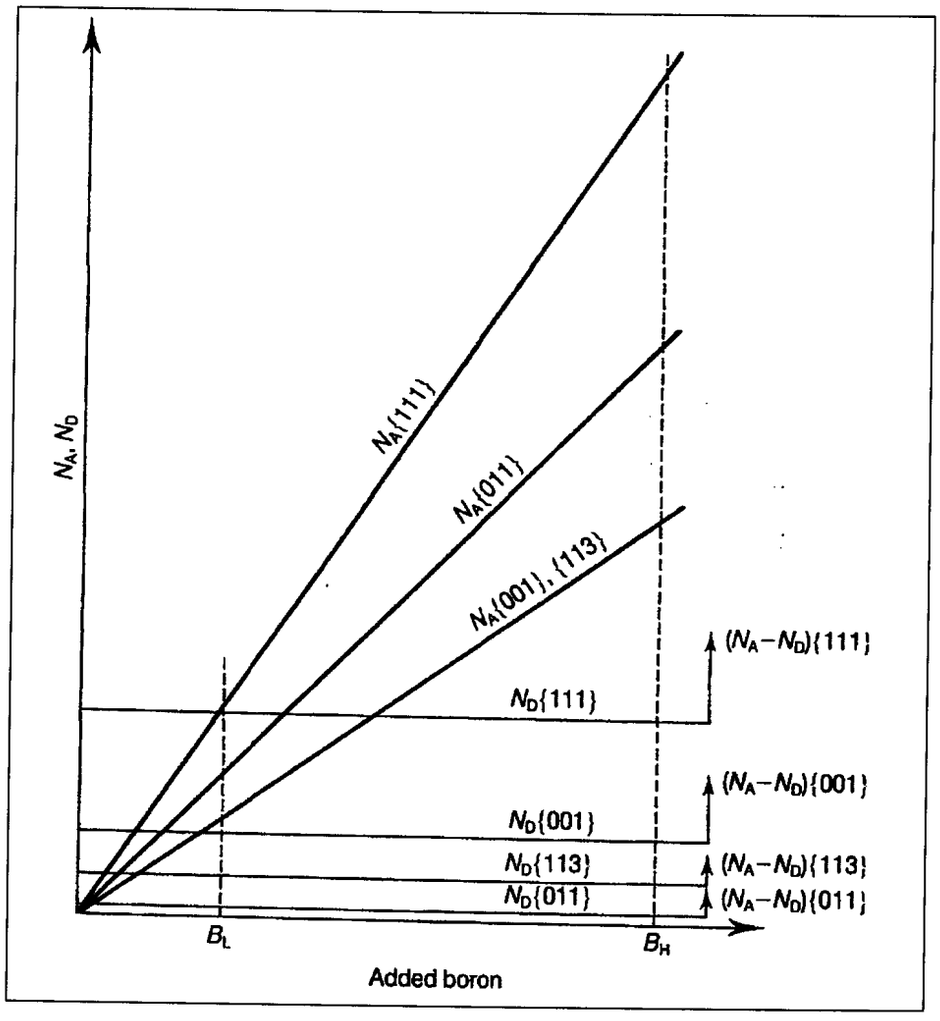

Figure 2.7 : Schematic diagram (Kanda diagram) depicting the behaviour of the relative uncompensated boron acceptor concentrations, ($N_A - N_D$), in the various growth sectors on moving from low (B_L) to high (B_H) levels of boron doping [9]

2.5 References

[1] http://www.chm.bris.ac.uk/pt/diamond/end.htm

[2] X K Zhang, J G Guo and Y F Yao, **Phys. Stat. Sol., (a) 133** (1992) 377.

[3] K Okano, H Naruki, Y Akiba, T Kurosu, M Iida and Y Hirose, **Japanese Journal of Applied Physics, 27** (1988) L173.

[4] K Okada, H Kanda, S Komatsu and S Matsumoto, **Mat. Res. Soc. Symp. Proc., 593** (2000) 459.

[5] K Miyata, K Kumagai, K Nishimura and K Kobashi, **J. Mater. Res., 8** (1993) 2845.

[6] J Xu, M C Granger, Q Chen, J W Strojek, T E Lister and G M Swain, **Analytical Chemistry News & Features, 69** (1997) 591A.

[7] H B Martin, A Argoitia, U Landau, A B Anderson and J C Angus, **J. Electrochem. Soc., 143** (1996) L133.

[8] P Chen and R L McCreery, **Anal. Chem., 68** (1996) 3958.

[9] J E Field, **The Properties of Natural and Synthetic Diamond,** Academic Press Limited (1992) 429.

[10] A Hussain, D Zhou, L Chow and V Desai, **The Minerals, Metals and Materials Society,** (2000) 141.

[11] A R West, **Solid State Chemistry and its Applications,** John Wiley & Sons Limited (1984) 75.

[12] A Butler and R Nicholson, **Chemistry in Britian,** (1998) 34.

[13] Y V Pleskov, **Russian Chemical Reviews, 68** (1999) 381.

CHAPTER 3

Surface structure and chemistry of diamond and boron-doped CVD diamond

3.1 Surface structure and chemistry of diamond

Naturally occurring diamonds are found in two types of deposits, namely alluvial and kimberlite deposits [1]. There is a tendency for the alluvial diamonds to be predominantly hydrophilic and those from a kimberlite pipe to be hydrophobic. Separation techniques for these two types of diamonds were thus developed based on their respective surface chemical properties [2]. Using grease tables or flotation techniques [1], it was found that hydrophobic diamonds readily adhered to the grease, whereas hydrophilic diamonds did not.

The reason why some diamonds were hydrophobic and others hydrophilic was initially not well understood. It was believed that the hydrophilic properties of the alluvial diamonds arose as a result of the adsorption of inorganic salts such as sodium chloride and ferric oxides onto the surface of the diamond [1]. After extensive research, it was found that hydrophobic diamonds became hydrophilic on exposure to water [1,2], which led researchers to believe that diamonds are hydrophilic because of the oxidation and hydration of the diamond surface rather than the adsorption of inorganic salts onto the

surface. This was to ultimately lead to, and inevitably be the foundation for the developing research into the importance of the surface chemistry of diamond.

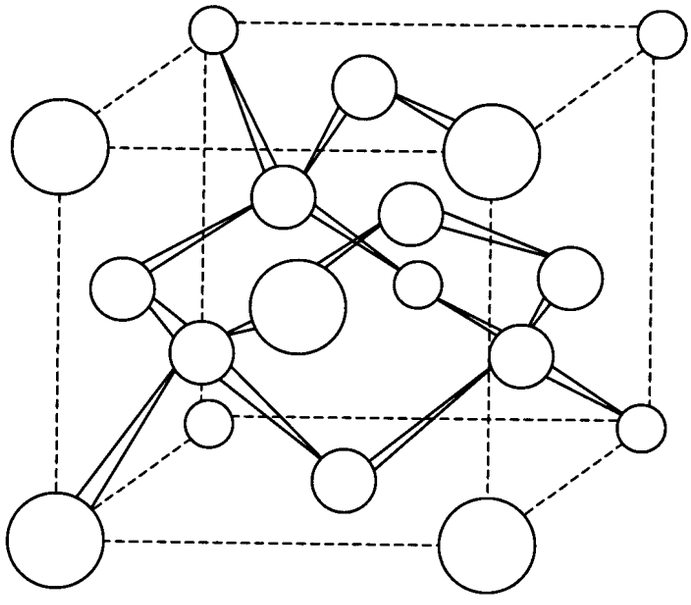

Figure 3.1 : Crystal structure of the diamond lattice [1]

Figure 3.1 represents the crystal structure of a diamond lattice. Each carbon atom is tetrahedrally surrounded by four other carbon atoms. The most frequently occurring facets are the octahedral (111), cubic (100) and rhombic dodecahedral (110) facets [3]. Carbon atoms may be singly bonded on the edges and corners of diamond crystals or anchored with two or three valence bonds to the bulk structure in the (100) and (111) crystal faces (**Figure 3.2**).

11595191
b15367927

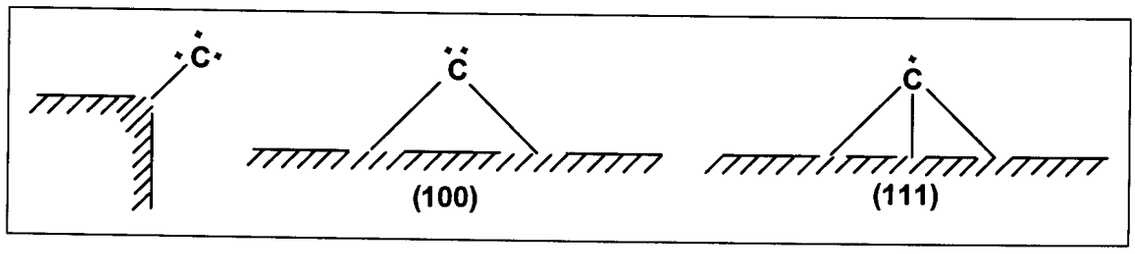

Figure 3.2 : Bonding of carbon atoms to the diamond surface [4]

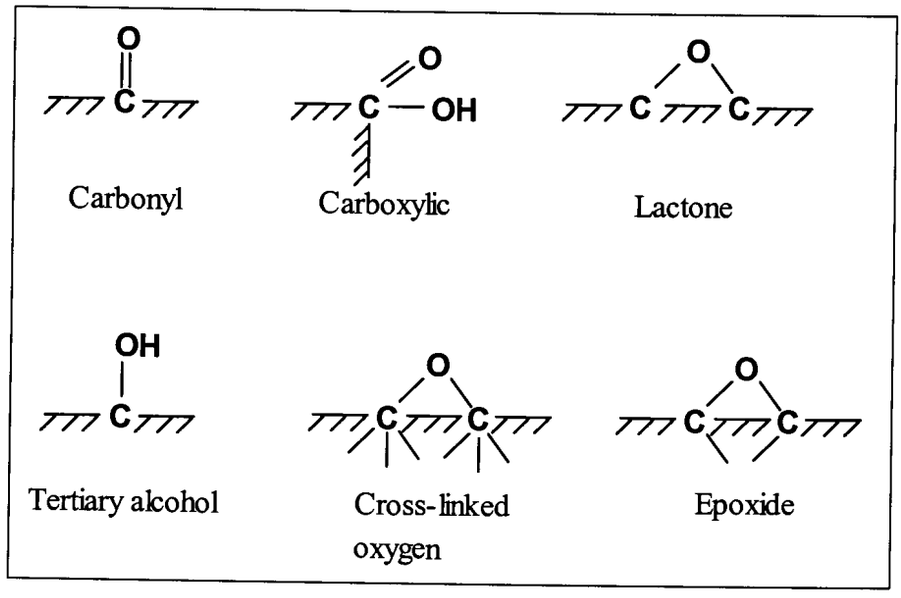

Figure 3.3 : Possible oxygen groups on the diamond surface [2]

Figure 3.3 represents possible oxygen groups on the surface of diamond. Shergold et. al. [2] found that less than 10% of surface carbon atoms are involved in acidic and carbonyl groups. According to the classification of Boehm [4], about 55% of the acidic and carbonyl groups are carboxylic and lactonic in nature and the rest alcohol and carbonyl groups. These carboxylic and lactonic groups are probably found on the edges of the diamond surface rather than on a flat diamond surface because both groups involve a carbon atom with only one bond linking it to another carbon atom within the solid. **Table**

3.1 illustrates the surface groups possibly arising from the saturation of the free valences of carbon with oxygen and hydrogen.

Table 3.1 : Surface groups possibly arising from the saturation of the free valences of carbon with oxygen and hydrogen [3]

Facet	Free valence electrons on carbon	Oxygen group	Hydrogen group
(111) or (110)	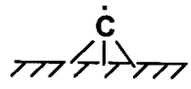	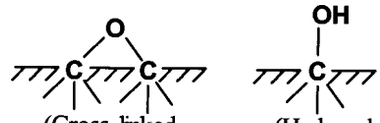 (Cross-linked oxygen) (Hydroxyl group)	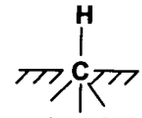 (tert. C-H group)
(100)		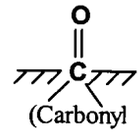 (Carbonyl group)	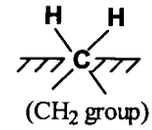 (CH_2 group)
Edges and Corners	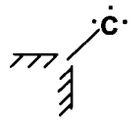	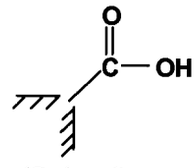 (Carboxylic group)	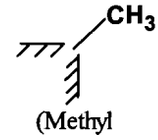 (Methyl group)

Gordeev and Smirnov [5] investigated the effect of the various functional groups synthesised on the surface of synthetic diamond submicron powders on their respective water vapour adsorption isotherms. Chloride, hydride, methyl and hydroxyl functional groups were used in the experiment. They found that the preparations containing a large number of strongly hydrophilic centres (hydroxyl or carbonyl functional groups)

adsorbed far more water than did the other diamond preparations. The activities of the functional groups were ranked according to their decreasing adsorptivity towards water vapour : OH > COOH > Cl > CH_3 > H. Since the activity is related to the polarity of the surface groupings, this implies that the hydroxyl group is much more polar than the methyl or hydride groups. The above ranking agrees with the fact that the adsorption of polar water molecules takes place preferentially on the surface centres that have a high dipole moment (**Table 3.2**) and are also capable of forming hydrogen bonds with the adsorbate.

Table 3.2 : Dipole moment of functional groups [6]

Functional group	Dipole moment, μ
-OH	1.51
-COOH	-
-Cl	1.47
$-CH_3$	0.4
-H	0.4

3.2 Surface structure and chemistry of boron-doped CVD diamond

Chemical vapour deposited diamond is polycrystalline in nature. Depending on the growth conditions, the crystalline structure of CVD diamond could consist predominantly of (111) facets, (100) facets or a mixture of randomly oriented facets. The growth and

surface structure of CVD diamond is best described using the Van der Drift model (**Figure 3.5**). CVD diamond is usually deposited on silicon or tungsten substrates. According to the model, the initial layer of CVD diamond consists of randomly oriented octahedral, cubic and rhombic dodecahedral facets. The facet which grows the fastest will become predominant. This will result in the CVD diamond film consisting of acicular crystallites. The specific conditions for CVD diamond will determine which facet becomes predominating.

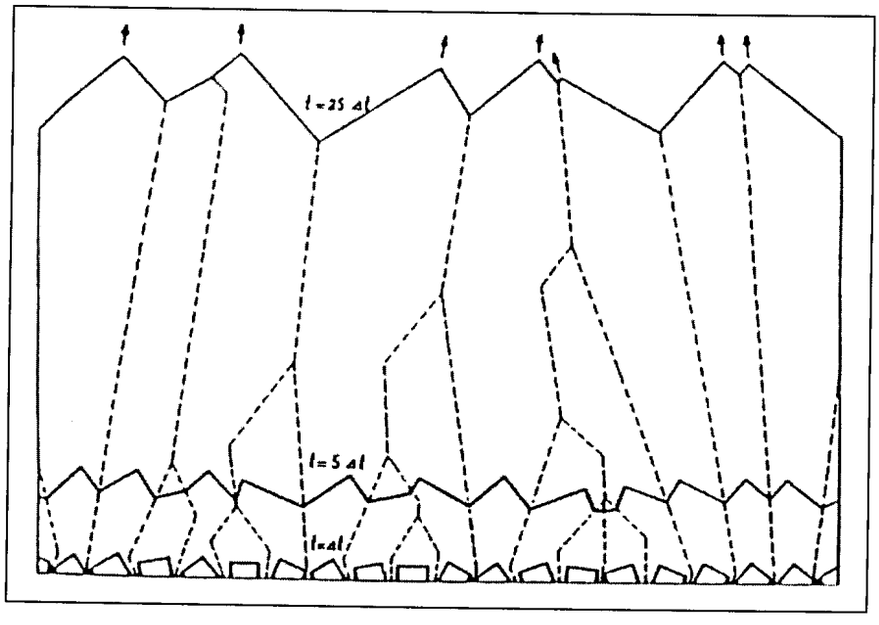

Figure 3.5 : Van der Drift model [7]

Since boron-doped CVD diamond consists primarily of sp^3 carbon covalently bonded in the polycrystalline lattice, it can be assumed that the surface chemistry of boron-doped CVD diamond is analogous to that of natural or synthetic diamond. Since CVD diamond also possesses the three most frequently occurring facets (i.e. (111), (110) and (100)), it is

presumed that similar oxygen functional groups will occur on the boron-doped CVD diamond surface as compared to natural or synthetic diamond (**Table 3.1**).

According to the investigations undertaken by Beamson et. al. [8], hydroxyl, ether, carbonyl and carboxyl functional groups could be identified on organic polymers by their respective peak shifts using X-ray photoelectron spectroscopy (XPS). Using this information and XPS, Goeting et. al. [9] identified the presence of these functional groups on the surface of the boron-doped CVD diamond.

3.3 References

[1] C J Hartley and H L Shergold, **Chemistry and Industry,** (1980) 224.

[2] C J Hartley and H L Shergold, **International Journal of Mineral Processing, 9** (1982) 219.

[3] H P Boehm, **Kolloid Zeitschrift & Zeitschrift fuer Polymere, 227** (1968) 17.

[4] H P Boehm, **Adv. Catalysis, 16** (1966) 219.

[5] S K Gordeev and E P Smirnov, **Kolloidnyi Zhurnal, 44** (1992) 554.

[6] A J Gordon and R A Ford, **The Chemist's Companion,** Wiley, New York (1972).

[7] A Van der Drift, **Philips Res. Rep., 22** (1967) 267.

[8] G Beamson and D Briggs, **High Resolution XPS of Organic Polymers,** Wiley, Chichester, UK (1992).

[9] C H Goeting, F Marken, A Gutierrez-Sosa, R G Compton and J S Foord, **New Diamond and Frontier Carbon Technology, 9** (1999) 207.

CHAPTER 4

Characterisation of boron-doped CVD diamond

4.1 Introduction

There exist various analytical techniques that can provide information on the surface structure as well as on the surface chemistry of solid materials. The information that is gained by using these analytical techniques is invaluable in understanding the characteristics and behaviour of these solid materials. One of the frequently used techniques is scanning electron microscopy (SEM). Unlike ordinary microscopes, the SEM allows for magnifications up to approximately 100 000x to be easily reached, thereby enabling the structures of, for example nano sized particles to be easily obtained.

Another well used technique is X-ray photoelectron spectroscopy (XPS). This is a surface technique that permits the identification of elements on solid surfaces. Another effective technique is Auger electron spectroscopy (AES). XPS and AES are the two major surface analytical techniques and are largely complementary. XPS is more sensitive and gives more useful chemical information, whilst AES has the advantages of greater speed and the potential for high spatial resolution.

Secondary ion mass spectrometry (SIMS) is a technique well known for its high-sensitivity elemental analysis. Laser ablation inductively coupled plasma mass spectrometry (LA-ICP-MS) is less sensitive compared to SIMS, but can readily be applied to solid samples.

The techniques used to analyse the as-received CVD samples were SEM, LA-ICP-MS, Raman and XPS. Contact angle and resistance measurements of the samples were also performed in order to determine the surface state as well as the conductivity of the samples respectively.

4.2 Scanning electron microscopy (SEM)

4.2.1 Theory

Scanning electron microscopy involves the interaction of a beam of primary electrons (produced by an electron gun) with the material being examined. When the primary electron beam strikes the sample, three types of emissions occur, namely secondary electrons, backscattered electrons and X-rays (**Figure 4.1**). These emissions emanate either from the surface of the sample or within the sample.

The secondary electrons are emitted from the surface of the sample and are used to determine the sample topography. Backscattered electrons are emitted from deeper within the specimen, and these electrons provide information related to the atomic number of the specimen. Finally, the emitted X-rays can be used in conjunction with an X-ray detector

to determine which elements are present in the sample. This technique of X-ray emission is called energy dispersive spectroscopy (EDS).

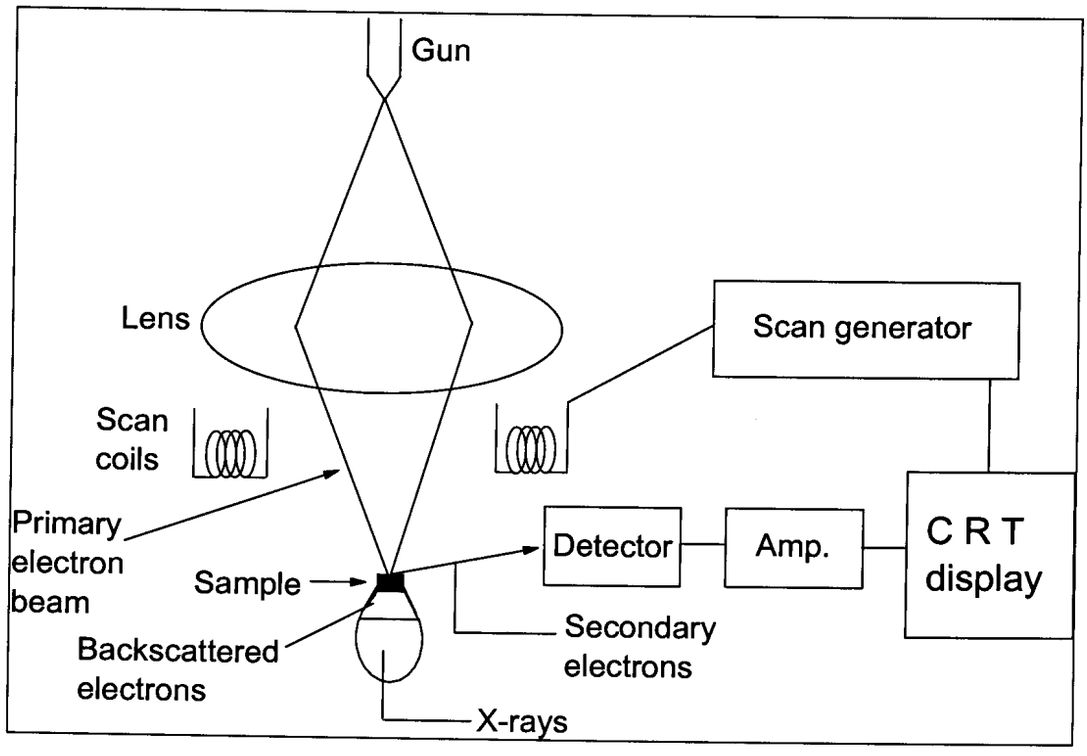

Figure 4.1 : Schematic of the scanning electron microscope (SEM) (modified extract from [1])

During the imaging of a sample, the electron beam scans across the surface of the sample in a raster type pattern. Since the secondary electron detector is connected to the display monitor, as the primary electron beam is scanned across the surface of the sample, the image is shown on the monitor instantaneously. The image formed is based on the intensity of the secondary electrons emitted from the specimen.

In order to obtain a good quality image, the specimen under investigation must be electrically conductive. Otherwise, there will be a build-up of electrons in and around the sample, and this will result in the primary electron beam being repelled from the sample, thereby producing a "poor" quality image.

Various boron-doped diamond samples were analysed using the SEM. Diamond, in the absence of a satisfactory dopant, is rendered non-conductive. One of the techniques adopted to make non-conductive specimens conductive is gold plating of the sample surface. Since the boron-doped diamond samples were conductive due to the presence of boron, gold plating of the surface of the CVD sample was not essential.

4.2.2 Experimental

A Philips ESEM XL 30 was used to analyse the surfaces of six boron-doped CVD diamond samples, obtained from De Beers. The dimensions of each sample were: length = 1 cm, width = 1 cm and thickness = 0.07 cm. CVD samples were initially ultrasonically cleaned with water and acetone before analysis. The boron-doped samples were mounted onto stainless steel stubs using graphite tape and then inserted into the SEM sample chamber. After the chamber was evacuated, the electron beam was focused onto the sample surface and the desired magnification attained. The image was then acquired electronically.

4.2.3 Results and discussion

CVD samples of varying boron content were characterised using the SEM. The manufacturer's estimated boron content of the samples is given in **Table 4.1**. CVDBD6 is the highest boron-doped sample, whereas CVDBD2 is the lowest boron-doped sample. CVDBD1 is undoped. The SEM images of the various boron-doped samples are shown in **Figures 4.2 – 4.7**. From these images, it can be seen that the CVD samples consist of randomly oriented facets.

Table 4.1 : Estimated boron concentrations of CVD samples

Sample	[B] / mg/L	[B] / atoms.cm^{-3}
CVDBD1	0	0
CVDBD2	76	1.50×10^{19}
CVDBD3	438	8.64×10^{19}
CVDBD4	799	1.58×10^{20}
CVDBD5	1160	2.29×10^{20}
CVDBD6	1521	3.00×10^{20}

Numerous grain boundaries are also present. This observation is important from a sample homogeneity point of view, as it is known that impurities concentrate at grain boundaries [2]. The undoped and medium boron-doped samples were found to be similar in terms of their crystallite sizes, which were considerably larger than those of the low boron-doped and high boron-doped samples. This will impact on the surface area of the samples, with

the medium doped sample expected to have a slightly smaller surface area, and therefore to generate a slightly smaller current when used as an electrode, than the other samples. One way of ensuring that all the sample surface areas are the same, is to polish the sample. However, this would alter the surface state in terms of chemical functionalities, and it was therefore decided to work with cleaned but unpolished samples during the voltammetric investigation.

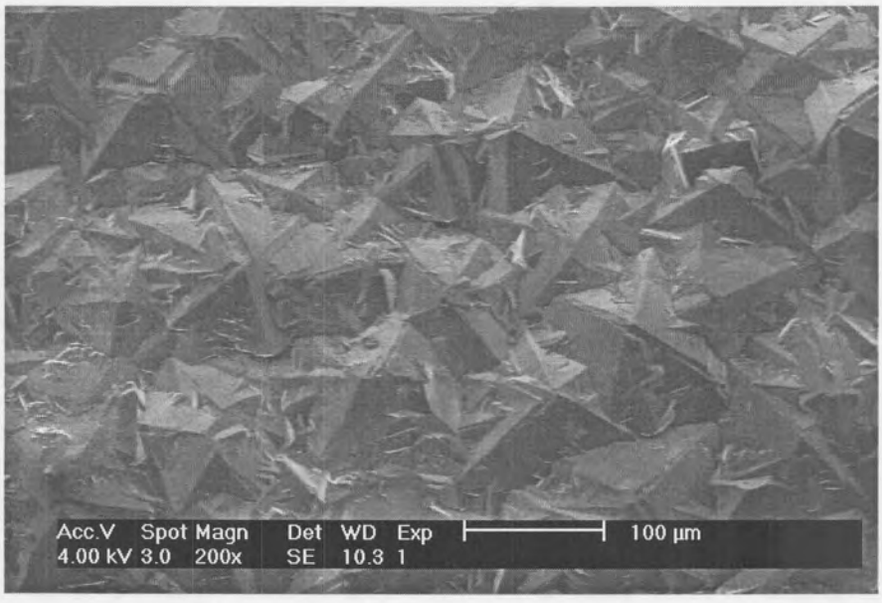

Figure 4.2 : SEM image of undoped CVD diamond

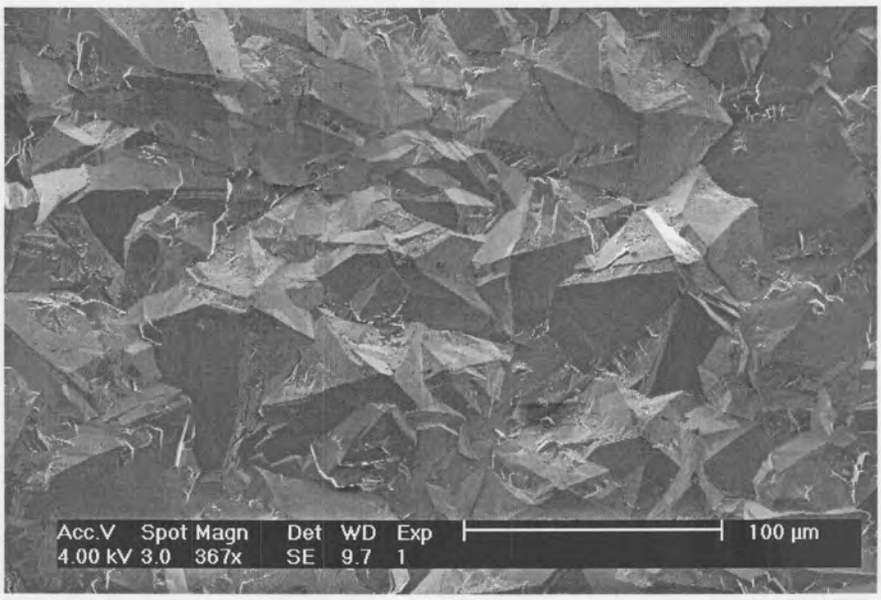

Figure 4.3 : SEM image of low boron-doped CVD diamond (CVDBD2)

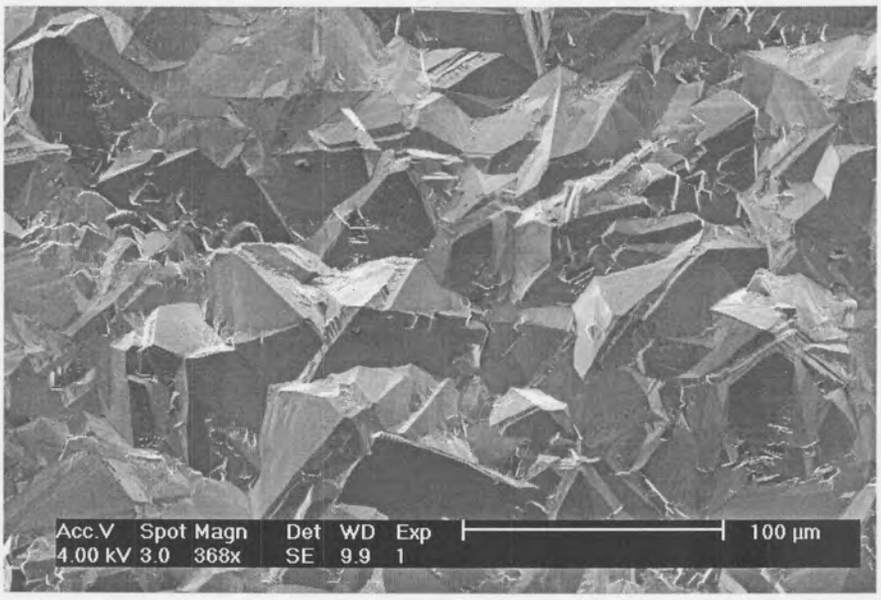

Figure 4.4 : SEM image of low-medium boron-doped CVD diamond (CVDBD3)

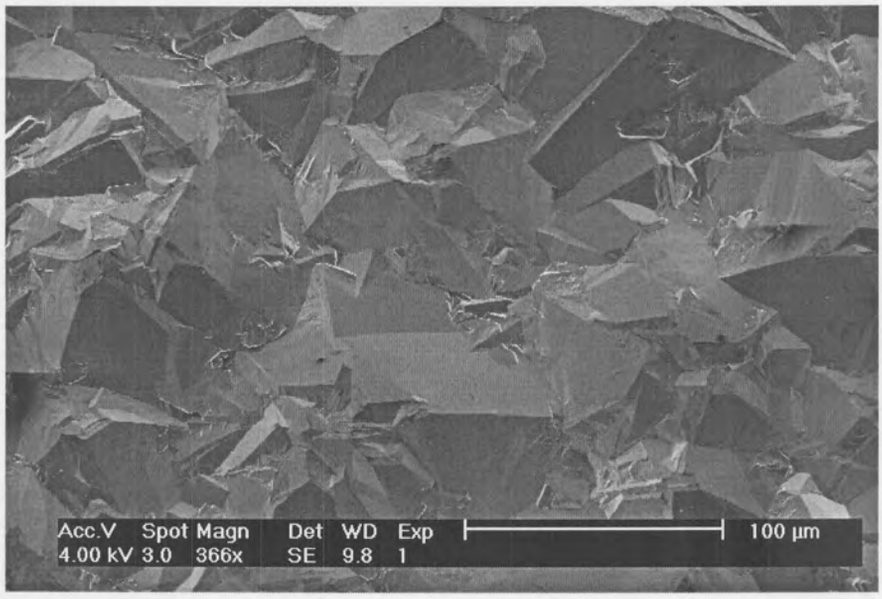

Figure 4.5 : SEM image of medium boron-doped CVD diamond (CVDBD4)

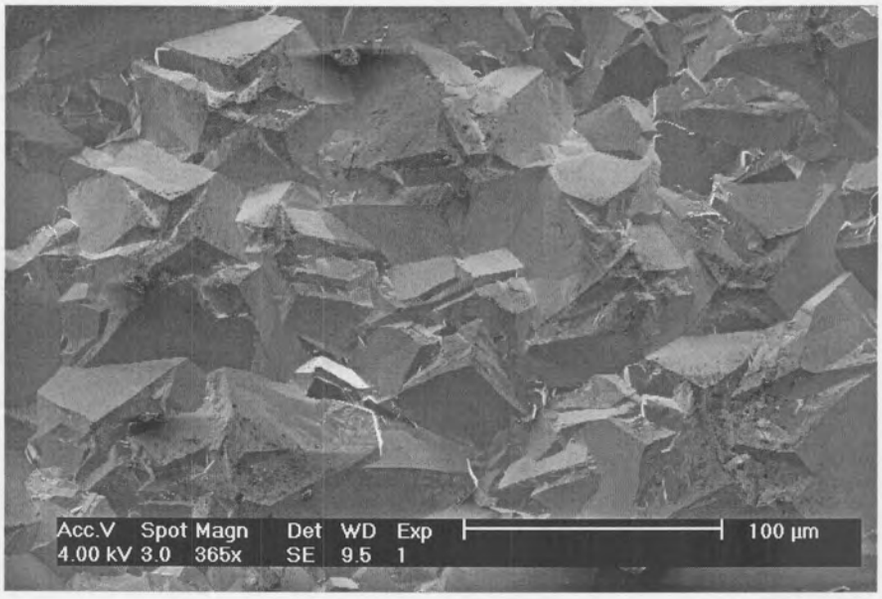

Figure 4.6 : SEM image of medium-high boron-doped CVD diamond (CVDBD5)

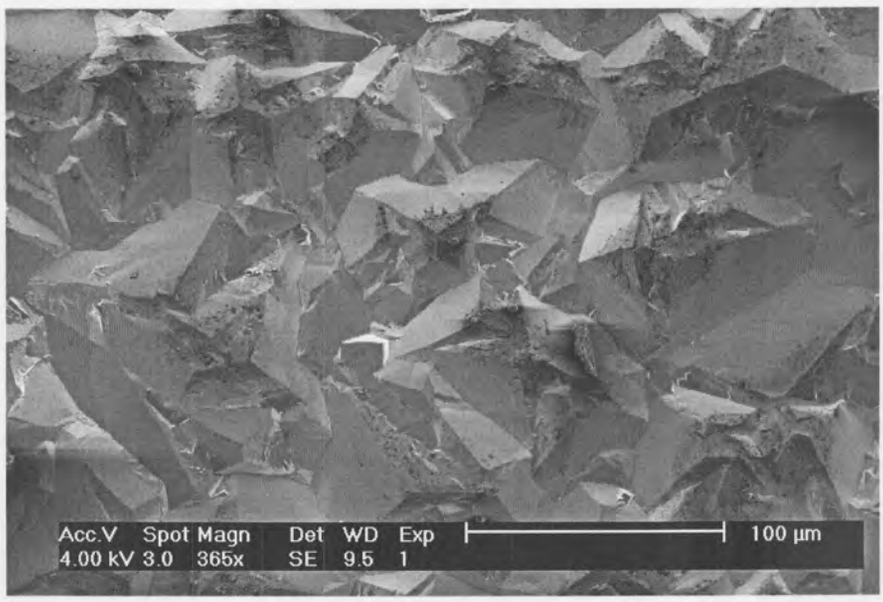

Figure 4.7 : SEM image of high boron-doped CVD diamond (CVDBD6)

4.3 Laser ablation inductively coupled plasma

4.3.1 Theory

The laser ablation ICP-MS is a trace element microprobe which combines the spatial resolution of an ultraviolet laser beam with the mass resolution and elemental sensitivity of an inductively coupled plasma mass spectrometer (ICP-MS). This system is thus suitable for the analysis of boron concentration in the CVD samples. A schematic diagram depicting the laser ablation ICP-MS system is shown in **Figure 4.8**.

The laser beam is generated from a Nd-YAG laser with a wavelength range from 1 micron (infra-red region) to 266 nanometers (ultraviolet region). Samples are located in an enclosed sample cell that is continuously purged with argon gas. The top surface of the

sample cell, which consists of a thin flat plate of quartz or a thin mylar film, is transparent to the laser light and the laser beam can therefore be focused onto the sample surface causing ablation.

Samples may either be mounted as irregular shapes or polished/unpolished thin sections. The physical form of the sample is irrelevant as long as the sample is positioned under the laser beam. Samples are usually viewed through a high-resolution colour video camera. A small volume of material is ablated from the sample surface using the laser beam. The ablated material is then transported in an argon carrier gas directly to the inductively coupled plasma. The resulting ions are then drawn into a quadrupole mass spectrometer for detection. LA-ICP-MS has various advantages and disadvantages [4].

Advantages

- There is no need for chemically dissolving samples, thereby reducing the risk of contamination and sample losses
- Very small samples can be analysed
- The spatial distribution of elements can be determined

Disadvantages

- There is a need for an internal standard to correct for the differences in the ablation rate of the sample and of the standard
- The instrument needs to be routinely calibrated

LA-ICP-MS has several geological applications, which may include analysis of rocks, minerals, glasses, fluid and solid inclusions.

4.3.2 Experimental

The analysis of the boron concentration of the CVD samples using the LA-ICP-MS system (Cetac LSX200, Elan 6000 ICP-MS) was carried out at the De Beers GeoScience Centre. **Table 4.2** illustrates the LA-ICP-MS system configuration. A carbon-based oil was used as a standard in order to calibrate the instrument. Small portions of glass capillary tubes were mounted horizontally in epoxy mounts and the surfaces polished to flatten the top portion of each capillary tube. The standard oil (which was doped with boron) was then syringed into the capillaries and these capillaries were thereafter sealed with tape.

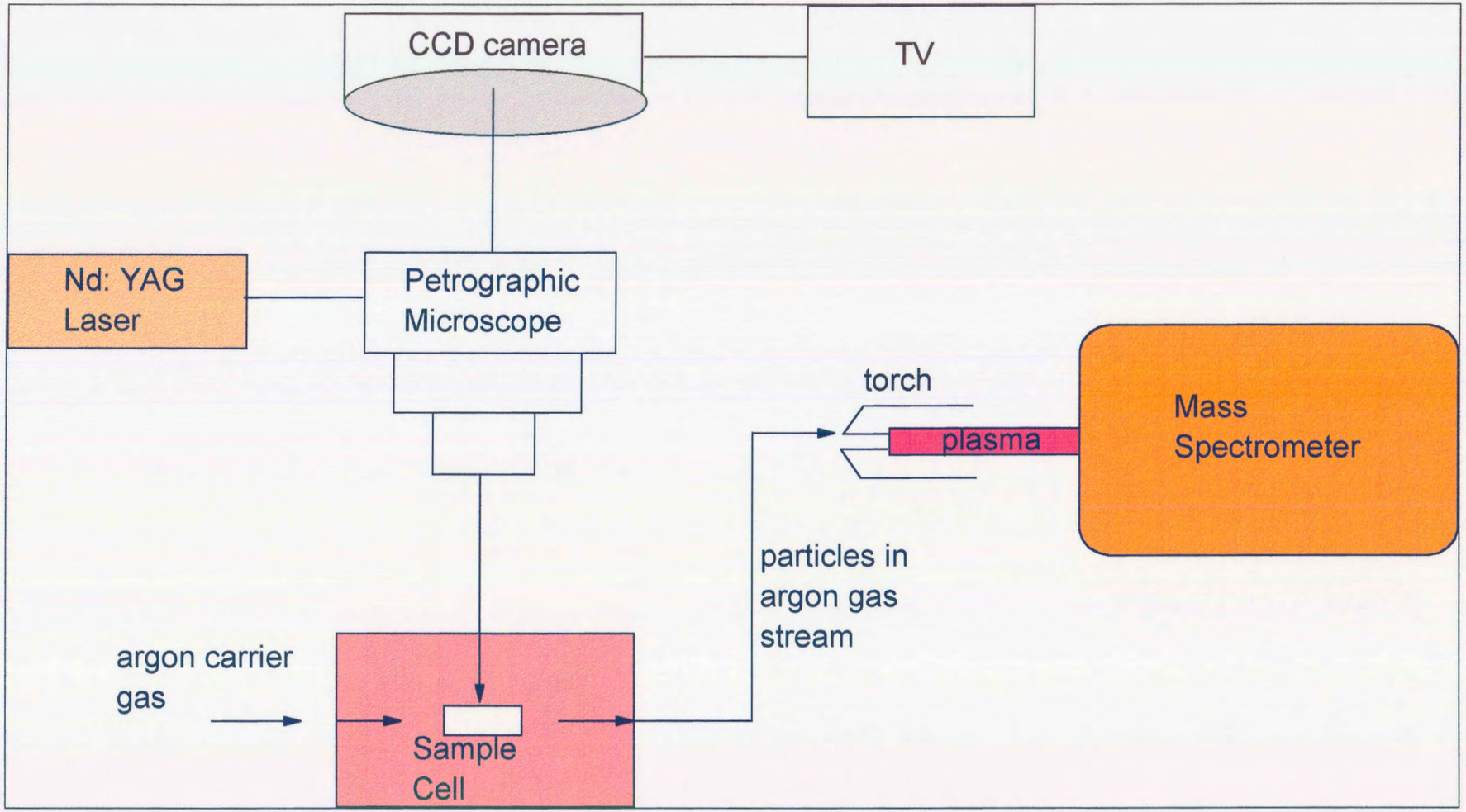

Figure 4.8 : Schematic setup of a LA-ICP-MS unit [3]

Table 4.2 : LA-ICP-MS system configuration

Cetac LSX200	
Laser type :	Q-switched Nd:YAG, frequency quadrupled to 266 nm
Laser energy :	20 mJ
Pulse frequency :	10 Hz
Spot size :	150 micron
Ablation method :	Drill on oil
Elan 6000 ICP-MS	
RF forward power :	1350 V
Carrier gas flow :	1.14 l/min argon and ~1.5 l/min helium
Detector mode :	Peak hopping
Autolens facility :	Activated
Dwell times / sweep :	10 ms per element (except for carbon, 4 ms)
No. of Replicates :	150
Blank acquired for :	30 – 40 s
Ablated sample data acquired for :	10 – 20 s

The carbon in both the oil and the samples was used for internal standardisation to compensate for differential ablation. The carbon concentration of the oil is 86% and that of the diamond films is assumed to be 99.9%. The three samples were ablated using the same laser parameters applied to the standard and quantitative data were obtained.

4.3.3 Results and discussion

Table 4.3 represents the boron concentration results for the three samples analysed. CVDBD1 is the "undoped" sample, CVDBD2 the low boron-doped sample and CVDBD4 the medium boron-doped sample. The estimated boron concentration values were taken from **Table 4.1**. It is seen from **Table 4.3**, that the measured boron concentration values of the CVD samples are very similar to that of the estimated values.

The small amount of boron present in CVDBD1 may be due to boron contamination of the CVD sample during its growth stage. The lower limit of detection for boron with the LA-ICP-MS system was found to be 1 mg/L, and the relative standard deviation for this element ranged from 3.1% to 4.8% for the three pits drilled. **Figure 4.9** illustrates the detailed SEM image of the ablation pit in the glass capillary surface, whilst **Figure 4.10** depicts the SEM image of the diamond thin film surface with two ablation pits.

Table 4.3 : Boron concentrations of CVDBD1, CVDBD2 and CVDBD4

Sample	Measures values		Estimated values
	[B] / mg/L	[B] / atoms.cm^{-3}	[B] / atoms.cm^{-3}
CVDBD1	1.19	2.32×10^{17}	0
CVDBD2	83.8	1.64×10^{19}	1.50×10^{19}
CVDBD4	543	1.06×10^{20}	1.58×10^{20}

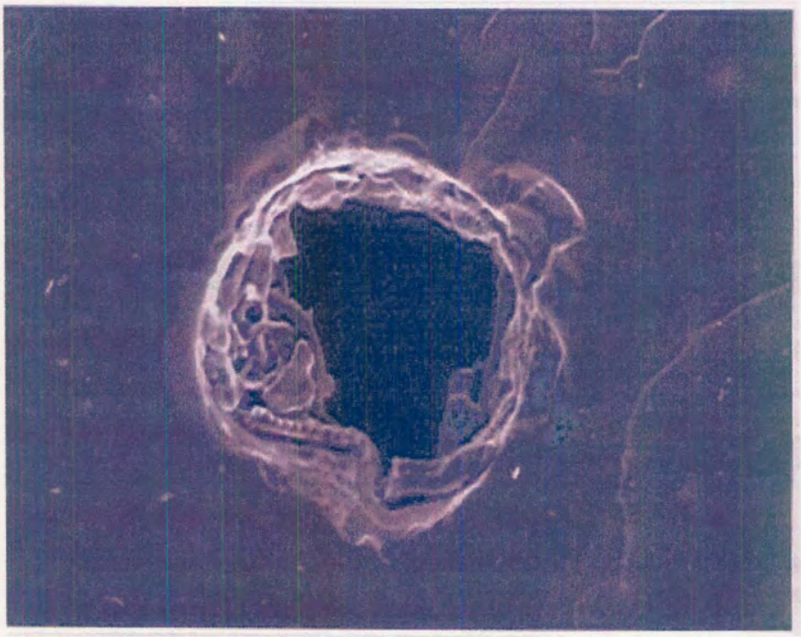

Figure 4.9 : Detailed SEM image of ablation pit in the glass capillary surface

(Magnification ~320x)

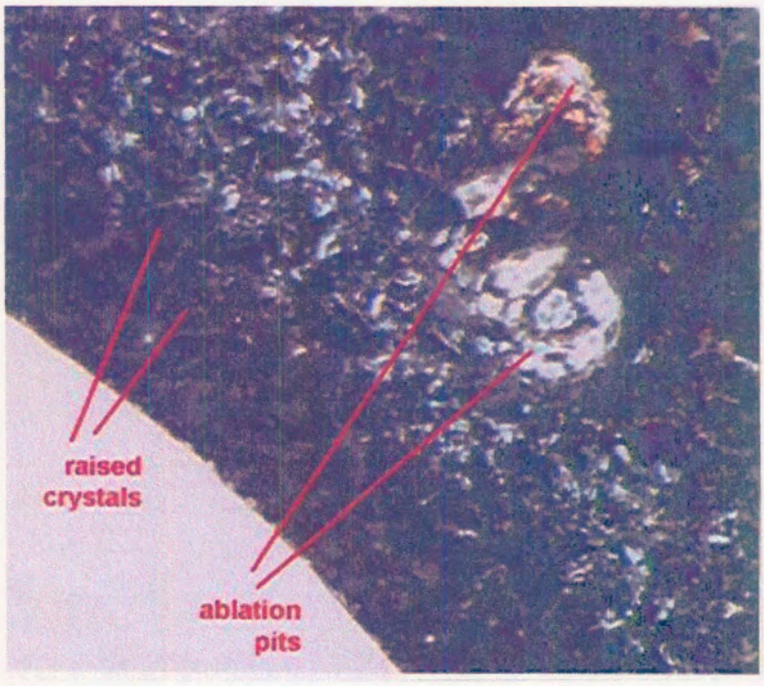

Figure 4.10 : Diamond thin film surface with two ablation pits

An equipment malfunction resulted in decreased sensitivity of the LA-ICP-MS system, so that the boron concentrations of CVDBD3 and CVDBD5 could not be measured. However, the boron concentrations of these samples were estimated using the low, medium and high boron concentration samples (CVDBD2, CVDBD4 and CVDBD6). The boron concentration for all the CVD samples is therefore given in **Table 4.4**.

Table 4.4 : Boron concentrations of CVD samples

Sample	[B] / mg/L	[B] / atoms.cm^{-3}
CVD1	1.19	2.35×10^{17}
CVD2	84	1.64×10^{19}
CVD3	313*	6.18×10^{19} *
CVD4	543	1.06×10^{20}
CVD5	1032*	2.04×10^{20} *
CVD6	1521*	3.00×10^{20} *

*estimated values

4.4 Raman spectroscopy

4.4.1 Theory

The electrochemical behaviour of CVD diamond electrodes can be affected drastically by the presence of sp^2 carbon (graphitic carbon) on the electrode surface. Depending on the growth conditions, sp^2 carbon may be co-deposited with diamond on the substrate surface. It is therefore vital that the extent of graphitisation of the CVD samples be

determined. One of the very few techniques that is extremely useful in distinguishing between the presence of sp^2 carbon and sp^3 carbon in a diamond lattice is Raman spectroscopy. This technique was discovered by an Indian physicist C.V.Raman in 1928 [5]. He was awarded the 1931 Nobel prize in physics for this discovery and his systematic exploration of it.

Raman spectroscopy is a nondestructive method to study the vibrational band structure of materials. It has been extensively used for the characterisation of diamond [6-9], graphite [10] and diamond-like carbon (DLC) [11,12]. This technique can also be applied to the qualitative and semi-quantitative analysis of organic, inorganic and biological systems [5].

A schematic diagram of the Raman spectrometer is given in **Figure 4.11**. The laser is used as the photon source due to its high monochromatic nature. In the visible spectral range, Raman spectrometers use notch filters to cut out the signal from a very narrow range centred on the frequency corresponding to the laser radiation. A microscope is used to focus the laser beam onto the sample. Light from the sample is then passed back through the microscope optics into the spectrometer. Raman shifted radiation is detected with a charge-coupled device (CCD) detector, and a computer is used for data acquisition and curve fitting.

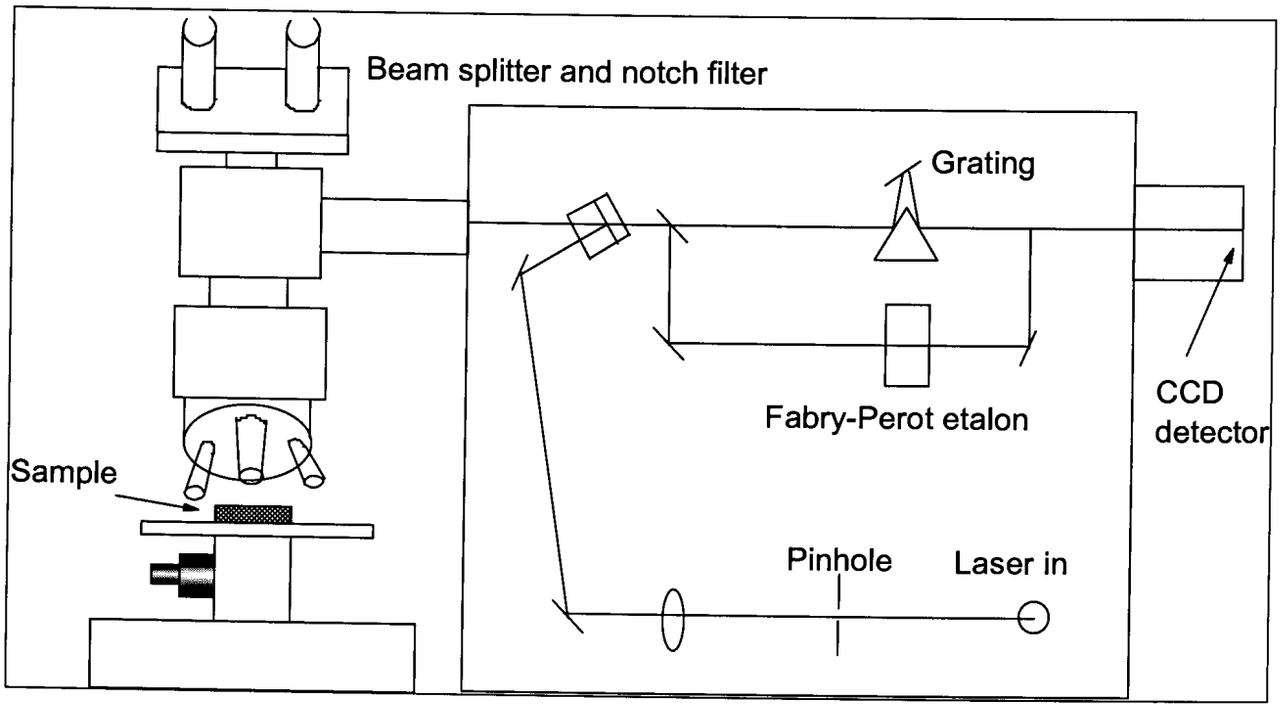

Figure 4.11 : Schematic diagram of a Raman spectrometer [13]

The Raman effect arises when incident light of a particular wavelength excites molecules in the sample, which subsequently scatter the light. While most of this scattered light is at the same wavelength as the incident light (Rayleigh scattering), some of the light is scattered at a different wavelength. This inelastically scattered light is called Raman scatter.

The energy difference between the incident light (E_i) and the Raman scattered light (E_s) is equal to the energy involved in changing the molecule's vibrational state (E_v) (**Equation 4.1**). This energy difference is called the Raman shift.

$$E_v = E_i - E_s \qquad (4.1)$$

Different vibrational or rotational motions of molecules in the sample give rise to different Raman shifted signals being observed. A plot of Raman intensity versus Raman shift is a Raman spectrum.

4.4.2 Experimental

The CVD samples were analysed using a Jobin-Yvon T64000 Raman spectrometer with an Olympus Bx40 microscope attachment. A grating of 1800 grooves/mm was employed to disperse the scattered light onto a liquid nitrogen–cooled CCD detector. The 514.5 nm line of an argon ion laser was used as the excitation radiation for the sample. The Olympus Bx40 microscope attachment with a 100x objective was utilised to focus the argon ion laser to about 3 μm spot size onto the surface of the CVD sample. Spectra for both the rough and smooth surfaces of each sample were recorded.

4.4.3 Results and discussion

Each of the samples had a rough upper surface and a smooth lower surface. Both the rough and the smooth surfaces of the samples were analysed using Raman spectroscopy. **Figure 4.12** denotes the Raman spectra for the rough upper surfaces of the samples. The spectra for CVDBD2 to CVDBD6 are characteristic of high quality diamond films (narrow line width and low background signal).

A very intense one phonon diamond sp^3 carbon peak occurs at a wavelength of approximately 1332 cm^{-1}. This peak is accompanied by a broad flat sp^2 carbon peak occurring at about 1550 cm^{-1}. This non-diamond peak representing the sp^2 carbon impurity phases in the boron-doped samples is clearly observed in the undoped sample and unseen in the boron-doped samples. If the intensity scale of the spectra is expanded, extremely low levels of these impurity phases can be detected. It should be noted that the magnitude of the Raman signal on the ordinate is 50 times more sensitive to the non-diamond carbon form than to the crystalline diamond [14].

Table 4.5 illustrates the sp^2/sp^3 ratio of the rough surface of the CVD samples. This ratio is an average of three sample measurements. From **Figure 4.12** and **Table 4.5**, it may be deduced that the presence of boron in the sample suppresses the formation of sp^2 carbon. However, as the concentration of boron in the sample increases, the ratio of sp^2/sp^3 carbon also increases. This may be due to the decrease of sp^3 carbon as the boron replaces carbon atoms in the diamond lattice, which effectively decreases the Raman cross section for the diamond lattice [15], or it may mean that the boron has improved the quality of the lightest-doped samples by decreasing the content of graphitic and amorphous carbon.

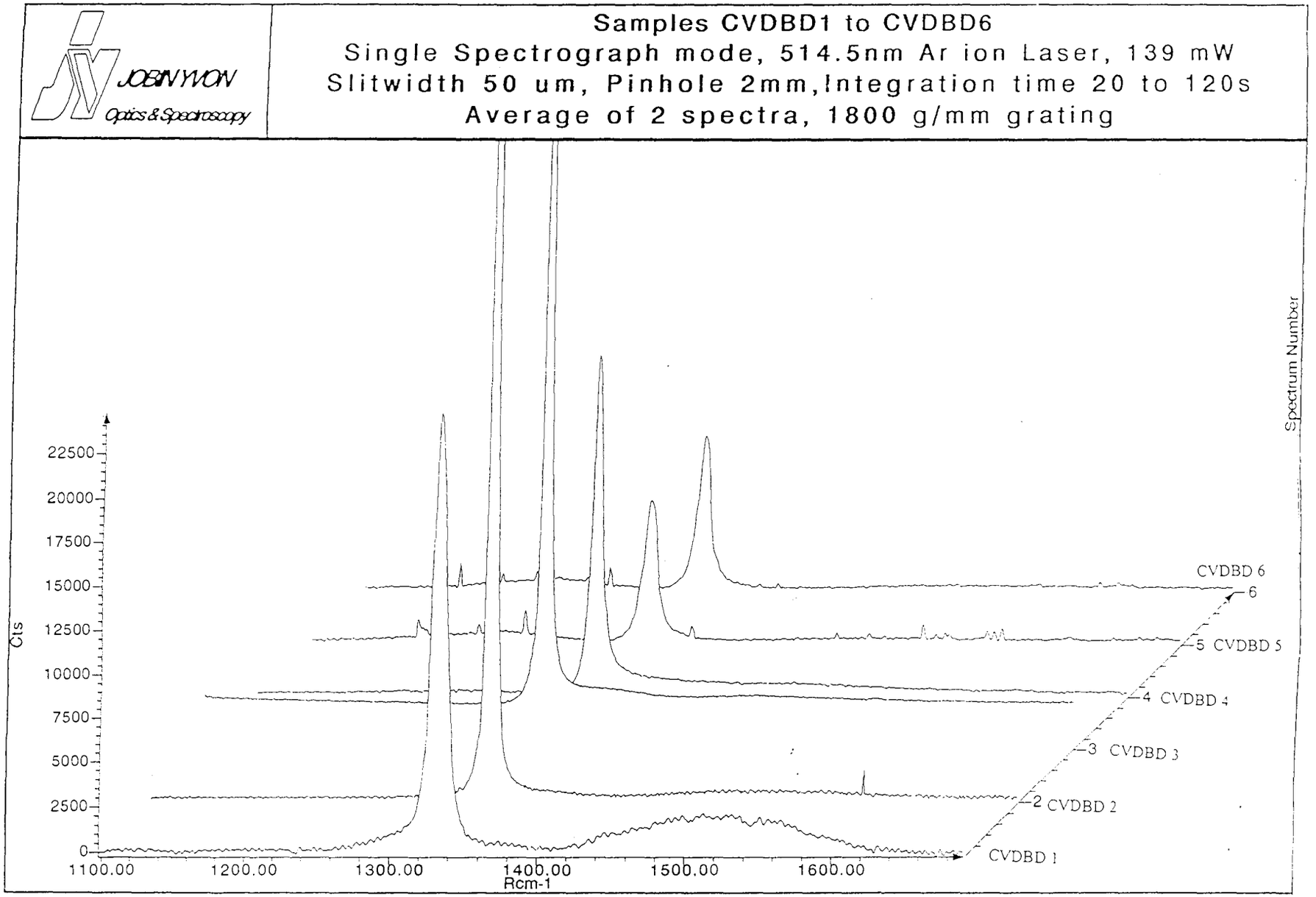

Figure 4.12 : Raman spectra for the rough upper surfaces of the CVD samples

Table 4.5 : Ratio of the sp^2/sp^3 carbon peak areas of the rough surface of the CVD samples

CVD sample	Average sp^2/sp^3 ratio
CVDBD1	2.19
CVDBD2	0.23
CVDBD3	0.71
CVDBD4	1.22
CVDBD5	2.50

Polo et. al. [16] investigated the effect of increasing boron concentration of CVD diamond samples on their respective Raman spectra (**Figure 4.13**). They observed a decrease and a broadening of the diamond peak as the boron concentration increased. The heavily doped sample (75000 mg/L of boron) presents a Raman spectrum with the typical features of amorphous carbon with two broad bands centred around 1350 cm^{-1} and 1570 cm^{-1}.

Figure 4.14 illustrates the Raman spectra for the smooth lower surface of the CVD samples. This surface has a smooth texture due to it being in contact with the substrate (usually silicon or tungsten) during growth. The Raman spectra indicate the strong presence of sp^2 carbon in all the CVD samples. This broad peak occurs at approximately 1550 cm^{-1}.

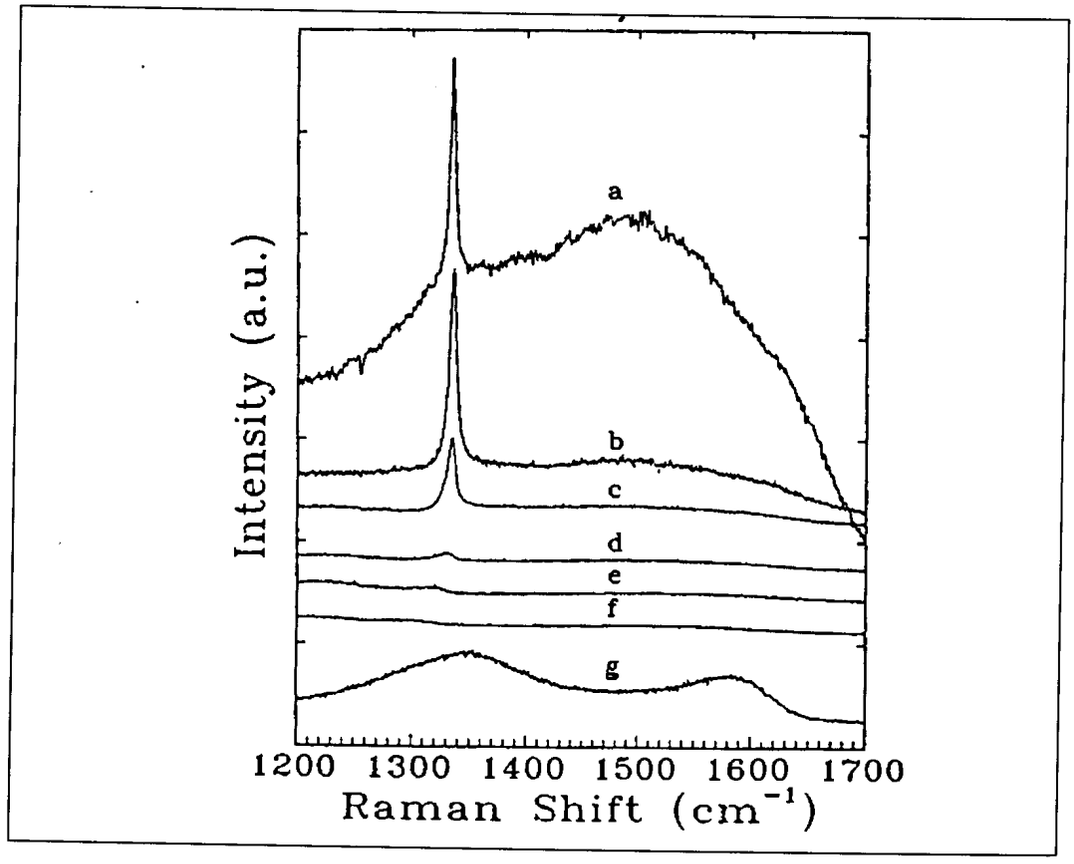

Figure 4.13 : Raman spectra of diamond samples with different boron contents; (a) undoped film, (b) 1333 mg/L B, (c) 2250 mg/L B, (d) 5250 mg/L B, (e) 17500 mg/L B, (f) 2750 mg/L B, (g) 75000 mg/L B [16]

An interesting feature in the spectra illustrated in **Figure 4.14** is that as the boron concentration increases from CVDBD2 to sample CVDBD6, the sp^2 non-diamond peak seems to become more narrow and sharp. This may imply that the graphitic carbon tends to become more crystalline. The smooth lower surface of the CVD samples (i.e. the initial layer deposited during manufacture) was found to contain more sp^2 carbon than the rough upper surface.

UNIVERSITEIT VAN PRETORIA
UNIVERSITY OF PRETORIA
YUNIBESITHI YA PRETORIA

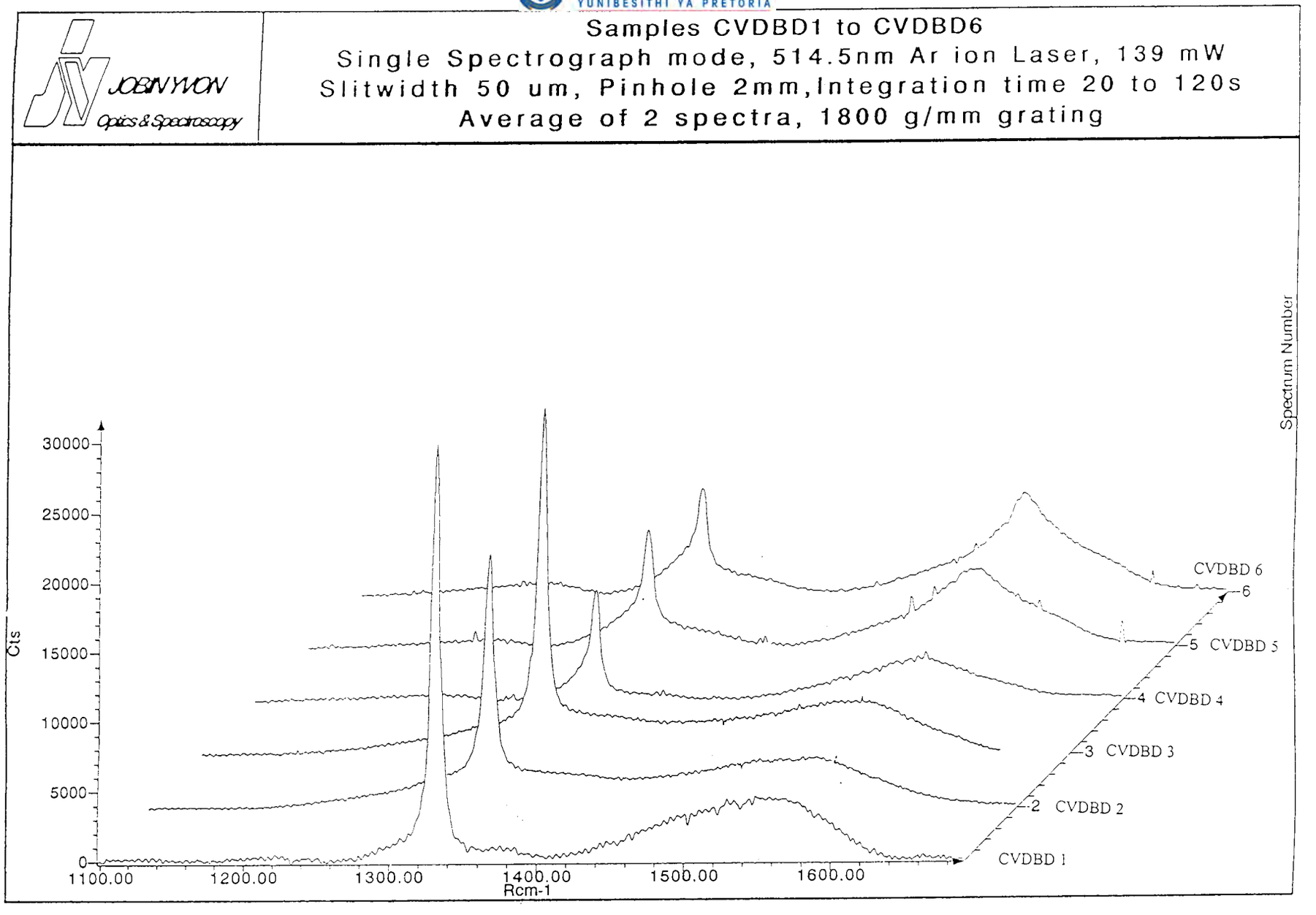

Figure 4.14 : Raman spectra for the smooth lower surface of the CVD samples

4.5 X-ray photoelectron spectroscopy (XPS)

4.5.1 Theory

X-ray photoelectron spectroscopy (XPS, also called electron spectroscopy for chemical analysis, ESCA) was developed in the mid 1960s by K.Siegbahm and his research group [17]. K. Siegbahm was awarded the Nobel Prize in 1981 for his work in XPS. The phenomenon of XPS is based on the photoelectric effect outlined by Einstein in 1905 where the concept of the photon was used to describe the ejection of electrons from a surface when photons impinge upon it. XPS may be used in various areas of application such as polymers, organics, biological specimens, fibres, films, powders and particles [18].

In XPS, the photon is absorbed by an atom in a molecule or solid, leading to ionization and the emission of a core (inner shell) electron [19]. The kinetic energy, E_k, of these emitted photoelectrons is determined by the energy of the X-ray radiation, $h\nu$, and the electron binding energy, E_b, as given in **Equation 4.2** [20].

$$E_k = h\nu - E_b \qquad (4.2)$$

The experimentally measured energies of the photoelectrons are given in **Equation 4.3**, where E_w is the work function of the spectrometer.

$$E_k = h\nu - E_b - E_w \qquad (4.3)$$

Each element yields a characteristic binding energy associated with each core atomic orbital, that is, each element will give rise to a characteristic set of peaks in the photoelectron spectrum at kinetic energies determined by the photon energy and the respective binding energies.

Specific elements in a sample can be identified by the presence of specific peaks occurring at particular energies in the photoelectron spectrum. Furthermore, the intensity of the peaks is related to the concentration of the element within the sampled region. Thus, the XPS technique produces qualitative as well as semi-quantitative information on solid samples. A schematic diagram of the XPS apparatus is found in **Figure 4.15**.

The XPS instrument consists of an X-ray source, an energy analyser for the photoelectrons and an electron detector. In order to analyse and detect the emitted photoelectrons, the sample has to be placed in a high-vacuum chamber. The energy of the photoelectrons is analysed by a spherical analyser, and a channeltron electron detector detects the photoelectrons.

4.5.2 Experimental

A VG Scientific XPS instrument together with VGX 900-W data acquisition and analyzing software were used for the characterisation of the as-received sample, CVDBD4, in terms of its oxygen content. The sample was strapped to a molybdenum sample holder and the holder inserted into the UHV (Ultra High Vacuum) chamber via a

Leybold Heraeus sample introduction rod. The vacuum was then pumped down to 10^{-11} < Pressure < 10^{-10} millibar. Since XPS is a surface analytical technique, the UHV is needed to prevent the atoms in the air from landing on the sample surface and changing its properties.

X-rays from the X-ray source (AlK_{α} radiation) were then focused onto the sample and the resulting photoelectrons emitted. These photoelectrons were then analysed via a channeltron electron detector and an XPS spectrum was produced. The photon energy was 1486.6 eV and the resolution of the spectrometer was 0.1 eV.

4.5.3 Results and discussion

Figure 4.16 represents the XPS spectrum for CVDBD4. The carbon peak occurs at a binding energy of 288 eV and the oxygen peak occurs at a binding energy of 536 eV. For natural diamond, the carbon peak occurs at a binding energy of 284 eV and the oxygen peak occurs at a binding energy of 532 eV. The observed peak shift could be due to the presence of boron on the CVD sample or the oxygen functionalities on the sample.

UNIVERSITEIT VAN PRETORIA
UNIVERSITY OF PRETORIA
YUNIBESITHI YA PRETORIA

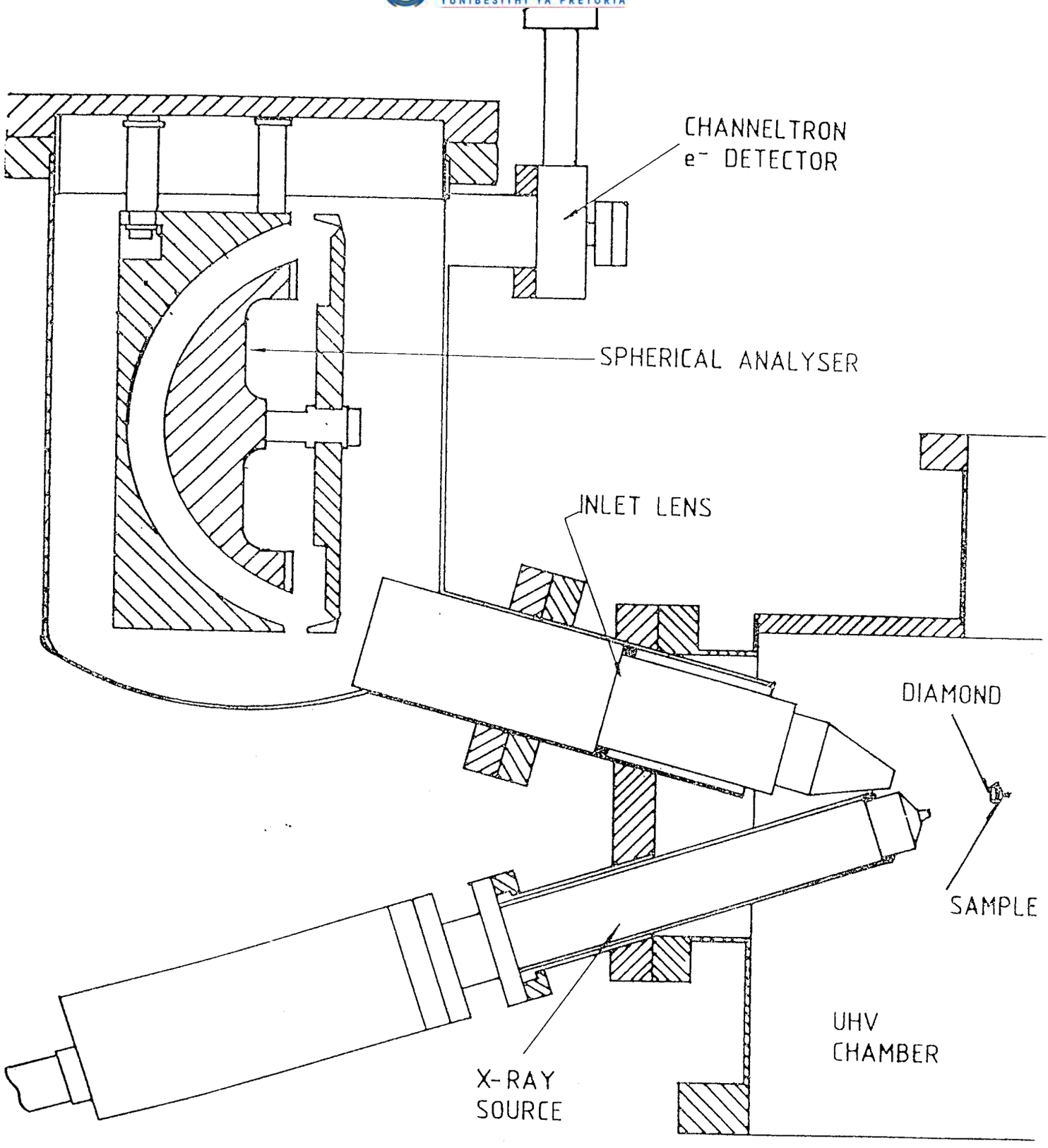

Figure 4.15 : Schematic diagram of the XPS apparatus [21]

UNIVERSITEIT VAN PRETORIA
UNIVERSITY OF PRETORIA
YUNIBESITHI YA PRETORIA

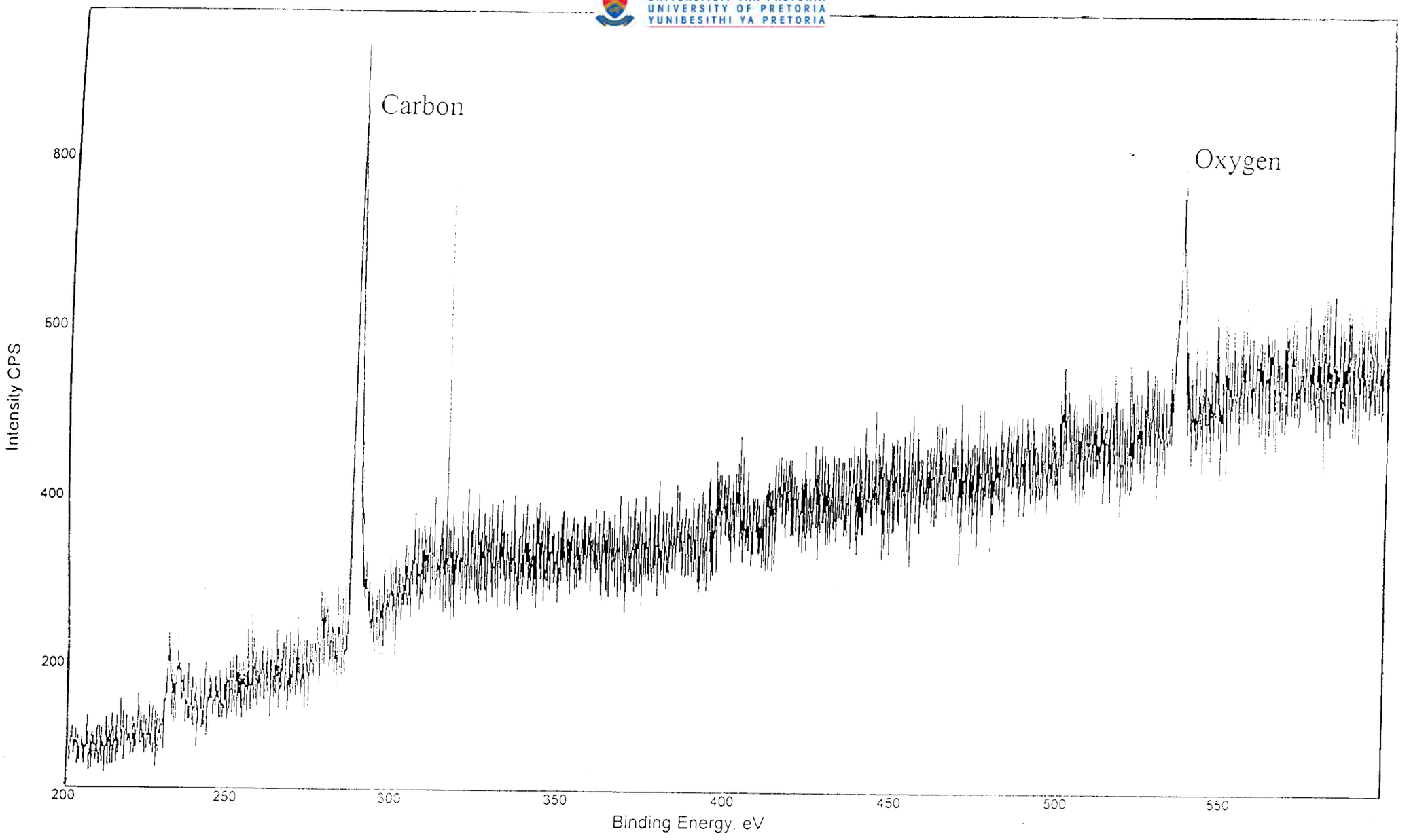

Figure 4.16 : XPS spectrum for CVDBD4

By integrating the peak areas, applying a Gaussian fit to the peaks and using **Equation 4.4**, the oxygen content of the CVD sample was calculated to be 2.37 x 10^{15} atoms/cm^2.

$$\sigma = \frac{Y_m}{Y_s} \times \frac{N \cos\theta\ \mu_s\ \rho_s\ \lambda}{\mu_m\ M_s} \qquad (4.4)$$

Where :

σ = surface oxygen content, atoms/cm^2

Y_m = integrated XPS peak area for adsorbed oxygen atoms corrected for the increase in analyser sensitivity with decreasing kinetic energy

Y_s = integrated peak area for substrate carbon

N = Avogadro's number, 6.023 x 10^{23} atoms/mole

θ = system geometrical constant, 25°

μ_s = photoionization cross-section for carbon, 1.0

μ_m = photoionization cross-section for oxygen, 2.92

ρ_s = diamond density, 3.51 g/cm^3

λ = photoelectron escape depth (AlK_α)

M_s = mass number of carbon, 12.01

Hansen et. al. [21] reported the amount of a full monolayer of oxygen on each of the surfaces (111), (110) and (100) to be 1.82 x 10^{15} atoms/cm^2, 2.22 x 10^{15} atoms/cm^2 and 1.57 x 10^{15} atoms/cm^2 respectively. Since CVD diamond is polycrystalline, that is it

contains randomly oriented facets, the average of the full monolayer of oxygen for the above surfaces was taken, which was calculated to be 1.87 x 10^{15} atoms/cm^2. Using this value, the oxygen coverage of CVDBD4 was thus calculated to be 1.26 monolayers. The results obtained therefore confirm the presence of oxygen functionalities on the surface. An alternative technique that may be used to calculate the oxygen monolayer coverage is by altering the take-off angles for the electrons thereby giving them a geometrically longer path length [22]. Since the IMFP of electrons is quite small at Al K-alpha wavelengths, this method may be used to calculate monolayer coverages.

4.6 Contact angle measurements

4.6.1 Theory

The contact angle is a measure of the surface state, that is the hydrophilicity or hydrophobicity, of a solid sample. A hydrogen terminated diamond surface may be expected to be more hydrophobic, and an oxygen terminated surface more hydrophilic. Contact angle measurements were therefore used as a quick feedback method to evaluate the hydrogenation and oxygenation techniques used later in this work to modify the diamond surface. The two most widely used techniques to measure contact angles are the tensiometric method [23] and the drop method [21].

In a tensiometric method, the sample is suspended from an electrobalance and is slowly immersed into a liquid, for example water. The advancing angle is measured when the

sample is immersed into the aqueous solution and the receding angle is measured when the sample is extracted out of solution.

The drop method involves generating a droplet of water on the tip of a syringe and then applying the water droplet to the surface of the sample. If the drop completely wets the sample surface, the sample is said to be hydrophilic. If the droplet does not wet the surface, the sample is hydrophobic. To determine the hydrophobicity or hydrophilicity of the boron-doped CVD samples, the drop method was employed. It should be noted that the drop method is not a very accurate method and will only give an indication of the surface state of a sample by means of the contact angle measurement.

Figure 4.17 shows a schematic diagram of a droplet of water on the surface of a substrate. A low contact angle (θ) value implies a hydrophilic surface, whereas a high contact angle value implies a hydrophobic surface.

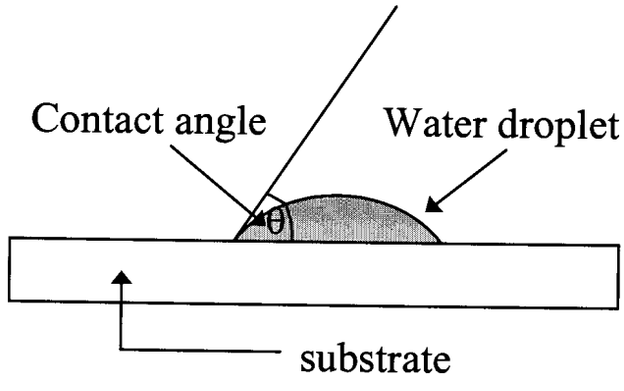

Figure 4.17 : Schematic diagram of a droplet of water on the surface of a substrate

4.6.2 Experimental and discussion

A Wild microscope (M420), prism and digital camera were used to measure the contact angles of the boron-doped CVD samples. A droplet of water was placed on the surface of the sample and, using a microscope, prism and a digital camera, an image representing the sideview of the sample was captured (**Figure 4.18**). Using a protractor, the contact angle for each sample was measured. A total of twenty measurements were taken for each sample and the average and standard deviation were calculated.

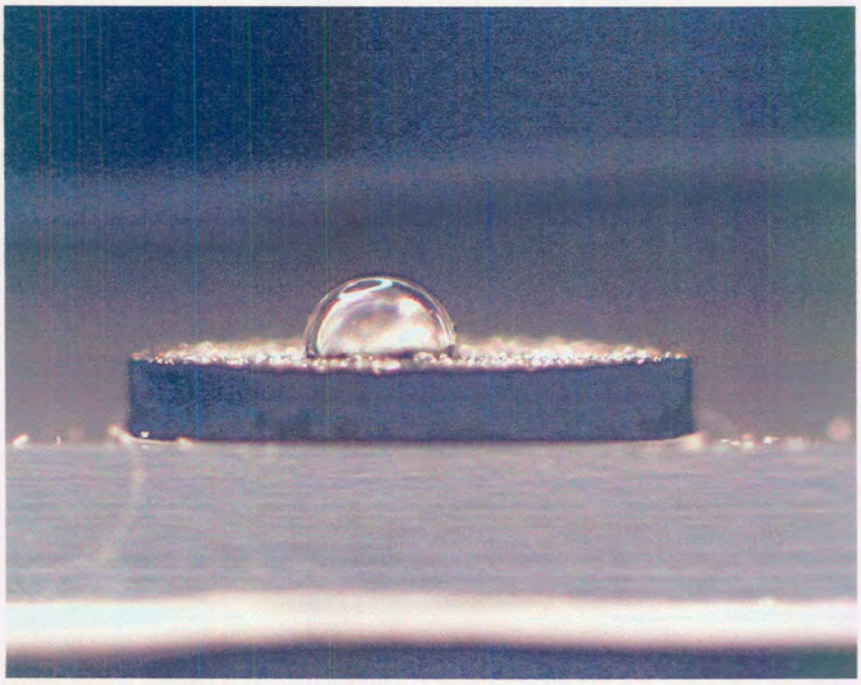

Figure 4.18 : Image of CVDBD2 containing a droplet of water

The results for the contact angle measurements are given in **Table 4.6**. The standard deviation for the respective measurements is quite high. Nevertheless, the differences

between the contact angles were sufficient to reveal a trend. It is evident from the contact angle measurements that CVDBD1 and CVDBD2 are hydrophobic, whilst CVDBD3 and CVDBD4 are partially hydrophobic. CVDBD5 and CVDBD6 tend to be more hydrophilic than the rest of the samples. It appears therefore that an increase in boron dopant level is accompanied by an increase in hydrophilicity, which indicates an increased presence of surface oxygen functionalities.

Table 4.6 : Contact angle measurements

CVD sample	Contact angle		
	Range / °	Average/ °	Std Deviation
CVDBD1 (undoped)	87 - 92	89.60	2.43
CVDBD2 (84 mg/L boron)	87 – 92	89.50	2.28
CVDBD3 (313 mg/L boron)	71 – 85	77.80	6.90
CVDBD4 (543 mg/L boron)	72 – 88	79.95	8.36
CVDBD5 (1032 mg/L boron)	54 – 67	60.50	6.15
CVDBD6 (1521 mg/L boron)	57 – 68	62.20	5.53

4.7 Resistance measurements

4.7.1 Experimental and discussion

In electrochemical applications, the electrode material should have a high conductivity (low resistance), in order to facilitate electron transport and to minimise the potential drop through the electrochemical cell. The total resistance (bulk and surface resistances) of the various boron-doped diamond samples was measured using a voltmeter and two copper electrodes. The copper electrodes were initially cleaned with hydrochloric acid to remove any passivating layer formed on the electrode surface. **Figure 4.19** illustrates the setup for the resistance measurements. The sample was placed between the two copper electrodes and a resistance measurement taken (**Figure 4.20**).

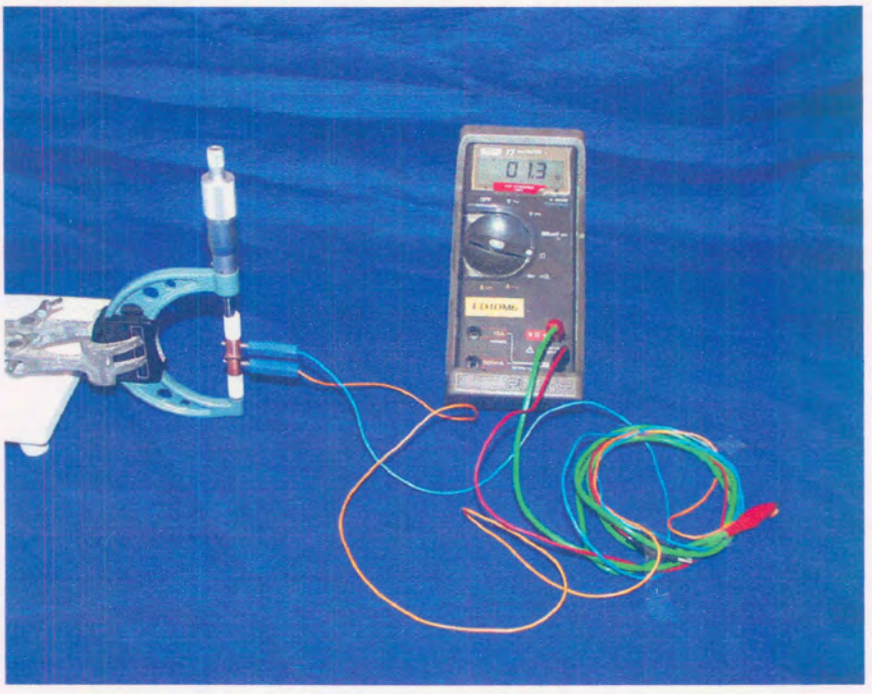

Figure 4.19 : Resistance measurement setup

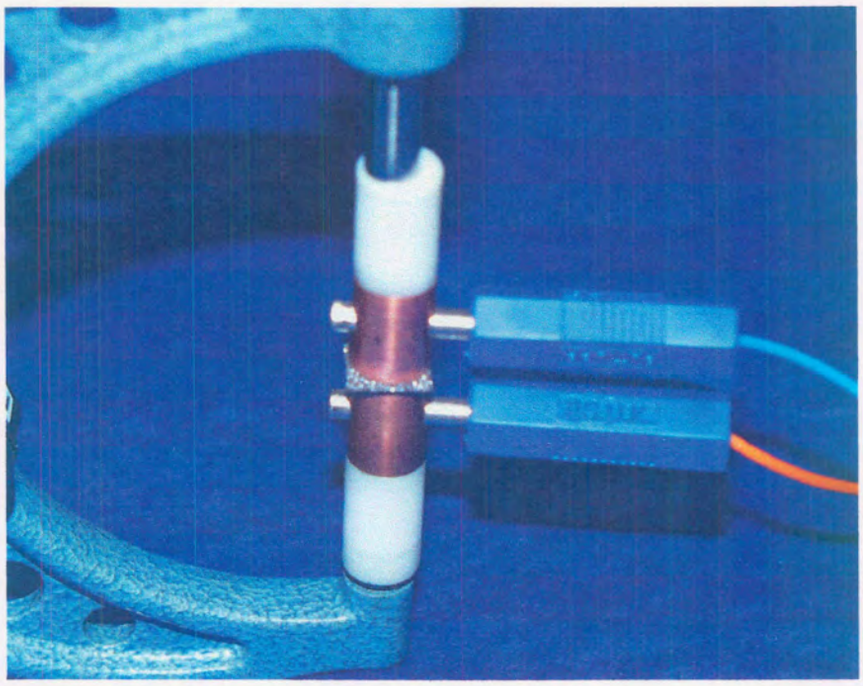

Figure 4.20 : Boron-doped CVD sample between two copper electrodes

Table 4.7 illustrates the resistance measurements of the various samples. CVDBD1 was found to have a resistance reading of mega Ω to overload. The conductivity of CVDBD2 and CVDBD3 seemed to be very low according to the resistance measurements, whilst the conductivity of CVDBD4 – CVDBD6 was found to be fairly high. From these measurements, it may be deduced that since CVDBD4 – CVDBD6 are fairly conductive, the minimum level of boron required to make diamond suitable as an electrode material is approximately 500 mg/L.

Table 4.7 : Resistance measurements of boron-doped CVD samples

CVD sample	Resistance / Ω
CVDBD1 (undoped)	-
CVDBD2 (84 mg/L boron)	1198 – 2183
CVDBD3 (313 mg/L boron)	74.20 – 214.18
CVDBD4 (543 mg/L boron)	1.02 – 1.43
CVDBD5 (1032 mg/L boron)	1.07 – 2.39
CVDBD6 (1521 mg/L boron)	2.29 – 3.77

As the boron concentration of the samples increases, the resistance of the samples should decrease. However, the resistance of CVDBD6 is higher than that of CVDBD4. According to the work carried out by Hansen et. al. [21], the resistance of diamond samples decreases as the hydrophobicity of the sample surfaces increase. Since CVDBD6 was found to be more hydrophilic than CVDBD4 (see **Section 4.6**), this could be a possible explanation of why CVDBD6 has a higher resistance than CVDBD4.

4.8 Conclusion

SEM analysis showed the surface of the boron-doped diamond samples to contain randomly oriented facets, whilst LA-ICP-MS measurements indicated that CVDBD2 contains the lowest boron concentration and CVDBD6 contains the highest boron concentration. According to the Raman spectroscopy analysis, the presence of boron in the sample appears to suppress the formation of sp^2 carbon. However, if the sample is doped with excessive amounts of boron, the amount of sp^2 carbon in the sample increases.

Using XPS, the oxygen content of CVDBD4 was found to be 2.37×10^{15} atoms/cm^2, with a surface oxygen coverage of 1.26 monolayers. The contact angle measurements revealed CVDBD1 and CVDBD2 to be hydrophobic, CVDBD3 and CVDBD4 to be partially hydrophobic and CVDBD5 and CVDBD6 to be more hydrophilic. And finally, the resistance measurements show CVDBD2 and CVDBD3 to have a low conductivity, whilst CVDBD4 – CVDBD6 were found to have a high conductivity. Thus, the minimum level of boron required to make diamond a suitable electrode material was found to be 500 mg/L.

4.9 References

[1] D Chescoe and P J Goodhew, **The Operation of Transmission and Scanning Electron Microscopes,** Oxford University Press (1990) 1.

[2] M C Granger, M Witek, J Xu, J Wang, M Hupert, A Hanks, M D Koppang, J E Butler, G Lucazeau, M Mermoux, J W Strojek and G M Swain, **Anal. Chem., 72** (2000) 3793.

[3] http://minerals.cr.usgs.gov/webdocs/icpms/laser.htm

[4] http://www.gfz-potsdam.de/pb4/pg3/equipment/laicpms.html

[5] H H Willard, L L Merritt, Jr., J A Dean, **Instrumental Methods of Analysis,** 5th Edition, D. Van Nostrand Company, New York, (1974) 189.

[6] S A Solin and A K Ramdas, **Phys. Rev. B 1** (1970) 1687.

[7] J Wagner, M Ramsteiner, C H Wild and P Koidl, **Phys. Rev., B 40** (1989) 1817.

[8] R J Nemanich, J T Glass, G Lucovsky and R E Shroder, **J. Vac. Sci. Technol., A 6** (1988) 1783.

[9] R E Schroder and R J Nemanich, **Phys. Rev., B 41** (1990) 3738.

[10] F Tuinstra and J L Koenig, **J. Chem. Phys., 53** (1970) 1126.

[11] M Yoshikawa, G Katagiri, H Ishida, A Ishitani and T Akamatsu, **Appl. Phys. Lett., 52** (1988) 1639.

[12] M Yoshikawa, N Nagai, M Matsuki, H Fukuda, G Katagiri, H Ishida and A Ishitani, **Phys. Rev., B 46** (1992) 7169.

[13] http://www-personal.umich.edu/~jshaver/virtual/explain.html

[14] P Bou and L Vandenbulcke, **J. Electrochem. Soc., 138** (1991) 2991.

[15] S R Sails, D J Gardiner, M Bowden, J Savage and D Rodway, **Diamond Relat. Mater., 5** (1996) 589.

[16] M C Polo, J Cifre and J Esteve, **Vacuum, 45** (1994) 1013.

[17] http://www.uksaf.org/tech/xps.html

[18] J M Walls, **Methods of surface analysis**, Cambridge University Press, Great Britian (1989).

[19] http://www.chem.qmw.ac.uk/surfaces/scc/scat5_3.htm

[20] http://www.chem.vt.edu/chem-ed/spec/material/xps.html

[21] J O Hansen, **Wetting of the Diamond Surface,** PhD Thesis, (1987).

[22] S Evans and C E Riley, **J. Chem. Soc., Faraday Trans. 2, 82** (1986) 541.

[23] J O Hansen, R G Copperthwaite, T E Derry and J M Pratt, **Journal of Colloid and Interface Science, 130** (1989) 347.

CHAPTER 5

Hydrogenation and oxygenation techniques

5.1 Introduction

The surface chemistry of boron-doped CVD diamond is deemed extremely important as far as the electrochemical behaviour of boron-doped diamond electrodes is concerned, i.e. the electrochemical response of the diamond electrode to several redox systems depends on the chemical surface state of the electrode. The chemical state of the boron-doped diamond electrode can be modified using hydrogenation and oxygenation techniques. Hydrogenation of the surface results in the surface becoming more hydrophobic due to the increased presence of hydrogen atoms (accompanied by an increase in the contact angle), whilst oxygenation of the surface results in the surface becoming more hydrophilic due to the increased presence of oxygen atoms (accompanied by a decrease in the contact angle).

5.1.1 Hydrogen treatment

According to the work carried out by Matsumoto et. al. [1], the most rapid thermal desorption of CO and CO_2 from diamond powders occurs at approximately 500°C. In addition, Hansen et. al. [2] suggests that the hydrogenation process, if carried out above

500°C, requires the desorption of a carbonyl group from the diamond surface, exposing a reactive surface carbon atom for hydrogenation, rather than the splitting of a C-O bond.

According to subsequent work carried out by Tapraeva et. al. [3], it was found that hydrogen treating a diamond sample at 20 – 300°C produced a layer of adsorbed hydrogen on the diamond surface. At 600 – 900°C, the hydrogen is chemically bound to the surface, and between 300 – 600°C, both forms of the hydrogen may be present. It is further stated that hydrogen can adsorb onto the diamond surface or chemically react with the oxygen-containing groups on the surface, leading to partial reduction (**Figure 5.1**) or replacement by hydrogen groups (**Figure 5.2**).

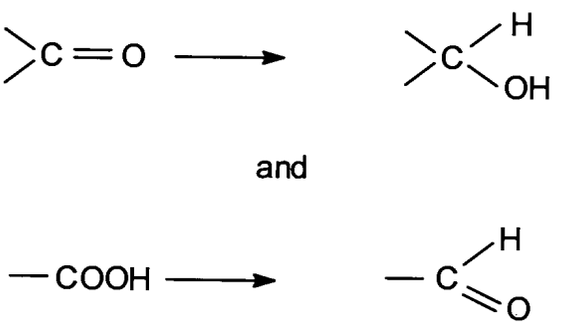

Figure 5.1 : Partial reduction of oxygen group

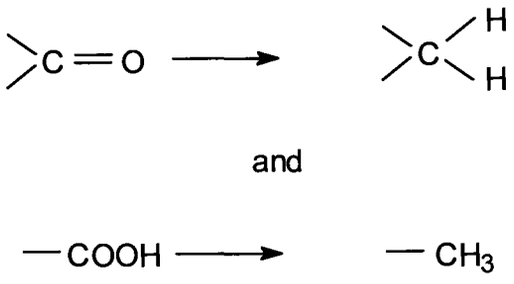

Figure 5.2 : Replacement by hydrogen groups

Examples of techniques for hydrogenation are :

(a) Heat treatment of the diamond samples in a tube furnace or a thermogravimetric analyser at 700°C under a flowing gas stream of either 10% hydrogen in argon or 99% hydrogen

(b) Hydrogen plasma treatment of the diamond sample

5.1.2 Oxygen treatment

Oxygen functional groups are always present on the surface of solids under normal conditions mostly due to exposure to air. These oxygen functional groups are chemisorbed on the carbon atoms, and are held very strongly by covalent bonds. As a result, a pure carbon surface can only be obtained and preserved for some time in an ultrahigh vacuum.

Various techniques exist for the attachment of oxygen functional groups onto a diamond surface. These are :

(a) Heat treatment of the diamond samples in a tube furnace or a thermogravimetric analyser between 260°C – 700°C in air or under a flowing gas stream of pure (99%) oxygen

(b) Heat treatment of the diamond samples in chromic acid, hydrogen peroxide or a mixture of sulphuric acid and potassium nitrate

(c) Anodisation of the diamond sample in a strong base, for example aqueous potassium hydroxide (KOH)

5.2 Hydrogenation techniques : experimental and discussion

5.2.1 Tube furnace treatment

A boron-doped CVD sample (CVDBD6(1)) was heat treated at 700°C in a tube furnace **(Figure 5.3)** under a flowing gas stream of 10% hydrogen in argon, for one hour. The contact angle of the sample was then measured **(Table 5.1)** and compared with the contact angle measured before furnace treatment. From a total of twenty contact angle measurements per sample, the average (Avg) and standard deviation (Std) were calculated. The decrease in the contact angle indicated that, in this experiment, the sample was in fact oxygenated instead of hydrogenated. This result may be ascribed to the presence of oxygen in the tube furnace during the reaction, either as an impurity in the feed gas, or due to insufficient sealing of the system. To prevent oxygen from the feed gas entering the system, an oxygen trap may be inserted in the gas line between the gas cylinder and the flow meter.

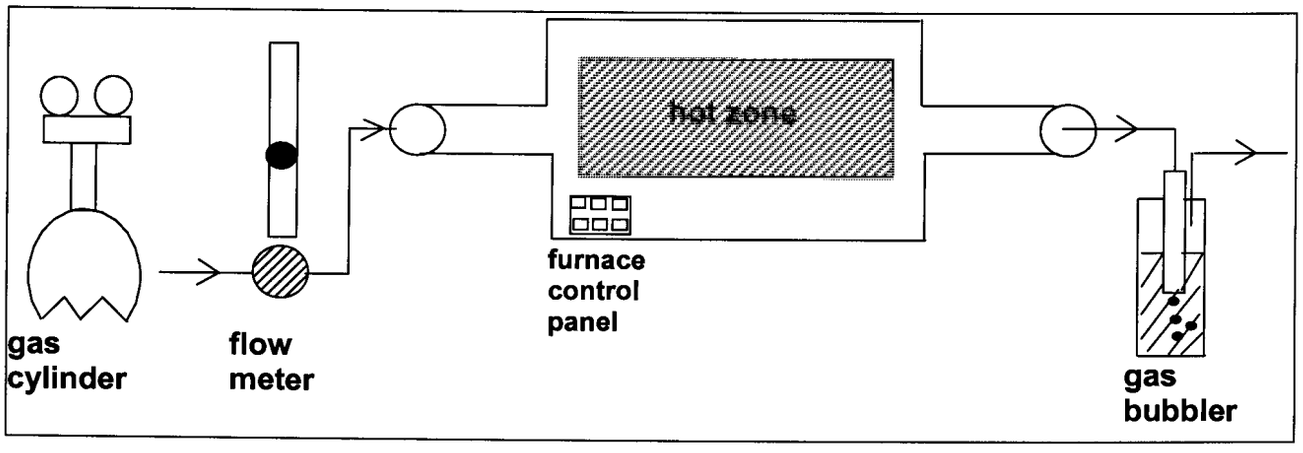

Figure 5.3 : Experimental tube furnace setup

To ensure that the surface of the sample is completely hydrogenated, 99% hydrogen can be used as the source gas. This system, however, becomes highly explosive if the system components and gas lines are not adequately sealed to prevent the escape of hydrogen into the atmosphere. To enable the safe running of the system, a hydrogen igniter may be installed at the end of the exhaust line.

Table 5.1 : Contact angle measurements : Hydrogenation

Diamond sample	Before hydrogenation	Hydrogenation technique		
		Tube furnace	TGA	Hydrogen plasma
CVDBD6(1)	Range : 57°-68° Avg : 62.2° Std : 5.53°	Range : 22°-35° Avg : 29.95° Std : 6.86°	-	-

CVDBD4(2)	Range : 66°-80° Avg : 73.1° Std : 6.96°	-	Range : 80°-91° Avg : 85.25° Std : 4.13°	-
CVDBD4	Range : 72°-88° Avg : 79.95° Std : 8.36°	-	-	Range : 88°-91° Avg : 89.78° Std : 1.22°

Avg : Average

Std : Standard deviation

5.2.2 Thermogravimetric analyser (TGA) treatment

The TGA apparatus is normally used to measure the mass change of a sample as a function of time. It consists of a six decimal place electronic balance with a weighing pan suspended in a small furnace. Some of the uses of a TGA include burn-off of organic matter, moisture determination and the oxidation and reduction temperature measurements of solid materials.

Since the furnace and sample chamber of the TGA are enclosed in a flowing gas stream, the problem of oxygen contamination from the surrounding atmosphere is eliminated. This makes the TGA more effective than the tube furnace for the hydrogenation of small samples.

A boron-doped CVD sample (CVDBD4(2)) was weighed into a platinum pan and the pan inserted into the TGA. The temperature was then ramped up to 700°C at 50°C/min and held there for two hours, under a flowing stream of 10% hydrogen in argon. The contact angle measurement of the sample after treatment is given in **Table 5.1**. This result confirmed that the TGA treatment is an effective method to obtain a hydrogenated surface.

5.2.3 Hydrogen plasma treatment

A standard microwave was converted into a hydrogen plasma treatment apparatus (**Figure 5.4**). A glass tube, which contained the sample, a thermocouple and a heating element was inserted into the centre of the microwave. Pure hydrogen (99%) was then introduced into the system. The microwaves that were generated by the microwave oven converted the hydrogen gas into hydrogen plasma. A mesh surrounding the tube helped prevent the escape of microwaves into the surrounding area and the cooling water helped absorb excess microwave radiation. For the microwave plasma treatment, the temperature was increased to 580°C at a pressure of 350 mTorr. The duration of the reaction was 30 minutes. The contact angle measurement after treatment **(Table 5.1)** suggests the hydrogen plasma treatment to be a very effective method for surface hydrogenation.

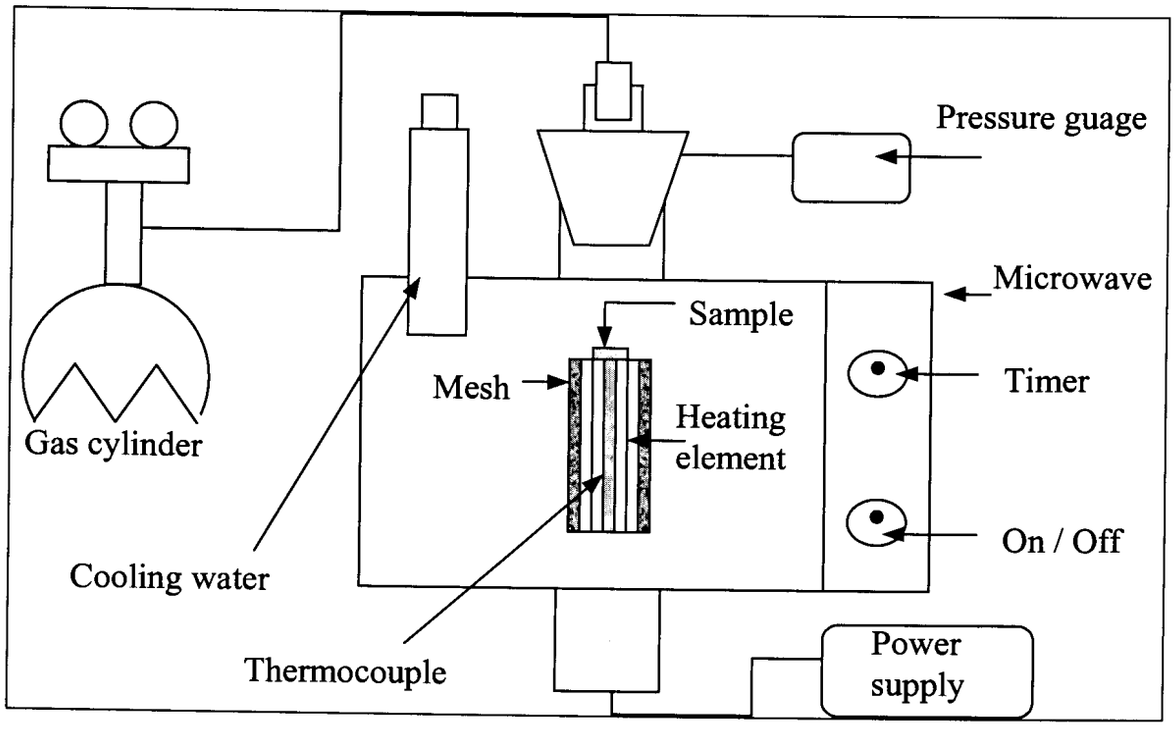

Figure 5.4 : Experimental setup of a microwave plasma apparatus

5.3 Oxygenation techniques : experimental and discussion

5.3.1 Chromic acid treatment

Chromic acid solution was prepared by the addition of 1 g of analytical grade potassium dichromate (obtained from Saarchem) to 20 ml of fuming sulphuric acid. CVDBD3 was then boiled in this solution for 30 minutes. Afterwards, contact angle measurements were taken **(Table 5.2)**, and the measurement showed that chromic acid treatment is very effective for obtaining hydrophilic diamond surfaces.

Table 5.2 : Contact angle measurements : Oxygenation

Diamond sample	Before oxygenation	After oxygenation	
		Chromic acid treatment	TGA
CVDBD3	Range : 71°-85° Avg : 77.80° Std : 6.90°	0°	-
CVDBD6(2)	Range : 57°-68° Avg : 62.20° Std : 5.53°	-	0°

However, it has one major drawback : during the acid treatment, chromium species are deposited onto the surface of the CVD sample, and this contamination subsequently occurs as a redox couple in the cyclic voltammogram of the CVD sample (see **Chapter 8**). The chromium species are removed on boiling the sample in hydrochloric acid for 10 minutes.

5.3.2 Anodisation treatment

The CVD sample (CVDBD4) which was obtained as a plate (length = 1 cm, width = 1 cm and thickness = 0.07 cm) from De Beers was laser cut (**Figure 5.5**) into smaller

circular discs to be used as working electrodes. The schematic construction of the diamond electrode is shown in **Figure 5.6**.

The electrode holder, which consisted of Teflon, was designed and manufactured for the easy insertion of a graphite insert. The laser cut diamond sample was subsequently glued onto the graphite insert using carbon paste. Electrical contact was made by the attachment of silver wire to the graphite insert via a screw thread. The assembled diamond electrode is shown in **Figure 5.7**.

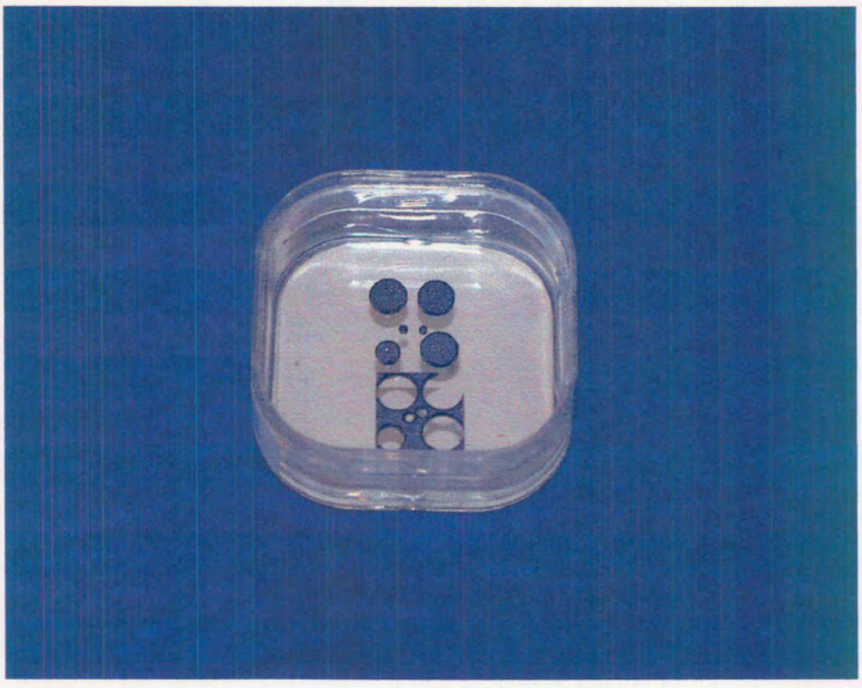

Figure 5.5 : Laser cut CVD sample

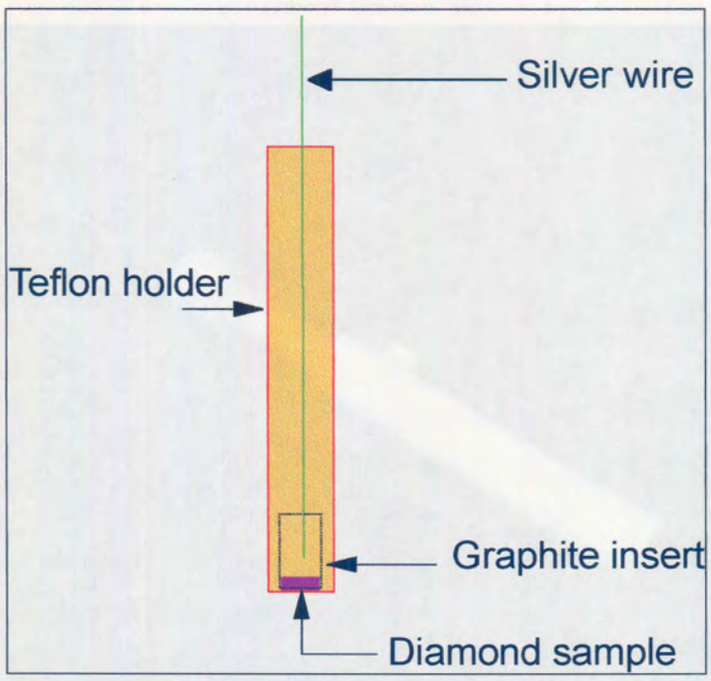

Figure 5.6 : Schematic construction of the diamond electrode

The diamond working electrode was then inserted into a three electrode electrochemical cell, containing 0.1 mol/L potassium hydroxide (KOH) (obtained from SMM Chemicals) solution. This cell was connected to an AutoLab PGStat 100 potentiostat. A constant potential of 2.7 V versus Ag/AgCl reference electrode was then applied to the boron-doped diamond electrode (BDD) for a period of 90 minutes. KOH was chosen for the anodisation reaction since it is a strong base.

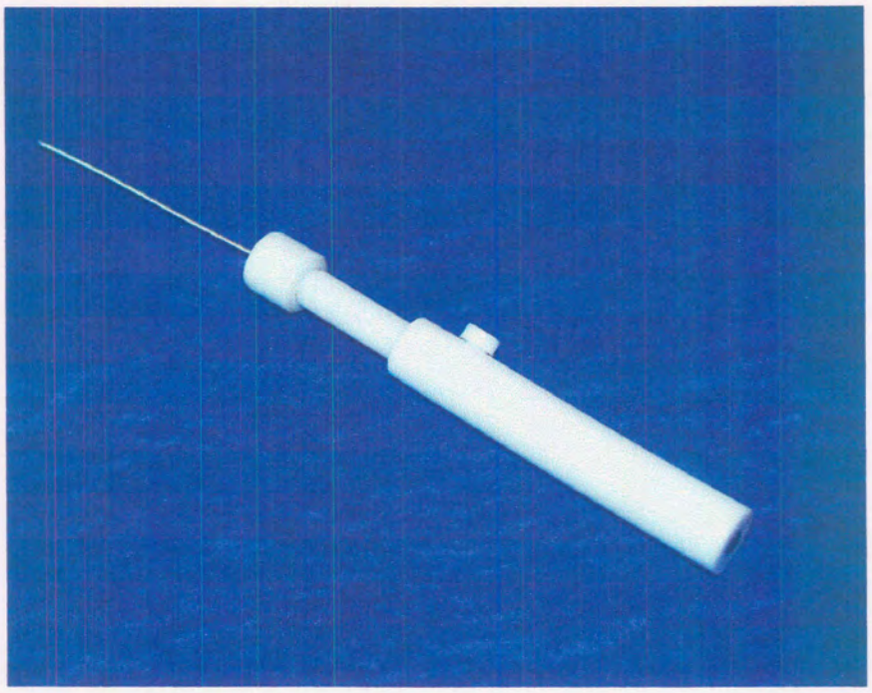

Figure 5.7 : Assembled diamond electrode

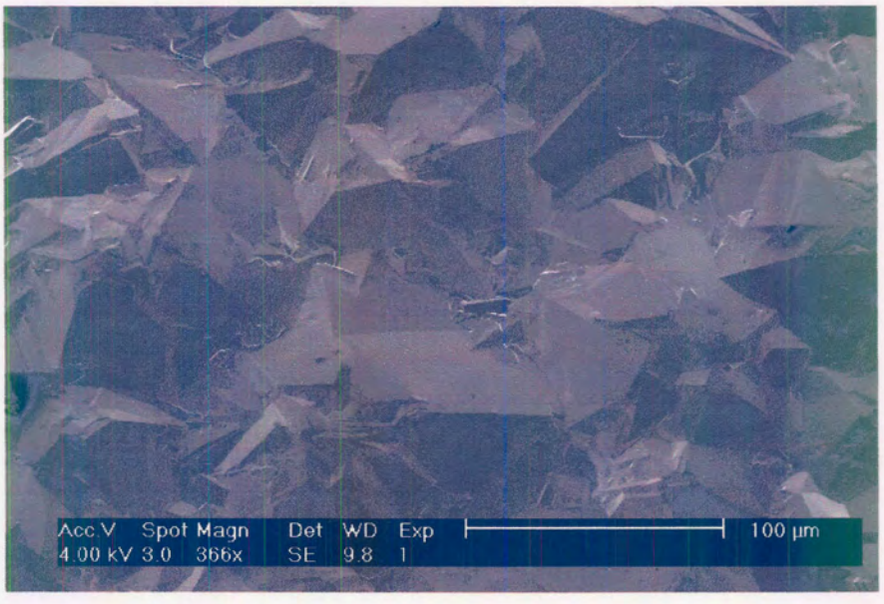

Figure 5.8 : SEM image of the as-received CVDBD4(2) sample

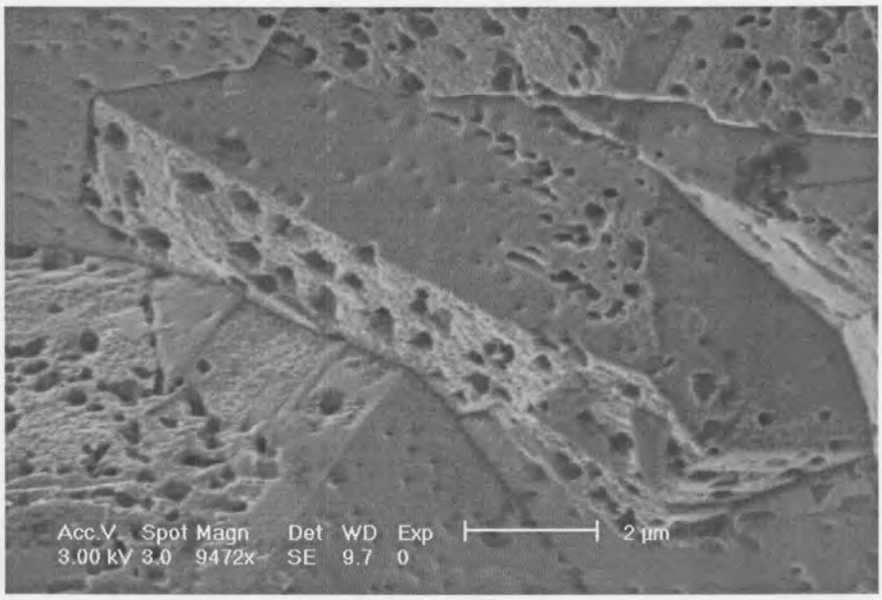

Figure 5.9 : SEM image of CVDBD4(2) after anodisation treatment

The SEM images of the CVD sample before and after treatment are shown in **Figure 5.8** and **Figure 5.9** respectively. Etch pits are apparent on the SEM image of the CVD sample after treatment. The oxygen content of the sample was subsequently analysed using XPS. **Figure 5.10** represents the XPS spectrum for the sample. A slight shift in the peak positions is observed in the treated sample as compared to the as-received sample (**Figure 4.16**). This could be attributed to the newly formed surface oxygen functionalities on the diamond surface.

The oxygen content as well as the oxygen coverage of the electrochemically treated sample and the as-received sample are shown in **Table 5.3**. It can be inferred from **Table 5.3** that a significant amount of oxygen atoms are either chemically or physically bound to the surface of the boron-doped CVD sample. The presence of these oxygen atoms renders the surface of the sample hydrophilic.

UNIVERSITEIT VAN PRETORIA
UNIVERSITY OF PRETORIA
YUNIBESITHI YA PRETORIA

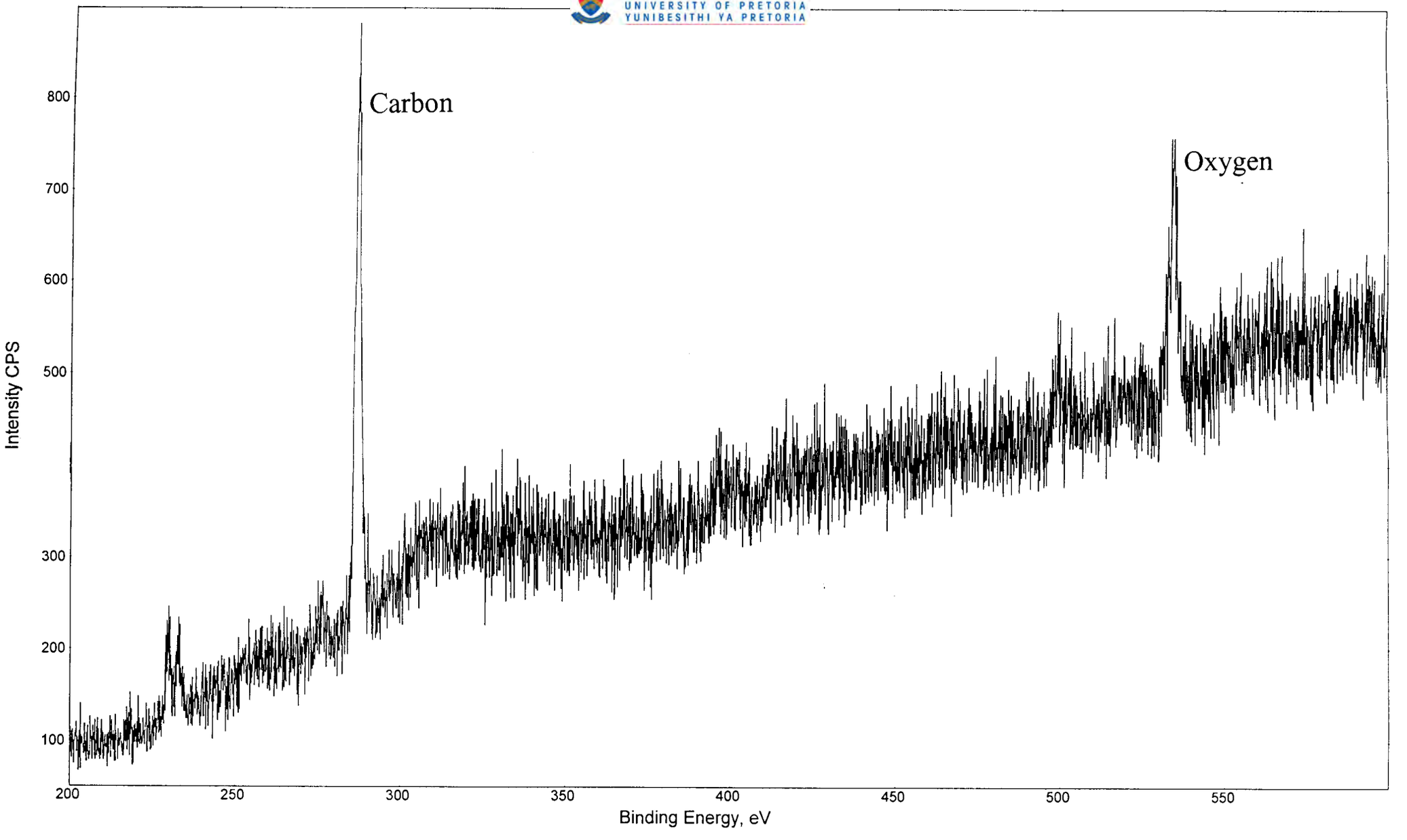

Figure 5.10 : XPS spectrum for CVDBD4(2) after anodisation

Table 5.3 : Oxygen content of boron-doped CVD samples

Diamond sample	Oxygen content / atoms.cm^{-2}	Surface oxygen coverage
CVDBD4(2) (as-received)	2.37 x 10^{15}	1.26 monolayers
CVDBD4(2) (anodised)	3.31 x 10^{15}	1.80 monolayers

5.3.3 Thermogravimetric analyser treatment

One of the undesirable characteristics of diamond is its susceptibilty to oxidation when heated. The onset of oxidation can occur at temperatures as low as 260°C [4]. Simons and Cannon [5] have reported that boron-doped diamond produced by the high pressure, high temperature (HPHT) process oxidised at 1/70 the rate of undoped HPHT diamond and at 1/100 the rate of a natural diamond. Further investigation of undoped CVD diamond [6-9] and boron-doped CVD diamond [10] confirmed that the boron-doping of CVD diamond decreases the oxidation rate of diamond.

In order to assess whether the boron-doping of De Beers CVD diamond decreases its oxidation rate, the work carried out by Farabaugh et. al. was repeated [10]. Two boron-doped CVD samples (CVDBD6 and CVDBD1, approximately 2 mg each) were weighed into a platinum pan and the pan inserted into the TGA. The temperature of the TGA was

programmed to increase from room temperature to 680°C at a rate of 50°C/min, and the temperature was then increased to 700°C at a rate of 20°C/min. The temperature was held at 700°C for five hours while high purity oxygen (99%) flowed through the sample chamber.

Figure 5.11 illustrates the TGA graph for the undoped (CVDBD1) and highest boron-doped (CVDBD6) samples. It is apparent from the two graphs that the total weight loss of the undoped sample is greater than that of the highest boron-doped sample. This observation confirms that boron-doping of CVD diamond decreases the oxidation rate of the diamond.

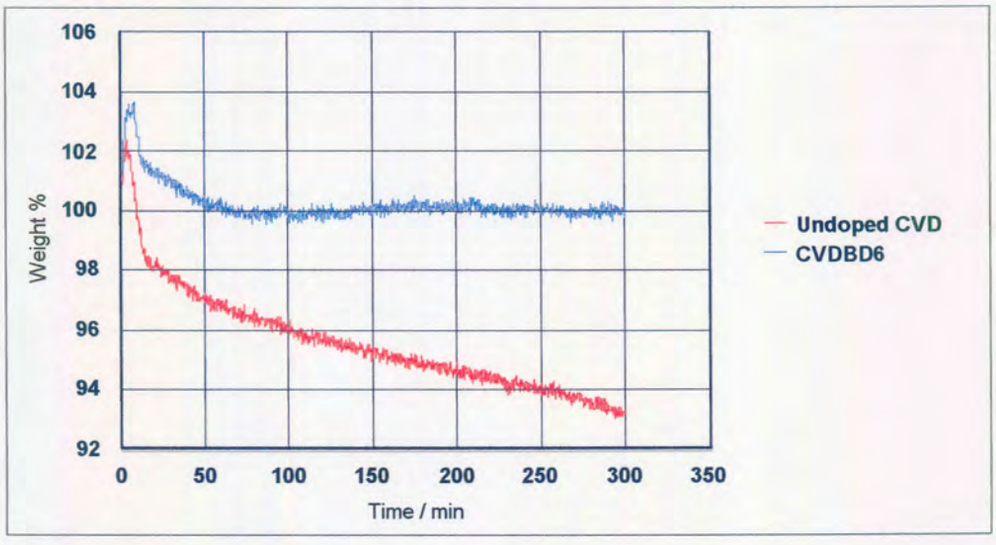

Figure 5.11 : TGA graph for the undoped and highest boron-doped sample (CVDBD6)

Farabaugh et. al. [10] further analysed the boron-doped CVD diamond residue from the TGA using Auger spectroscopy. They found an increase in the amount of oxygen and

boron on the CVD diamond surface. Furthermore, the boron peak shape very closely resembled the published boron peak shape in the Auger spectrum of boron oxide, indicating that during the oxidation of boron-doped CVD diamond, boron oxide is most likely formed on the diamond surface.

Assimilating the results as well as the suggestions reported in literature [1,3,6-9] and the results obtained in the current experiment, the following model for the oxidation of boron-doped CVD diamond may be proposed : when heating boron-doped CVD diamond in air, desorption of CO and CO_2 from the diamond surface begins at approximately 500°C. Oxygen atoms are initially chemisorbed onto the surface of the diamond, which contains tetrahedrally bonded carbon atoms and either a homogeneous or heterogeneous distribution of boron atoms. These oxygen atoms can then bind to the carbon atoms present to form oxygen functionalities on the surface of the diamond.

As the temperature increases to greater than 500°C, desorption of CO and CO_2 from the diamond surface occurs and an increase in the mass loss of the sample is observed **(Figure 5.11)**. As the carbon atoms together with the oxygen atoms begin to gasify and leave the surface, boron atoms become concentrated on the diamond surface. The boron atoms can then react with the incoming oxygen atoms to form boron oxide.

Literature suggests [10] that boron oxide forms a passivating layer on the diamond surface. This layer may inhibit the further reaction of oxygen atoms with carbon atoms to form CO and CO_2. The net result is a decrease in the mass loss of the sample as seen in

Figure 5.11. Further work needs to be done in order to verify the presence of boron oxide on the diamond surface after oxidation, using techniques such as Auger spectroscopy and X-ray diffraction. Whilst the presence of a passivating layer of boron oxide may be useful in reducing the rate of oxidation of the surface of boron-doped CVD diamond, this layer tends to decrease the conductivity of the sample. This may result in a poor electrochemical signal being observed.

5.4 Conclusion

The surface state of the CVD diamond electrode (i.e. whether it is hydrophilic or hydrophobic) affects the electrochemical behaviour of the electrode in various redox systems (see **Chapter 6** and **Chapter 7**). The most effective hydrogenation technique was found to be the hydrogen plasma treatment. The oxygenation of the diamond surface can easily be accomplished using the tube furnace, TGA, chromic acid and anodisation techniques.

Under a harsh oxygenation environment, for example temperatures greater than 700°C, etching, graphitisation as well as the formation of a boron oxide layer on the diamond surface may occur. This will drastically affect the observed electrochemical signal. The ideal oxygenation method for boron-doped CVD diamonds to be used as an electrode material would be one that yields oxygen functionalities on the surface of the electrode without the formation of a boron oxide passivating layer. A suitable oxygenation method could be to heat treat the CVD diamond in a tube furnace or TGA at temperatures below

250°C for a short period of time to minimise the formation of boron oxide. Alternatively, the CVD diamond can be mildly treated in hydrogen peroxide (H_2O_2).

5.5 References

[1] S Matsumoto, H Kanda, Y Sato and N Setako, **Carbon, 15** (1977) 299.

[2] J O Hansen, R G Copperthwaite, T E Derry and J M Pratt, **Journal of Colloid and Interface Science, 130** (1989) 347.

[3] F M Tapraeva, A N Pushkin, N I Epishina, I I Kulakova and A P Rudenko, **Russian Journal of Physical Chemistry, 60** (1986) 1092.

[4] H P Boehm, **Adv. Catalysis, 16** (1966) 219.

[5] E L Simons and P Cannon, **Nature (London), 210** (1996) 90.

[6] C E Johnson, M A S Hasting and W A Weimer, **J. Mater. Res., 5** (1990) 2320.

[7] M Alam and Q Sun, **J. Mater. Res., 8** (1993) 2870.

[8] A Joshi, R Nimmagadda and J Herrington, **J. Vac. Sci. Technol., A 8** (1990) 2137.

[9] K Tankala, T DebRoy and M Alam, **J. Mater. Res., 5** (1990) 2483.

[10] E N Farabaugh, L Robins and A Feldman, **J. Mater. Res., 10** (1995) 1448.

CHAPTER 6

Electroanalysis of inorganic redox systems – potassium iron (III) cyanide and cerium (III) sulphate

6.1 Introduction

Boron-doped diamond electrodes, according to literature [1,2], have several advantages over the conventional glassy carbon electrode :

- Wide potential window of water stability
- Low background current (low baseline current)
- Chemical and structural stability
- Resistance to fouling

Voltammetry studies were undertaken to investigate the advantages of diamond electrodes over glassy carbon electrodes and to compare the electrochemical behaviour of the De Beers diamond electrodes with that of other diamond electrodes reported in literature.

In voltammetric techniques, an electrical potential gradient is applied across an electrode-solution interface to oxidise or reduce species present in solution [3]. The potential of the working electrode is measured relative to the reference electrode, for example a Ag/AgCl

electrode. The current passed through the system is measured between the working electrode and a counter electrode, for example a platinum mesh electrode. The counter electrode is essential since current flow through a reference interface might perturb the reference potential. A total of three electrodes are therefore generally used: a working electrode at which the redox reaction of interest takes place, a reference electrode where no current flows, and the counter electrode at which the current is measured.

After a voltammetric analysis, a voltammogram (a current versus potential plot), is produced. A voltammogram reflects the chemical identity of the redox species (as indicated by its oxidation or reduction potential) and its concentration (by the magnitude of the current at a given potential). The current versus potential plot has three basic features that have useful thermodynamic, kinetic, and analytical information: the size of the current, the peak shape, and its position on the applied potential axis.

The voltammetric study entailed the use of three techniques: cyclic voltammetry, linear sweep voltammetry and chronoamperometry. Cyclic voltammetry is a popular technique that is particularly powerful for initial studies of a new system. Essentially, the potential applied to the working electrode is swept through the potential range where an electrochemical reaction occurs. The direction of the scan is then reversed in order to determine whether the product of electron transfer is stable or whether the reaction intermediates or the final product are electroactive [4]. Linear sweep voltammetry is similar to cyclic voltammetry except that the direction of scan is not reversed, i.e. the voltammetric scan is restricted to one direction only.

Chronoamperometry is a potential step experiment where the current versus time response is recorded. The potential of the electrode is changed almost instantaneously from a value where no current passes (i.e. no chemical reaction occurs at the electrode surface) to one where the electrode reaction of interest takes place [4]. This gives rise to a diffusion limited current whose value varies with time. The current-time relationship is described by the Cottrell equation [5].

In this study, diamond electrodes containing varying amounts of boron were characterised by observing the effect of boron concentration on the potential window in an aqueous solution, and on the size of the baseline current. The effect of the surface area of the diamond electrode in an ascorbic acid (AA) system was also investigated. The potassium iron (III) cyanide and cerium (III) sulphate redox systems were used to compare the electrochemical behaviour of boron-doped diamond electrodes with that of the glassy carbon electrode.

6.2 Experimental

An AutoLab PGStat 100 (**Figure 6.1**), connected to a computer with the GPES AutoLab software, was used for the voltammetric measurements. All measurements were carried out in a three-electrode electrochemical cell (**Figure 6.2**). The cell comprised a platinum mesh counter electrode, a boron-doped diamond working electrode (refer to **Section 5.3.2** for the construction of the diamond electrode) and a Ag/AgCl reference electrode with a Luggin capillary.

All electrochemical measurements were carried out at room temperature (25°C) in a stationary analyte solution. All solutions were deaerated using nitrogen prior to any electrochemical measurement. The chemicals used were analytical grade quality. Potassium iron (III) cyanide ($K_3[Fe(CN)_6]$), potassium nitrate (KNO_3) and sodium sulphate (Na_2SO_4) were obtained from Merck, cerium (III) sulphate ($Ce_2(SO_4)_3$) and the phosphate buffer were obtained from Sigma Aldrich and the sulphuric acid (H_2SO_4) was obtained from Saarchem.

The supporting electrolytes (KNO_3, H_2SO_4 and Na_2SO_4) and the phosphate buffer were made up to the desired concentration using ultrapure water from a Millipore purification system, having a conductivity of 18 μΩ.cm. The $K_3[Fe(CN)_6]$ and the $Ce_2(SO_4)_3$ stock solutions were made up to the predetermined concentrations using the supporting electrolyte solutions. $Ce_2(SO_4)_3$, however, is known to polymerise in solution on heating. $Ce_2(SO_4)_3$ was therefore slowly added to a stirred solution of H_2SO_4 at a temperature of below 0°C, until the $Ce_2(SO_4)_3$ had completely dissolved.

Figure 6.1 : An AutoLab PGStat 100 connected to a PC carrying the GPES AutoLab software

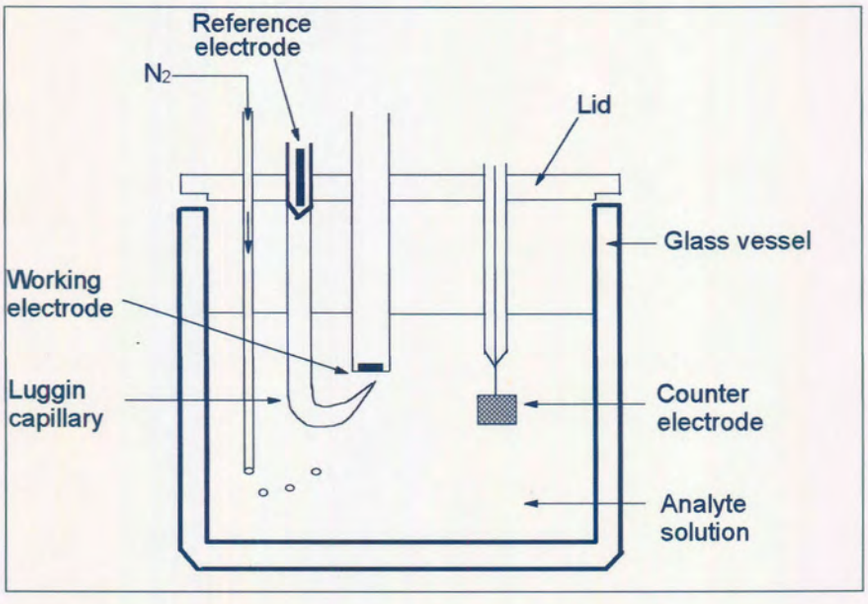

Figure 6.2 : Schematic diagram of a three electrode electrochemical cell

Voltammograms for the inorganic redox systems were then obtained at both glassy carbon and boron-doped diamond (BDD) electrodes. The surface areas of the glassy carbon and BDD electrodes were 0.071 cm^2 and 0.15 cm^2 respectively. The CVDBD4 electrodes having a boron concentration of 543 mg/L were used to investigate the $K_3[Fe(CN)_6]$ and $Ce_2(SO_4)_3$ redox systems.

6.3 Results and discussion

6.3.1 Electrochemical characterisation of diamond electrodes of varying boron concentrations

The boron concentrations for the various samples of the BDD are given in **Table 4.4.** CVDBD6 is the highest boron-doped sample whereas CVDBD2 is the lowest boron-doped sample. **Figure 6.3** represents the electrochemical behaviour of diamond electrodes containing varying amounts of boron in 0.5 mol/L perchloric acid ($HClO_4$).

The observed onset of water electrolysis, i.e. water oxidation and water reduction for the various BDD electrodes as well as the glassy carbon electrode, is found in **Table 6.1**. It appears that, as the boron concentration of the BDD increases, the potential window decreases. The decrease in the potential window of the BDD electrodes is thought to be due to the small increase of sp^2 carbon (graphitic or amorphous carbon) in the BDD electrodes. The observation was made previously in **Table 4.5** that, as the boron concentration of the CVD samples increases, the sp^2/sp^3 ratio of the respective samples also increases. It is clear, however, that the potential window for the highest BDD

electrode is still wider than that of glassy carbon, thereby confirming the advantage that the BDD electrode has over glassy carbon when investigating aqueous systems.

Table 6.1 : Onset of water oxidation and water reduction for the various boron-doped CVD diamond electrodes as well as that of the glassy carbon electrode, in 0.5 mol/L $HClO_4$ solution

CVD sample	Hydrogen evolution / V	Oxygen evolution / V
CVDBD2	-1.34	1.80
CVDBD3	-1.14	1.77
CVDBD5	-1.06	1.77
CVDBD6	-0.95	1.77
Glassy carbon	-0.88	1.65

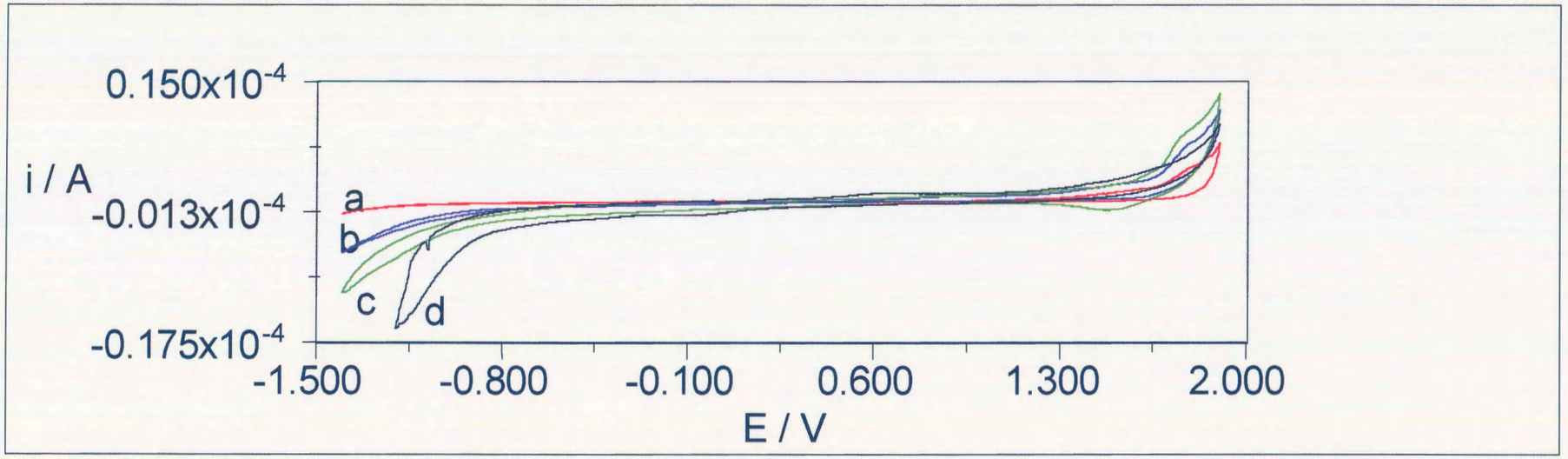

Figure 6.3 : Electrochemical behaviour of diamond electrodes containing varying amounts of boron in 0.5 mol/L $HClO_4$, (a) CVDBD2, (b) CVDBD3, (c) CVDBD5, (d) CVDBD6 – scan rate is 50 mV/s. E_i = -1 V, scan direction = positive.

6.3.2 Surface area effects

Three different diamond electrode projected surface areas were investigated: 0.1590 cm^2, 0.0707 cm^2 and 0.0078 cm^2. The electrochemical behaviour of these diamond electrodes was determined using an ascorbic acid (AA) system. The structure of AA is found in **Figure 6.4**. **Figure 6.5** represents the cyclic voltammograms for 6 mmol/L AA in 0.1 mol/L $HClO_4$ at diamond electrodes having varied surface areas. An anodic peak ascribed to the oxidation of the ascorbic acid molecule is seen at approximately 1.3 V. The magnified electrochemical response of the 0.0078 cm^2 diamond electrode in AA is given in **Figure 6.6**.

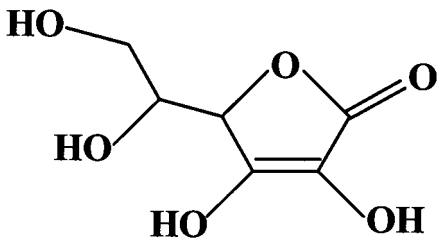

Figure 6.4 : Chemical structure of ascorbic acid [3]

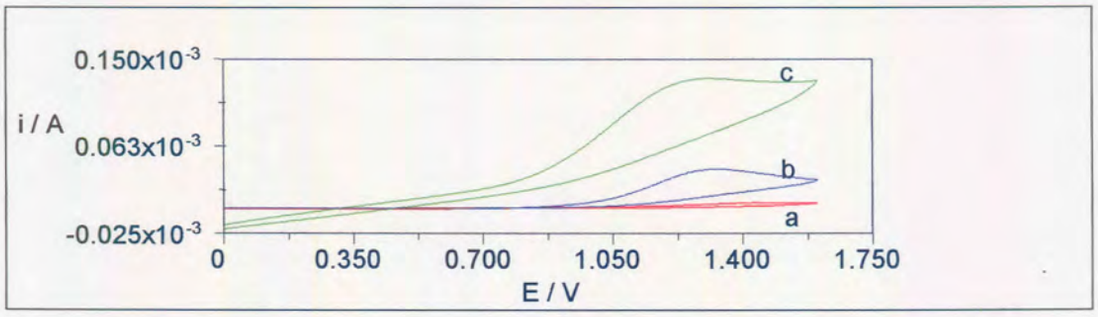

Figure 6.5 : Cyclic voltammograms for 6 mmol/L AA in 0.1 mol/L $HClO_4$ at CVDBD6 diamond electrodes with varying surface areas, (a) 0.0078 cm^2, (b) 0.0707 cm^2, (c) 0.1590 cm^2 - scan rate is 50 mV/s. E_i = 0 V, scan direction = positive.

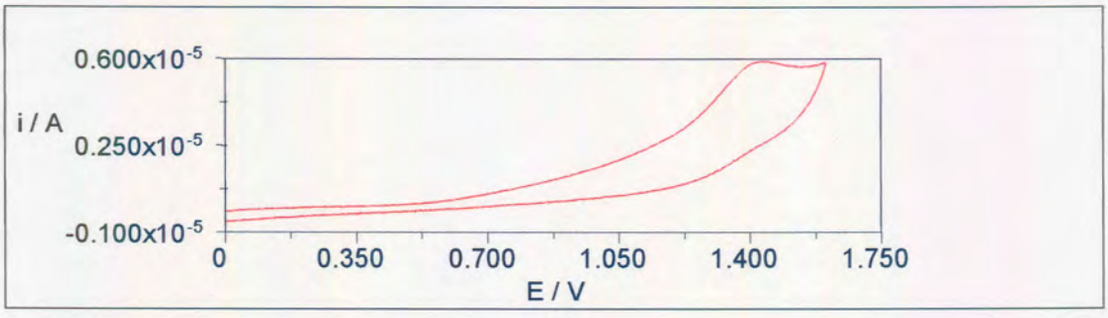

Figure 6.6 : Magnified electrochemical response of the 0.0078 cm^2 diamond electrode in AA. Scan rate is 50 mV/s.

From **Figure 6.5**, it can be seen that the largest diamond electrode surface area yields the greatest oxidation current. The oxidation current values are given in **Table 6.2**. This observation is in agreement with the fact that as the surface area of the electrode material increases, the corresponding electrochemical response also increases. The oxidation current values (**Table 6.2**) do not increase linearly with increasing surface area. This could be due to the difference between the true surface area and the projected surface area, brought about by the rough nature of the electrode surface. Polishing of the

electrode surface could rectify this, however, this would also alter the electrode surface state in terms of chemical functionalities. A method that could be employed to determine the true surface area of the BDD electrode is anodic stripping voltammetry.

Table 6.2 : Oxidation current values for boron-doped diamond (BDD) electrodes of varied surface areas - taken from Figure 6.5

Surface area of CVDBD6 / cm^2	Oxidation current values / μA
0.0078	5.90
0.0707	40
0.1590	132

6.3.3 Potassium iron (III) cyanide

The $[Fe(CN)_6]^{3-}/[Fe(CN)_6]^{4-}$ redox couple has a complex chemistry associated with it. Despite this complexity, the $[Fe(CN)_6]^{3-}/[Fe(CN)_6]^{4-}$ couple has been used to evaluate the performance of diamond electrodes [6-8]. Although it is often presumed that this redox couple undergoes electron transfer via a simple outer-sphere mechanism, there are several pieces of evidence suggesting otherwise:

(a) The electron-transfer rate constant of the $[Fe(CN)_6]^{3-}/[Fe(CN)_6]^{4-}$ system, k^o, has been shown to depend on the nature and concentration of the supporting electrolyte cation [9].

(b) A semipassivating layer of $[Fe(CN)_6]^{3-}/[Fe(CN)_6]^{4-}$ (Prussian blue) can be formed on the electrode surface and this layer serves to decrease the rate of electron transfer [10,11].

(c) Chen and McCreery [12-14] have reported a dependence of k^o on the electrode surface structure. This work indicates that the $[Fe(CN)_6]^{3-}/[Fe(CN)_6]^{4-}$ redox couple reacts on carbon via specific surface interactions through an innersphere pathway.

It has been suggested that boron-doped diamond electrodes are nothing more than an ensemble of non-diamond impurity domains isolated within an inactive diamond matrix. The relative role of the non-diamond carbon in electron transfer reactions at diamond electrode surfaces has also been questioned [15].

The work undertaken by Swain et. al. [16] subsequently entailed a direct comparison of the electrochemical behaviour of a high-quality boron-doped diamond electrode (containing a lower volume fraction of non-diamond carbon impurity) with that of a low-quality electrode (higher volume fraction of non-diamond carbon impurity) in the $[Fe(CN)_6]^{3-}/[Fe(CN)_6]^{4-}$ system.

They found that the high quality electrode was more active for $[Fe(CN)_6]^{3-}/[Fe(CN)_6]^{4-}$ than the low quality electrode. This implies that the electron transfer at diamond does not appear to occur through the non-diamond impurity sites but rather seems to occur through the doped diamond lattice.

Figure 6.7 shows the cyclic voltammetric i-E curve for 20 mmol/L $[Fe(CN)_6]^{3-}$ in 1 mol/L potassium nitrate (KNO_3) and 0.1 mol/L phosphate buffer, pH 6.7, at a BDD electrode (CVDBD4). The i-E curve shows two well-defined waves with a peak separation (ΔE_p) of 690 mV. This peak separation should, in fact, be 59 mV for a reversible one-electron transfer reaction such as the $[Fe(CN)_6]^{3-}/[Fe(CN)_6]^{4-}$ redox reaction. A large peak separation implies a slow electron-transfer reaction occurring at the electrode surface between the analyte and the electrode. This means that the response time for the electrode is slow.

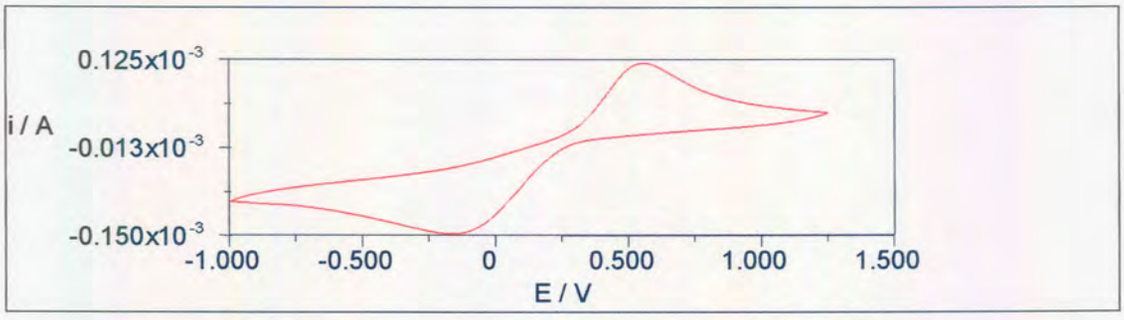

Figure 6.7 : Cyclic voltammetric curve for 20 mmol/L $[Fe(CN)_6]^{3-}$ in 1 mol/L KNO_3 and 0.1 mol/L phosphate buffer, pH 6.7, at a BDD electrode (CVDBD4) - scan rate is 50 mV/s. E_i = 1.25 V, scan direction = negative

Figure 6.8 illustrates the cyclic voltammogram for 20 mmol/L $[Fe(CN)_6]^{3-}$ in 1 mol/L KNO_3 at a BDD electrode as well as at a glassy carbon electrode. The cyclic voltammogram for $[Fe(CN)_6]^{3-}$ at the glassy carbon electrode yielded a ΔE_p of 61 mV which is an order of magnitude lower than that of the diamond electrode.

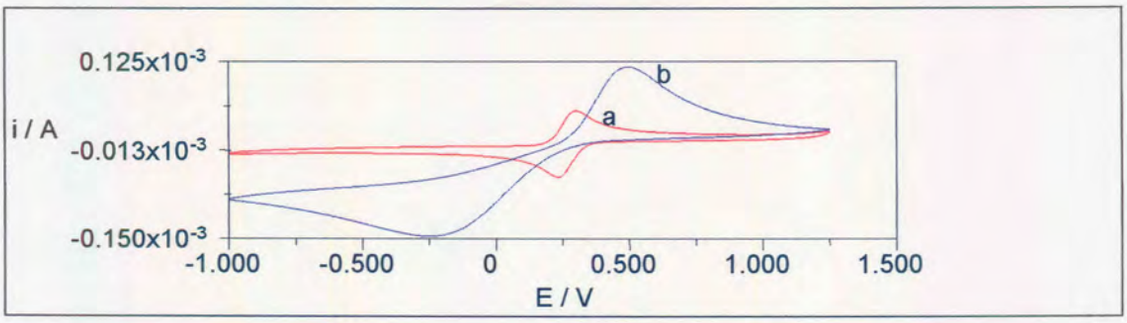

Figure 6.8 : Cyclic voltammograms for 20 mmol/L $[Fe(CN)_6]^{3-}$ in 1 mol/L KNO_3 at a BDD diamond electrode (b) as well as at a glassy carbon electrode (a). Scan rate is 50 mV/s. E_i = 1.25 V, scan direction = negative

The contact angle measurement of the diamond electrode (CVDBD4) used in this experiment was between 72°-88° (refer to **Section 4.6**). The XPS result (refer to **Section 4.5**) for the as-received sample showed the oxygen content to be 2.37 x 10^{15} atoms/cm^2, with an oxygen coverage of 1.26 monolayers. The contact angle measurement together with the XPS analysis implies that the surface of the diamond is partially hydrophobic. This therefore indicates that there are oxygen functionalities present on the diamond surface, i.e. the surface is partially oxygen terminated.

Many authors [17-19] report that the peak separation of the BDD electrode in the $[Fe(CN)_6]^{3-}/[Fe(CN)_6]^{4-}$ system is very sensitive to the surface termination of the electrode. The smallest ΔE_p is observed at the hydrogen terminated surface, whilst the largest ΔE_p is observed at the oxygen terminated surface. Ramesham and Rose [18] reported a ΔE_p of 192 mV in the $[Fe(CN)_6]^{3-}/[Fe(CN)_6]^{4-}$ system at a MA-CVD as-grown diamond electrode, whilst Yagi et. al. [20] reported a ΔE_p of 120 mV at a hydrogen

plasma treated diamond electrode and a ΔE_p of 1072 mV at an oxygen plasma treated electrode.

The evidence above suggests that oxygen termination inhibits $[Fe(CN)_6]^{3-}/[Fe(CN)_6]^{4-}$ electron transfer, because of chemical effects. These chemical influences could involve electrostatic or site-blocking effects. In the light of the above literature findings, the large peak separation of 690 mV observed for the $[Fe(CN)_6]^{3-}/[Fe(CN)_6]^{4-}$ redox couple could be explained as follows :

(a) Carbon-oxygen functionalities (for example carboxyl groups) on the surface of the diamond electrodes can be deprotonated, thereby producing a negative surface charge. This charge could repel the highly charged $[Fe(CN)_6]^{3-}/[Fe(CN)_6]^{4-}$ species and in so doing, reduce the rate of electron transfer. Hence, a large ΔE_p would be observed.

(b) Granger and Swain [17] believe that the hydrogen terminated surface appears to provide a specific site through which the $[Fe(CN)_6]^{3-}/[Fe(CN)_6]^{4-}$ couple can interact, which lowers the activation barrier for electron transfer. These surface interactions seem to be blocked on the oxygen terminated surface. This theory therefore explains the large ΔE_p observed since the surface of CVDBD4 is partially oxygen terminated.

It can therefore be assumed that in order to reduce the ΔE_p, the surface of the diamond electrode will have to be made hydrophobic.

The influence of the supporting electrolyte cation was also investigated. **Figure 6.9** represents the cyclic voltammogram for 20 mmol/L $K_3[Fe(CN)_6]$ in 1 mol/L KNO_3 and 0.1 mol/L sodium sulphate (Na_2SO_4) at a BDD electrode.

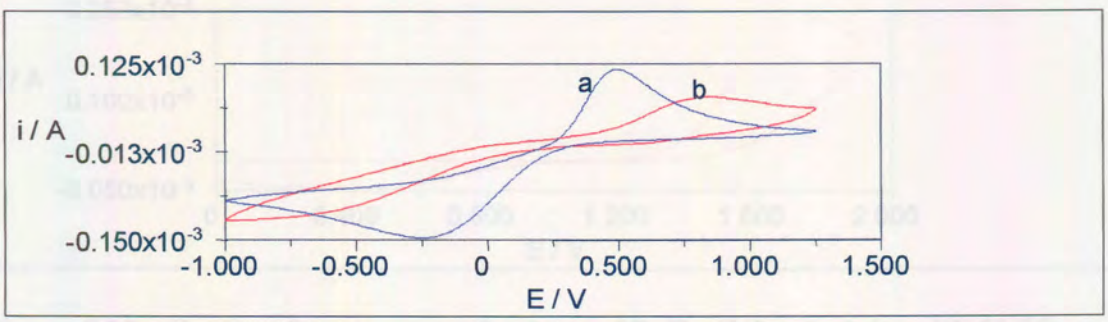

Figure 6.9 : Cyclic voltammogram for 20 mmol/L $K_3[Fe(CN)_6]$ in 1 mol/L KNO_3 and 0.1 mol/L Na_2SO_4 at a BDD electrode, (a) KNO_3, (b) Na_2SO_4 - scan rate is 50 mV/s. E_i = 1.25 V, scan direction = negative.

Using KNO_3 as a supporting electrolyte, a well-defined redox couple was obtained. However, when the supporting electrolyte was changed to Na_2SO_4, the ΔE_p increased significantly, and the peak size decreased. This result indicates a slower electron transfer reaction when a lower concentration of supporting electrolyte and a larger, less mobile ion such as the SO_4^{2-} ion is used. This finding clearly shows that the rate of the electron transfer of $[Fe(CN)_6]^{3-}/[Fe(CN)_6]^{4-}$ at a BDD electrode, is dependent on the nature of the supporting electrolyte.

6.3.4 Cerium (III) sulphate

One of the major advantages of diamond electrodes over all other electrodes is its wide potential window and high overpotential for oxygen evolution by water oxidation in aqueous electrolyte solutions. The Ce^{3+}/Ce^{4+} redox couple has a more positive standard potential than that of the H_2O/O_2 couple. It was for this reason that the Ce^{3+}/Ce^{4+} redox couple was chosen in order to highlight the fact that boron-doped diamond has a wider potential window than most other electrodes, especially the glassy carbon electrode. The anodic oxidation of Ce^{3+} cannot be clearly observed at conventional electrodes such as glassy carbon, platinum, gold, and other electrodes because of the influence of oxygen evolution [21].

Figure 6.10 illustrates the cyclic voltammogram for 3 mmol/L $Ce_2(SO_4)_3$ in 0.1 mol/L sulphuric acid (H_2SO_4) at a BDD electrode. A large, well-defined anodic peak is observed at approximately 1.7 V. This anodic peak represents the oxidation of Ce^{3+} to Ce^{4+}. A weak cathodic peak representing the reduction of Ce^{4+} can be seen at approximately 0.4 V on the reverse scan.

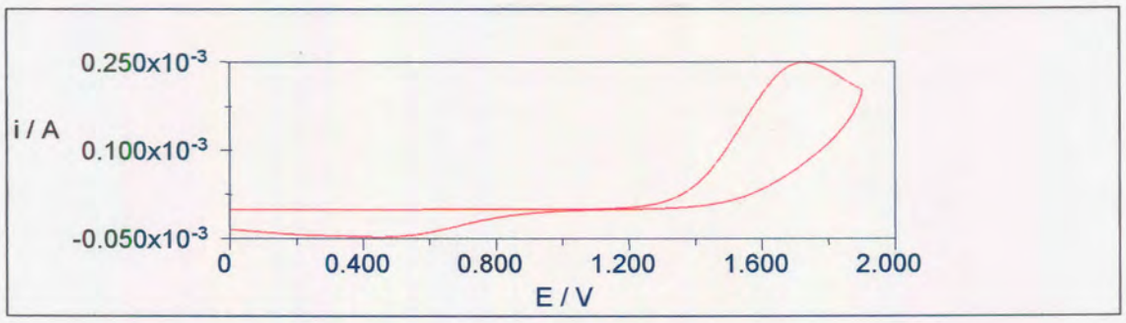

Figure 6.10 : Cyclic voltammogram for 3 mmol/L $Ce_2(SO_4)_3$ in 0.1 mol/L H_2SO_4 at a BDD electrode - scan rate is 50 mV/s. E_i = 0 V, scan direction = positive.

Figure 6.11 shows the cyclic voltammograms for 3 mmol/L $Ce_2(SO_4)_3$ in 0.1 mol/L H_2SO_4, at a glassy carbon electrode as well as at a BDD electrode. For the glassy carbon electrode, water oxidation occurs at about 1.7 V. The electrolysis of water and oxygen evolution therefore negatively affects the resolution of the anodic peak. A weak cathodic peak occurring at 0.4 V is also observed using the glassy carbon electrode.

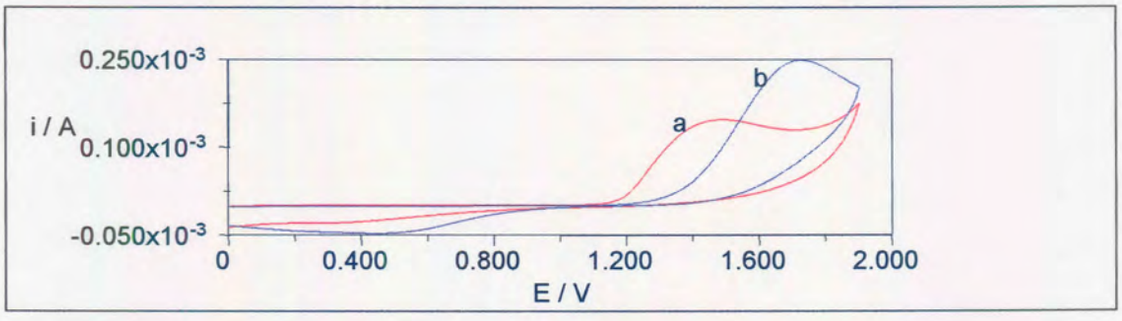

Figure 6.11: Cyclic voltammograms for 3 mmol/L $Ce_2(SO_4)_3$ in 0.1 mol/L H_2SO_4, at a glassy carbon electrode (a) as well as at a BDD electrode (b) - scan rate is 50 mV/s. E_i = 0 V, scan direction = positive.

On comparison of the voltammograms representing the glassy carbon and diamond electrodes, it is quite clearly seen that a better anodic peak resolution independent of water electrolysis is obtained for the diamond electrode. This implies that the use of diamond electrodes in systems such as that of the Ce^{3+}/Ce^{4+} redox couple, which require a large potential window, is favourable.

Figure 6.12 represents the effect of scan rate for 3 mmol/L $Ce_2(SO_4)_3$ in 0.1 mol/L H_2SO_4, at a BDD electrode. As the scan rate increases from 5 mV/s to 100 mV/s, the oxidation peak current also increases.

The cyclic voltammogram representing the reproducibility of the diamond electrode in cerium (III) sulphate is given in **Figure 6.13**. It can clearly be seen that as the number of scans increases, the oxidation peak potential shifts to more positive values, until it finally can no longer be resolved from the oxidation peak of water.

Initially, the surface of the diamond electrode [CVDBD4(3)] used in **Figure 6.13** was partially hydrophobic, i.e. contact angle measurements were between 72°-88° (see **Section 4.6**). This indicates that the diamond electrode surface contained oxygen functionalities. Cerium is known to react with oxygen to form a cerium-oxygen polymer. Cerium could therefore have reacted with the oxygen functionalities on the surface of the diamond electrode to form a polymeric layer on the surface. This layer could then act as a passivating layer, hindering oxidation of Ce^{3+} ions at the electrode surface, and necessitating more and more positive potentials to achieve electron transfer, as seen in **Figure 6.13**.

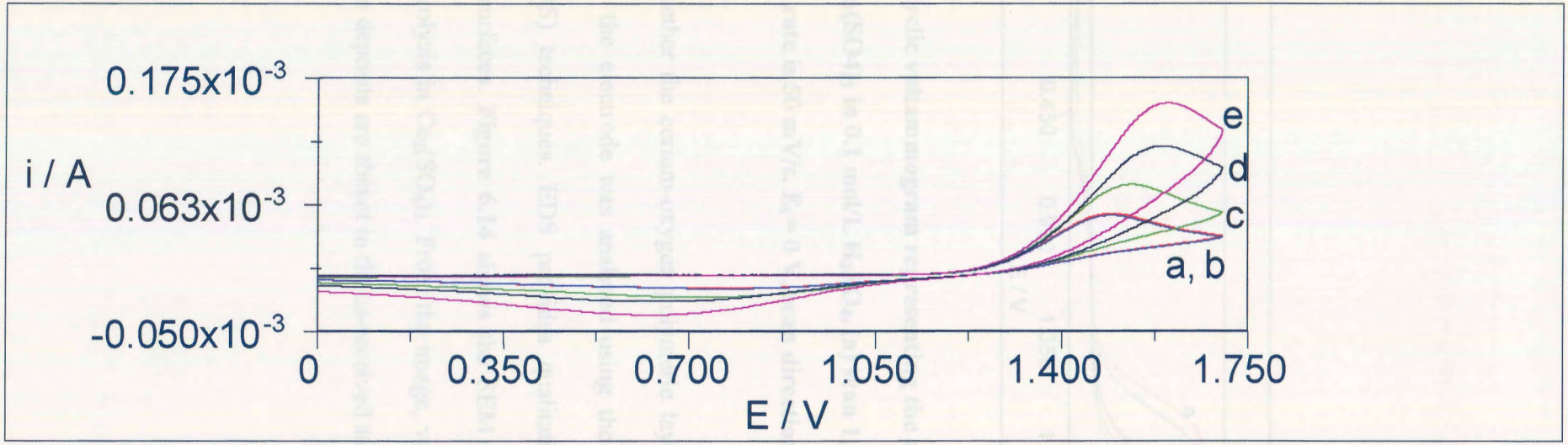

Figure 6.12 : Effect of scan rate for 3 mmol/L $Ce_2(SO_4)_3$ in 0.1 mol/L H_2SO_4, at a BDD electrode, (a) 5 mV/s, (b) 10 mV/s, (c) 25 mV/s, (d) 50 mV/s, (e) 100 mV/s. E_i = 0 V, scan direction = positive.

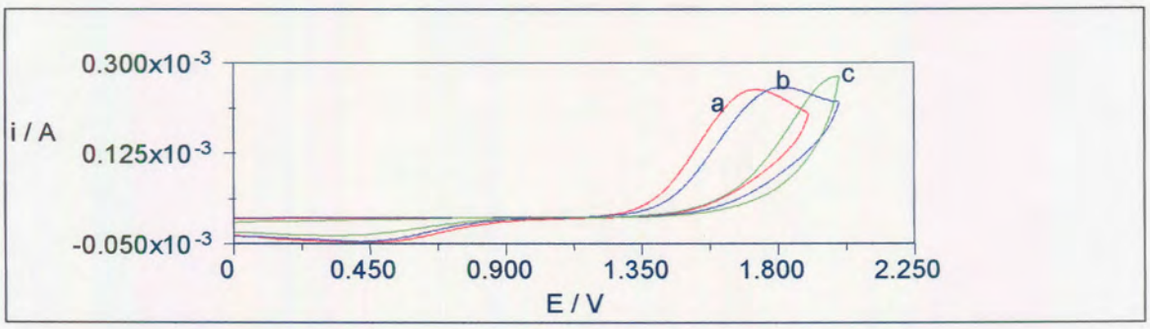

Figure 6.13 : Cyclic voltammogram representing the reproducibility of the BDD electrode for $Ce_2(SO4)_3$ in 0.1 mol/L H_2SO_4, (a) scan 1, (b) scan 3, (c) scan 7 - scan rate is 50 mV/s. E_i = 0 V, scan direction = positive

To investigate whether the cerium-oxygen polymeric layer had indeed formed on the electrode surface, the electrode was analysed using the SEM and energy dispersive spectroscopy (EDS) techniques. EDS provides qualitative information on elements present on solid surfaces. **Figure 6.14** shows the SEM image of the BDD electrode surface after electrolysis in $Ce_2(SO_4)_3$. From the image, various deposits or clusters can be observed. These deposits are absent in the as-received sample (**Figure 6.15**).

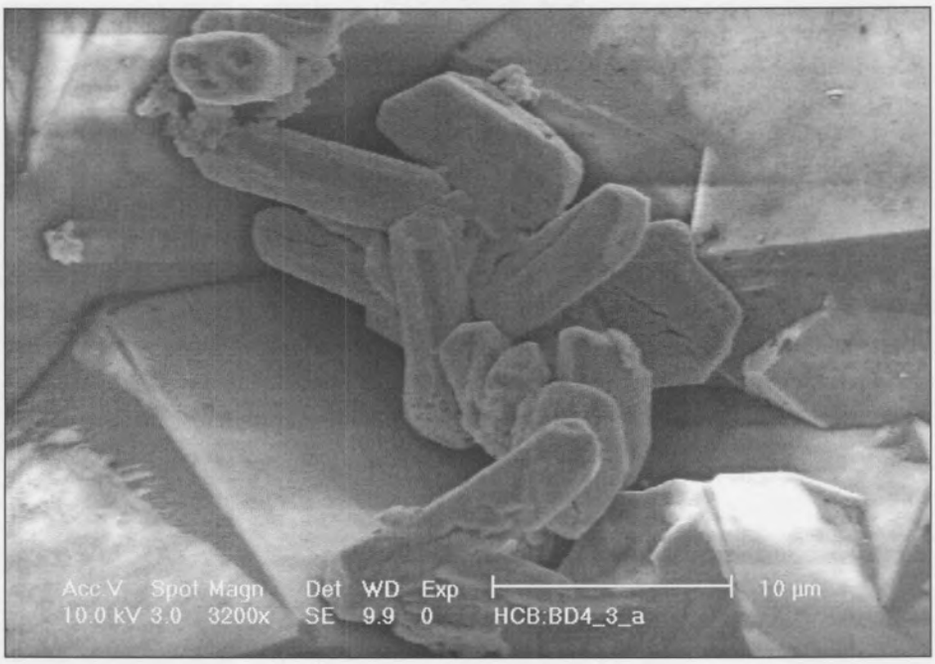

Figure 6.14 : SEM image of the BDD electrode surface after electroanalysis in $Ce_2(SO_4)_3$

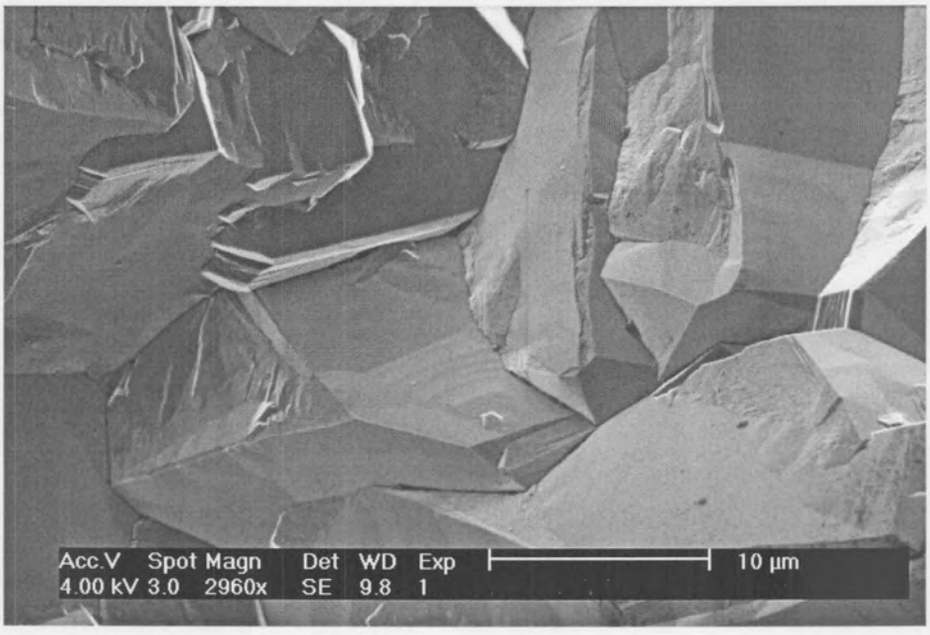

Figure 6.15 : SEM image of the as-received BDD electrode

EDS analysis identified these to be cerium deposits (**Figure 6.16**). The presence of cerium on the diamond electrode surface indicates that a cerium polymeric layer is likely to have formed on the electrode surface thereby hindering the further oxidation of Ce^{3+} to Ce^{4+}. In order to prevent the formation of the polymeric layer, the oxygen functionalities on the electrode surface would have to be removed via hydrogenation of the surface prior to analysis in $Ce_2(SO_4)_3$.

To test this theory, the diamond electrode (CVDBD4(3)) was acid cleaned in 20% H_2SO_4 and ultrasonically cleaned in hot water in order to remove the cerium deposits. The electrode was then hydrogenated in the TGA at 700°C under a flowing stream of 10% hydrogen in argon for 4 hours, in order to replace the oxygen atoms present on the surface with hydrogen atoms. A subsequent voltammetric scan for 3 mmol/L $Ce_2(SO_4)_3$ in 0.1 mol/L H_2SO_4 at the BDD electrode was carried out. A welcoming Ce^{3+} oxidation peak was evident at approximately 1.7 V. The peak potential and current remained constant on subsequent scans illustrating the reproducibility of the BDD electrode in $Ce_2(SO_4)_3$. However, the BDD electrode can only be reproducible in $Ce_2(SO_4)_3$ as long as the electrode surface is hydrophobic.

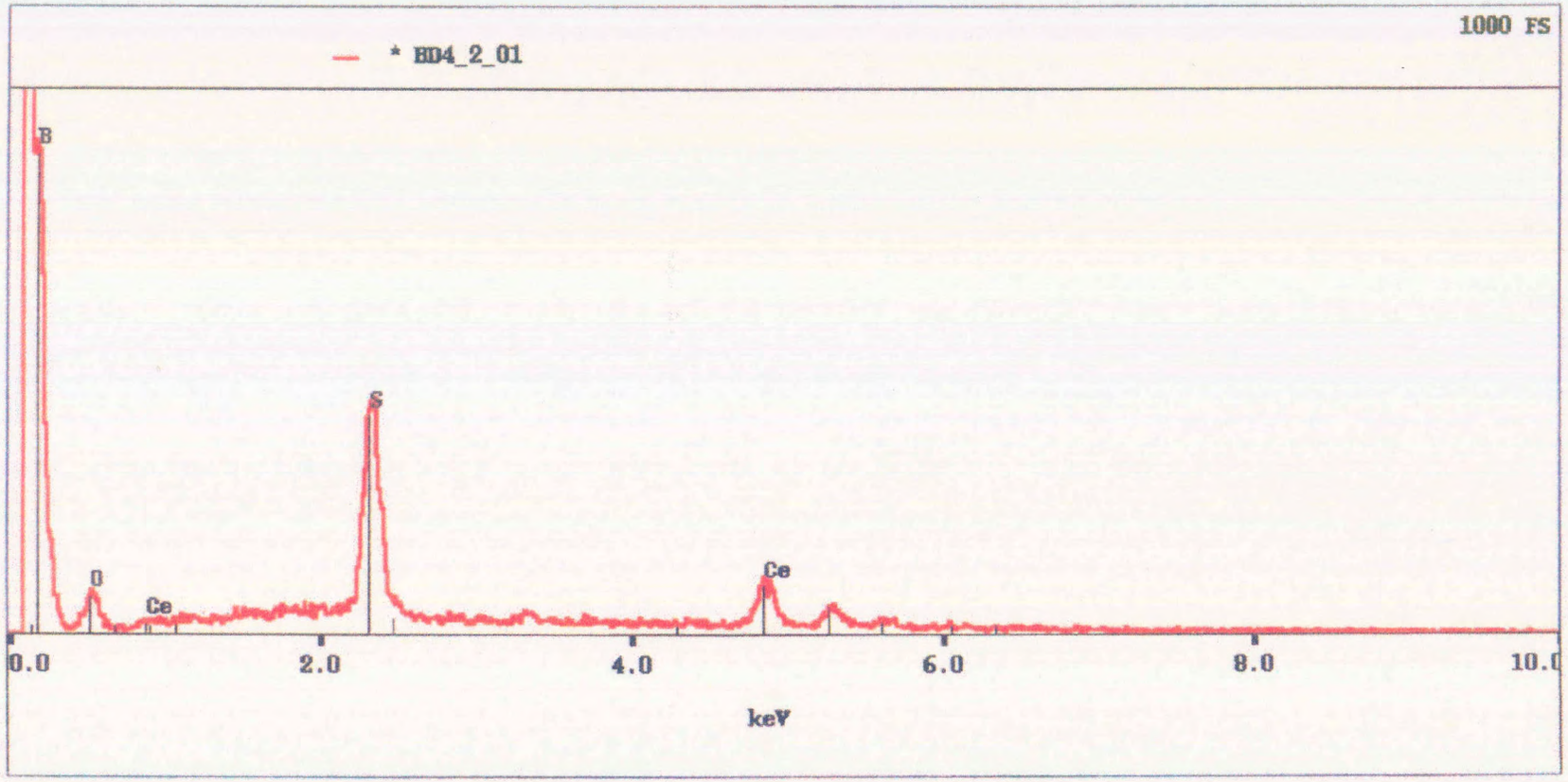

Figure 6.16 : EDS spectrum of CVDBD3 after electroanalysis in $Ce_2(SO_4)_3$

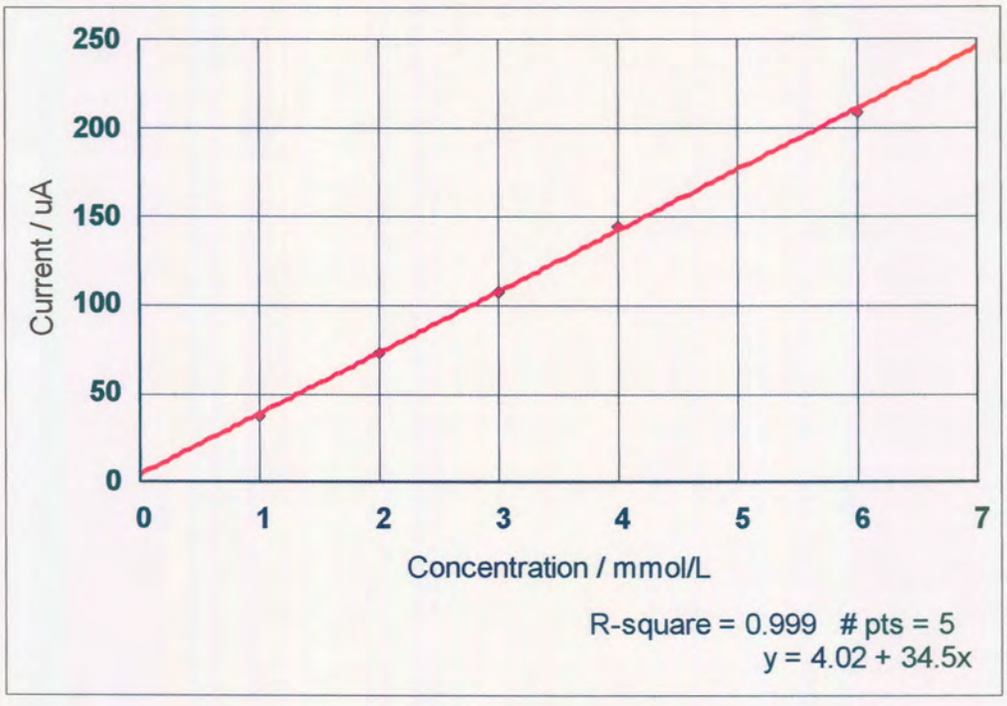

Figure 6.17 : Calibration plot for the BDD electrode

By varying the concentration of $Ce_2(SO_4)_3$ as a function of the respective oxidative peak current, a calibration plot was drawn for a partially hydrophobic BDD electrode (**Figure 6.17**) as well as the glassy carbon electrode (**Figure 6.18**). Percentage recoveries and the relative standard deviation of the samples measured are found in **Table 6.3**. The percentage recovery determines the ability of the electrode to analyse an unknown concentration. This value should be as close to 100% as possible in order to determine the reproduciblity and stability of the electrode.

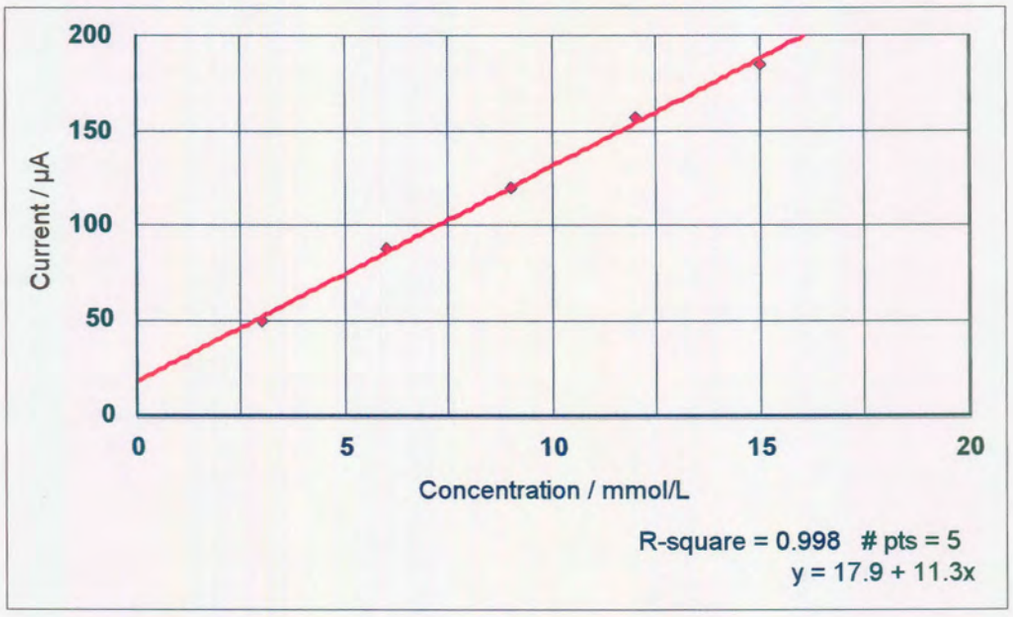

Figure 6.18 : Calibration plot for the glassy carbon electrode in $Ce_2(SO_4)_3$

Table 6.3 : Percentage recoveries and the relative standard deviation of the samples measured

Electrode	Sample	Percentage recovery	Average	Standard deviation
BDD	1	96.71	97.38	1.23
	2	98.80		
	3	96.63		
Glassy carbon	1	107.49	104.93	2.41
	2	102.70		
	3	104.59		

Both the BDD electrode and the glassy carbon electrode were linear in the concentration range measured. The linear regression (R-square) value for the diamond electrode (0.999) was found to be higher than that of the glassy carbon electrode (0.998). If all the points in a calibration graph lay in a straight line, then the R-square value would be 1. The R-square value is therefore regarded as a measure of the quality of the calibration plot. Thus, it can be clearly seen that the BDD electrode produces a better quality calibration plot than the glassy carbon electrode. Furthermore, the percentage recovery values (**Table 6.3**) for the BDD electrode is much closer to 100% than the glassy carbon electrode. This illustrates diamond to be preferable to glassy carbon for the quantitative analysis of $Ce_2(SO_4)_3$.

6.4 Conclusion

The electrochemical behaviour of diamond electrodes of varying boron concentrations was investigated. It was found that, as the boron concentration of the BDD increases, the potential window decreases. However, the potential window for the highest BDD electrode (CVDBD6) is still wider than that of the glassy carbon electrode, thereby confirming the advantage that the BDD electrode has over glassy carbon when investigating aqueous systems.

The peak separation of the $[Fe(CN)_6]^{3-}/[Fe(CN)_6]^{4-}$ redox couple (690 mV) was found to be an order of magnitude larger than that of the glassy carbon electrode (61 mV). It is suggested that oxygen termination of the BDD electrode surface inhibits the electron

transfer of the $[Fe(CN)_6]^{3-}/[Fe(CN)_6]^{4-}$ redox couple. It can thus be assumed that in order to reduce the peak separation, the surface of the electrode will have to be made hydrophobic.

The BDD electrode proved to be more effective (wider potential window, therefore better peak resolution) for the semi-quantitative analysis of cerium (III) sulphate, than the glassy carbon electrode. This is evidenced by the BDD electrode producing a better quality calibration plot and percentage recovery values than the glassy carbon electrode.

6.5 References

[1] S Jolley, M Koppang, T Jackson and G M Swain, **Anal. Chem., 69** (1997) 4041.

[2] M D Koppang, M Witek, J Blau and G M Swain, **Anal. Chem., 71** (1999) 1188.

[3] R D O'Neill, J P Lowry and M Mas, **Critical ReviewsTM in Neurobiology, 12** (1998) 69.

[4] D Pletcher, **A first course in Electrode Processes,** Alresford Press, (1991).

[5] C M A Brett and A M O Brett, **Electrochemistry Principles, Methods and Applications**, Oxford University Press, (1993).

[6] J Xu, M C Granger, Q Chen, T E Lister, J W Strojek and G M Swain, **Anal. Chem., 69** (1997) 591A.

[7] E N Farabaugh, L Robins and A Feldman, **J. Mater. Res., 10** (1995) 1448.

[8] A Argiotia, H B Martin, J C Angus and U Landau, **Electrochemical Society Proceedings, 97** (1997) 364.

[9] L M Peter, W Durr, P Bindra and H Gerischer, **J. Electroanal. Chem., 71** (1976) 31.

[10] M Datta and A Datta, **J. Phys. Chem., 94** (1990) 8203.

[11] C M Pharr and P R Griffiths, **Anal. Chem., 69** (1997) 4665.

[12] P Chen and R L McCreery, **Anal. Chem., 68** (1996) 3958.

[13] R J Rice and R L McCreery, **Anal. Chem., 61** (1989) 1637.

[14] K K Cline, M T McDermott and R L McCreery, **J. Phys. Chem., 98** (1994) 5314.

[15] S Alehashem, F Chambers, J W Strojek, G M Swain and R Ramesham, **Anal. Chem., 67** (1995) 2812.

[16] J W Strojek, M C Granger, T Dallas, M W Holtz and G M Swain, **Anal. Chem., 68** (1996) 2031.

[17] M C Granger and G M Swain, **Journal of the Electrochemical Soceity, 146** (1999) 4551.

[18] R Ramesham and M F Rose, **High Temperature and Materials Science, 38** (1997) 1.

[19] M C Granger, M Witek, J Xu, J Wang, M Hupert, A Hanks, M D Koppang, J E Butler, G Lucazeau, M Mermoux, J W Strojek and G M Swain, **Anal. Chem., 72** (2000) 3793.

[20] I Yagi, H Notsu, T Kondo, D A Tryk and A Fujishima, **J. Electroanal. Chem., 473** (1999) 173.

[21] Y Maeda, K Sato, R Ramaraj, T N Rao, D A Tryk and A Fujishima, **Electrochimica Acta, 44** (1999) 3441.

CHAPTER 7

Electroanalysis of organic systems – dopamine in the presence of ascorbic acid

7.1 Introduction

Dopamine belongs to the family of catecholamines and is found in the extracellular fluid (ECF) in the brain. It is synthesised in the body by a two step process from the 1-amino acid tyrosine. The hydroxylation of tyrosine by tyrosine hydroxylase results in the formation of the catechol dihydroyphenylalanine (DOPA). DOPA is then decarboxylated by the non-specific enzyme 1-amino acid decarboxylase to dopamine. **Figure 7.1** illustrates the reactions involved in the synthesis of dopamine.

Dopamine is a biologically important compound, which plays a key role in neurotransmission [2,3]. Neurotransmission is the conversion of an electrical impulse to a chemical event and subsequently to a second electrical event [4]. The mammalian brain contains approximately 10^{11} nerve cells or neurons, which assimilate and process information.

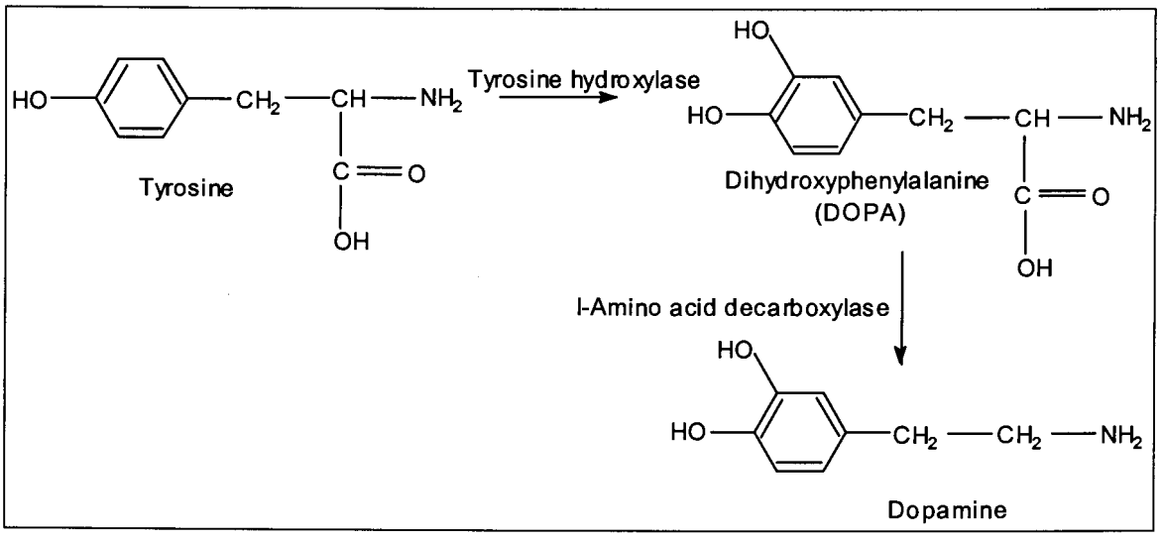

Figure 7.1 : Synthesis of Dopamine [1]

Figure 7.2 represents a schematic diagram of a neuron. Neurons receive information from cells via a treelike network called dendrites and then transfer this information in the form of electrical impulses along a cablelike axon to other nerves. These electrical impulses cause the release of a chemical messenger from a storage vesicle in the axon terminal. The chemical messenger, also called a neurotransmitter, travels across a synapse to bind to a postsynaptic receptor protein. The act of binding to the receptor sets in motion a series of events, which eventually brings about a change in the electrical state of the postsynaptic cell. As a chemical messenger, dopamine is similar to adrenaline. Dopamine affects brain processes that control movement, emotional response, and ability to experience pleasure and pain.

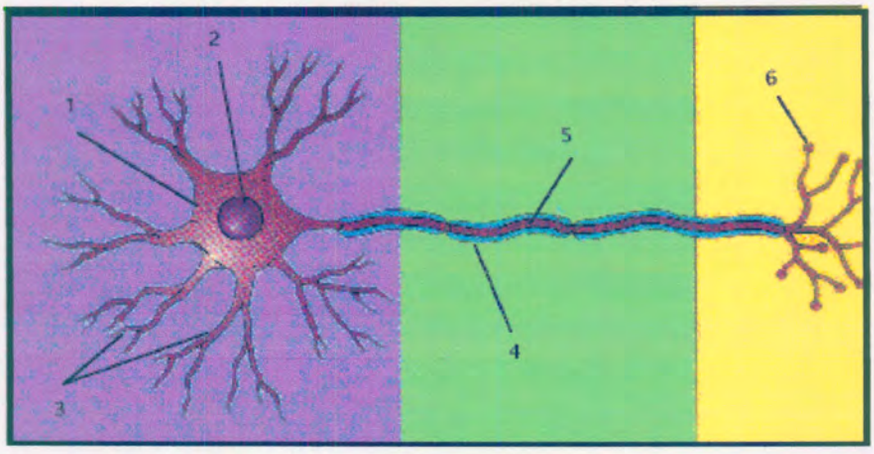

Figure 7.2 : Schematic diagram of a neuron - 1 = Cell Body, 2 = Nucleus, 3 = Dendrites, 4 = Axon, 5 = Myelin Sheath, 6 = Axon terminals [5]

Neurons containing the neurotransmitter dopamine are clustered in the midbrain in an area called the substantia nigra [6]. A deficiency of dopamine in the brain results in Parkinson's disease and an excess of dopamine results in schizophrenia. Dopamine is also one of the neurotransmitters that play a major role in the addiction to certain drugs such as cocaine. It is therefore vital that the presence of dopamine be efficiently detected in order to cure these dreaded diseases.

One of the methods used to detect for the presence of dopamine is voltammetry. Since dopamine, a neurotransmitter, is electroactive, it can be oxidised at an applied potential. The resulting current can then be measured and the concentration of analyte determined. The electro-oxidation of dopamine is illustrated in **Equation 7.1** [7].

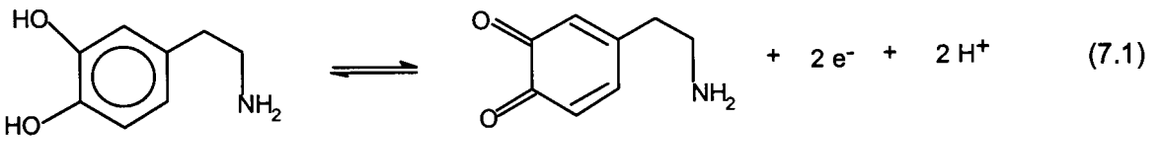

Dopamine Dopamine ortho-quinone

The ideal technique for the detection of dopamine would be *in vivo* voltammetry. This technique involves the insertion of an electrode into the brain of the subject, which enables online monitoring of the dopamine levels. Ralph Adams and his colleagues [8] first attempted this technique by inserting a carbon paste electrode, having a diameter of approximately 250 μm, into the brain of a rat to detect electroactive materials *in vivo*. Although oxidation currents were obtained, this technique was non-specific, unreliable and irreproducible.

At the time that Adams was doing his pioneering work in the United States, Francois Gonon and his colleagues in France had been investigating electrodes made of other carbon-based materials for detecting catecholamines [4,7]. They used carbon fibre electrodes made from glass pipettes and these electrodes were vastly reduced in size (having a diameter of approximately 10 μm). The implantation of an electrode is traumatic to brain cells, and obviously the smaller the electrode the less damage occurs. The size of the electrode can also alter the species detected [4]. For example, larger electrodes may disrupt the blood-brain barrier in the brain and allow blood-borne compounds to be detected, or they can evoke a local gliosis, which is a tissue reaction to a foreign object.

The carbon fibre electrode gave a considerable improvement in terms of reproducibility and reliability over the carbon paste electrodes. This electrode, however, like the carbon paste electrode was not selective in detecting only the catecholamine of interest. Although oxidation currents were produced, several other oxidizable molecules, notably ascorbic acid which coexists with the catecholamines in the ECF in the brain [9], obscured the currents from catecholamines such as dopamine. Because the oxidation potential of ascorbic acid is similar to that of dopamine, selective detection of dopamine became a challenging task. It was subsequently found that, in order to detect catecholamines such as dopamine in the presence of ascorbic acid and other acidic metabolites, an anionic Nafion membrane could be used to repel these acids, as reported by Ralph Adams [10].

Since the carbon paste and carbon fibre electrodes were used to detect the presence of catecholamines in brain tissue, it can be assumed that boron-doped diamond (BDD) electrodes can do the same, if not better. BDD electrodes, however, have a significant advantage over the carbon paste and carbon fibre electrodes, in that they are more resistant to fouling and more biocompatible than these carbon electrodes. Another very powerful advantage of BDD electrodes is their low baseline current, which enables them to detect extremely low concentrations of catecholamines such as dopamine in the brain tissue. These advantages make BDD electrodes potentially very useful as biosensors for the *in vivo* or *in vitro* detection of analytes.

7.1.1 Biocompatibility studies of chemically vapour deposited diamond (CVDD)

The surface of an implant (such as a biosensor) should not only be inert in the body, but should also stimulate cell proliferation and differentiation. Two biocompatibility studies of CVD diamond are reported in the literature. In the first, an internal study was commissioned by De Beers and carried out by researchers at De Montfort University (Leicester, United Kingdom), which compared the performance of boron-doped CVD diamond with that of porous silicon [11].

Three indicators of biocompatibility were measured : the deposition of protein, the deposition of hydroxyapatite (the inorganic constituent of bone tissue), and cell proliferation and morphology. The deposition of protein is essential for cells to become firmly anchored at the implant surface. Deposition of hydroxyapatite is a standard indicator of the compatibility of material for bone implants such as hip replacements, and may negatively affect the adherence and function of cells. Lastly, cell proliferation at an implant surface should be normal or above average, and the cells should adhere well to the surface and have a normal morphology.

It was found that hydroxyapatite deposited more slowly on the diamond sample than on porous silicon, and that the hydroxyapatite deposited more slowly than the protein layer. This is an excellent indication that boron-doped diamond would be a suitable candidate for a biomedical implant. Futhermore, B50 cells (transformed rat neuronal tissue) were

found to grow vigorously on the diamond surface, with good adhesion and normal morphology.

In the second study [12], the performance of a CVD (undoped) diamond coating was compared with that of pure titanium (titanium alloys are commonly used in hip replacements). Cell proliferation at the diamond coating was found to be equal to that at a titanium surface. However, attachment of cells at the diamond surface was retarded in comparison with titanium. Two reasons are proposed : firstly, the diamond surface was considerably rougher than the titanium surface, and secondly, the diamond surface was hydrophobic, which is expected to seriously interfere with protein adsorption and therefore cell adhesion. This lack of adhesion was not encountered in the De Montfort study, and may be due to the presence of boron dopant affecting the surface properties.

In conclusion, indications are that boron-doped diamond is an excellent biomaterial. However, care should be taken that the surface state has the right degree of hydrophilic/hydrophobic nature to balance the requirements for electroactivity and biocompatibility.

Since diamond is biocompatible, it would be an ideal biosensor for the *in vivo* or *in vitro* detection of catecholamines such as dopamine. However, there are many requirements that an electrode material has to meet in order to become an effective biosensor [13-17].

7.1.2 Commercial requirements and benefits of biosensors

Commercial biosensors must be accurate and repeatable [18-21]. In order to accomplish this, the electrode surface must be resistant to fouling, since any adsorbed species (for example quinones) on the surface of the electrode will result in a diminished level of accuracy and repeatability of the electrode.

The sensitivity of a biosensor is very important [22]. Biosensors must have very low detection limits when used to measure compounds in the body fluid, as the concentration levels are extremely low. Biosensors are specific and sensitive in that they can detect low concentrations of analytes which are present in a complex matrix. Another necessary requirement for a biosensor is its speed of response. If a biosensor is to be used to measure neurotransmitters in the ECF, where there is a major concentration flunctuation due to the speed at which chemicals are transferred from synapse to synapse, the biosensor has to respond quickly in order to detect these changes.

Other requirements for biosensors include reliability, physical robustness, low running costs and long lifetime. If they are physically robust, they can very easily be used by unskilled personnel.

Biosensors are potentially more efficient and less time consuming. Using conventional methods, rapid diagnosis and treatment cannot be carried out immediately because there is a long time delay between when the sample is taken and when the result is obtained

from a central laboratory. Biosensors, because of their excellent response time, are able to produce immediate results.

A vital requirement for a biosensor is biocompatibility. A biosensor must not contaminate nor poison the sample host system when inserted into the body. For this reason, diamond, being a purely carbon-based material, is ideal for use as a biosensor.

The investigations detailed below were carried out in order to evaluate the potential use of De Beers BDD electrodes as a biosensor for the *in vivo* detection of dopamine in brain tissue. The electrochemical behaviour of De Beers BDD electrodes was compared to that of other boron-doped diamond electrodes used in the literature, and to that of the glassy carbon electrode, in the dopamine and ascorbic acid systems.

7.2 Experimental

A three electrode cell consisting of a BDD working electrode, a platinum counter electrode and a Ag/AgCl reference electrode were used for the voltammetry investigation. All the chemicals used were analytical grade. Ascorbic acid (AA) and perchloric acid ($HClO_4$) were obtained from Saarchem. Dopamine was obtained from Sigma Aldrich. The supporting electrolyte ($HClO_4$) was diluted to the desired concentration using ultrapure Millipore water (18 μΩ.cm). Stock solutions of dopamine and AA were prepared using the supporting electrolyte. Each solution was deaerated prior to the electrochemical analysis by purging the solution with helium for 5 minutes.

All the electrochemical measurements were performed at room temperature (25°C).The surface areas of the glassy carbon and BDD electrodes were 0.071 cm^2 and 0.15 cm^2 respectively. CVDBD4, having a boron concentration of 543 mg/L, was used as the electrode material to investigate the dopamine and AA systems.

Prior to each electrochemical measurement, the glassy carbon electrode was polished for approximately 20 minutes in order to clean the electrode surface and remove any adsorbed organic species. An electrode holder was made from Perspex, consisting of a flat plate with a hole drilled in it through which the glassy carbon electrode was inserted during polishing. This was done in order to ensure that the electrode surface remained flat on the polishing cloth so that no curvature of the surface was introduced during the polishing process. The glassy carbon electrode was polished with a Leco polisher, using 6 μm diamond suspension, followed by 1 μm diamond suspension. The electrode surface was cleaned thoroughly with deionised water after polishing.

7.3 Results and discussion

7.3.1 Dopamine

Figure 7.3 illustrates the cyclic voltammogram for the oxidation of 0.2 mmol/L dopamine in 0.1 mol/L $HClO_4$ at a BDD electrode. A well-defined redox couple is observed with the oxidation of dopamine occurring at approximately 0.8 V and the ensuing reduction of dopamine occurring at about 0.2 V. The voltammogram shown in **Figure 7.3** was compared to that of literature. Fujishima et. al. [9] reported an oxidation

peak current density of 40 $\mu A/cm^2$ for 0.1 mmol/L dopamine in 0.1 mol/L $HClO_4$. The corresponding oxidation peak potential was reported to be approximately 0.8 V. These values are similar to the experimental values obtained for 0.2 mmol/L dopamine in 0.1 mol/L $HClO_4$, which gave an oxidation peak current density of 49 $\mu A/cm^2$ and an oxidation peak potential of approximately 0.8 V. The observed current was greater than that reported in literature due to a higher dopamine concentration. The shape of the experimentally obtained cyclic voltammogram (**Figure 7.3**) was identical to that depicted in literature [23].

The effect of deaerating the solution before any electrochemical analysis was also investigated. **Figure 7.4** shows the cyclic voltammograms for 0.2 mmol/L dopamine in 0.1 mol/L $HClO_4$ in a deaerated as well as in an aerated solution. Both cyclic voltammograms yielded a dopamine oxidation peak current of approximately 5 µA. The effect of purging the solution with helium was negligible.

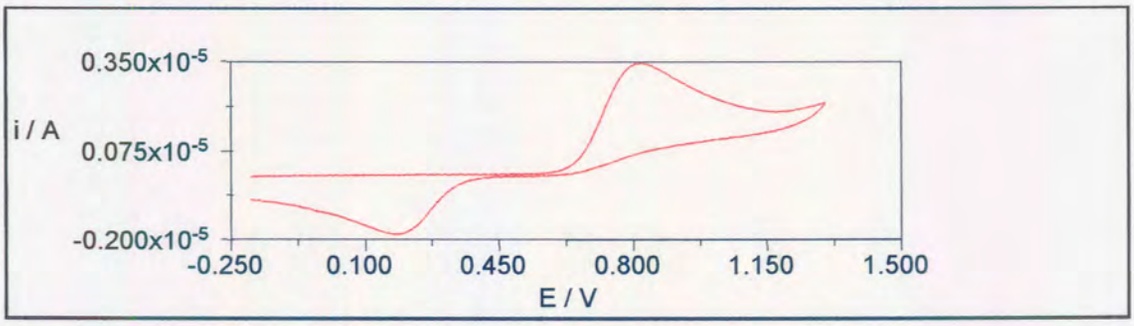

Figure 7.3 : Cyclic voltammogram for the oxidation of 0.2 mmol/L dopamine in 0.1 mol/L $HClO_4$ at a BDD electrode – scan rate is 50 mV/s. E_i = -0.2 V, scan direction = positive

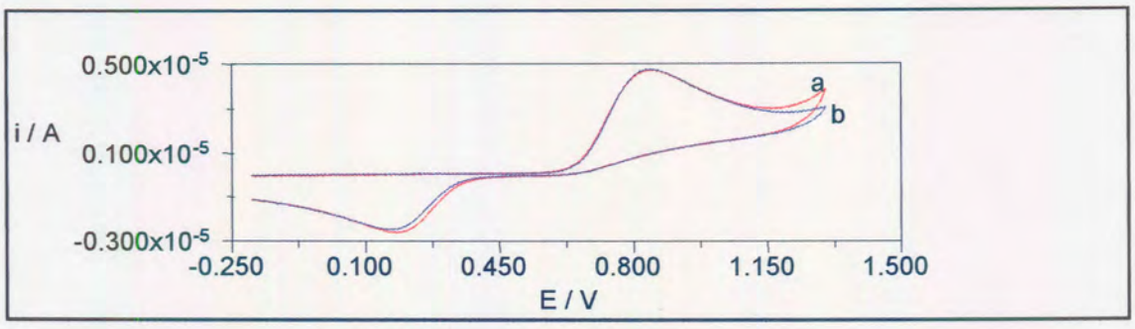

Figure 7.4 : Cyclic voltammograms for 0.2 mmol/L dopamine in 0.1 mol/L $HClO_4$ in an aerated (a), as well as in an deaerated (b) solution – scan rate is 100 mV/s. E_i = -0.2 V, scan direction = positive.

Linear sweep voltammetry was employed to investigate the reproducibility of the BDD electrode for 0.4 mmol/L dopamine in 0.1 mol/L $HClO_4$ (**Figure 7.5**). The oxidation peak current for both the first and the second scan was found to be 9.8 µA. This shows the reproducibility of the BDD electrode in the dopamine system to be quite acceptable.

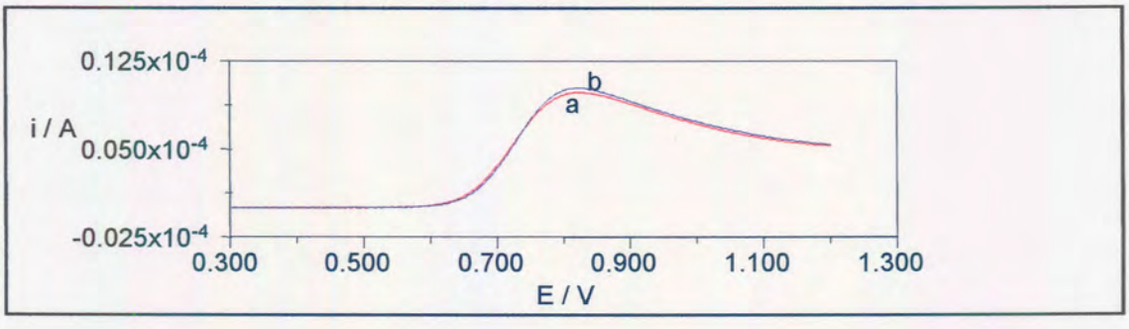

Figure 7.5 : Linear sweep voltammogram illustrating the reproducibility of the BDD electrode for 0.4 mmol/L dopamine in 0.1 mol/L $HClO_4$, (a) scan 1, (b) scan 2 – scan rate is 100 mV/s. E_i = 0.3 V, scan direction = positive.

Figure 7.6 represents the cyclic voltammograms for 0.2 mmol/L dopamine in 0.1 mol/L $HClO_4$ at a glassy carbon electrode and at a BDD electrode respectively. The separation between the oxidation peak and the reduction peak (peak separation, ΔE_p) for the BDD electrode was calculated to be 600 mV, whilst the ΔE_p for the glassy carbon electrode was calculated to be 56 mV. Granger et. al. [23] reported a ΔE_p of 480 mV for dopamine and a ΔE_p in the range of 125-175 mV at a polished glassy carbon electrode. Dopamine appears to therefore exhibit much more electrochemical irreversibility at the BDD electrode than at the glassy carbon electrode, as evidenced by the relatively large ΔE_p.

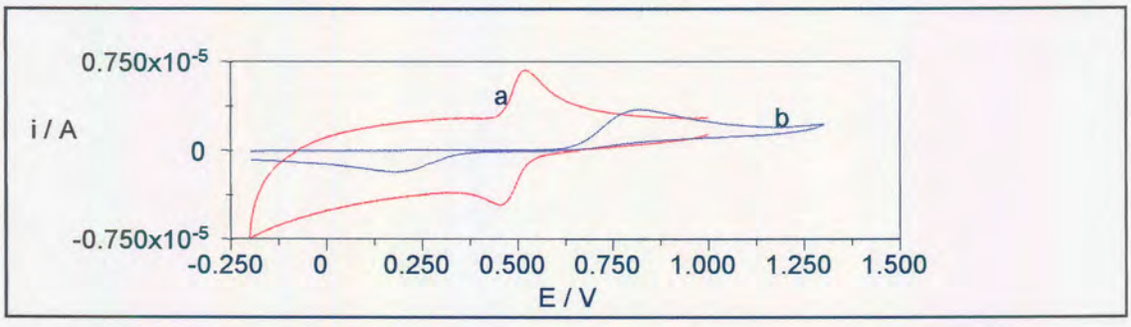

Figure 7.6 : Cyclic voltammograms for 0.2 mmol/L dopamine in 0.1 mol/L $HClO_4$ at a glassy carbon electrode (a), and BDD electrode (b) respectively – scan rate is 50 mV/s. E_i = -0.2 V and scan direction = positive.

The large ΔE_p for the BDD electrode can be ascribed to a slow electron transfer reaction occurring at the electrode surface. Swain et. al. [23] believe that a lack of adsorption of dopamine at the BDD electrode surface is one of the reasons for the relatively slow electrode kinetics. In addition, Hunt-Duvall and McCreery have presented a detailed

study showing that low ΔE_p values correlate with catechol and catecholamine adsorption on glassy carbon, and surface treatments that decreased adsorption also increased ΔE_p [24].

The apparent lack of adsorption of catecholamines such as dopamine on the BDD electrode surface demonstrates the high degree of resistance that BDD electrodes possess towards fouling. This feature is again one of the many advantages that BDD electrodes possess over most other electrode materials, for example glassy carbon. The surface of the glassy carbon electrode, like many solid electrodes, has a tendency to become deactivated over time when it is exposed to the atmosphere or working solution. The problem is more severe when biological sample solutions are used [25].

A further conspicuous feature in the above cyclic voltammogram (**Figure 7.6**), is the huge baseline current associated with the glassy carbon electrode. This observed baseline can be attributed to the sp^2 nature of the carbon in the glassy carbon electrode. BDD electrodes, however, possess a very low baseline current and this may be ascribed to several factors [26] :

(a) Since the as-grown BDD electrodes are hydrophobic or at least partially hydrophobic in nature, there is a lack of electroactive carbon-oxygen functional groups on the electrode surface. The presence of these oxygen functional groups would increase the baseline current associated with the electrode.

(b) Diamond possesses a low density of surface states at the Fermi level as compared to that of a metal. Thus, the baseline current associated with the BDD electrode is expected to be much lower than that associated with a corresponding metal electrode.

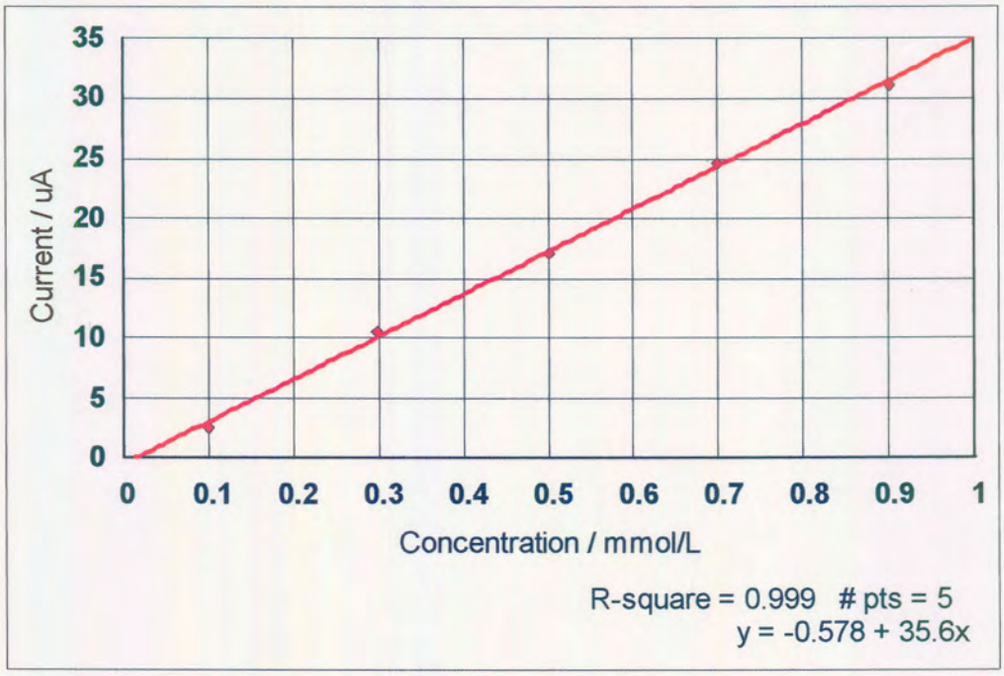

Figure 7.7 : Calibration plot for dopamine at a BDD electrode

Figure 7.7 and **Figure 7.8** illustrate the calibration plot for dopamine at a BDD electrode and at a glassy carbon electrode respectively. Percentage recoveries and the relative standard deviation of the samples measured are found in **Table 7.2**.

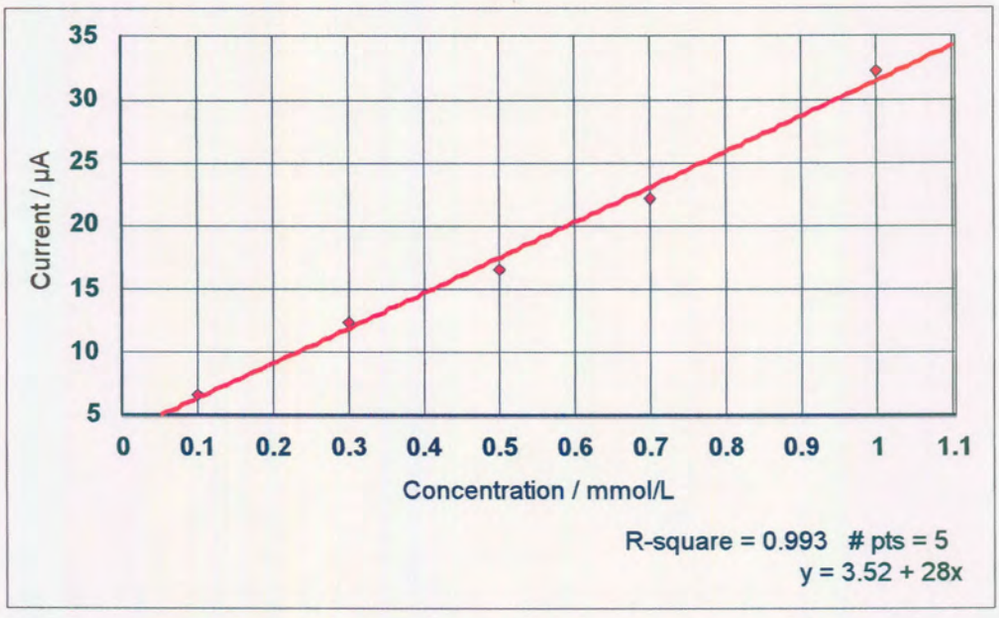

Figure 7.8 : Calibration plot for dopamine at a glassy carbon electrode

Table 7.2 : Percentage recoveries and the relative standard deviation of the samples measured

Electrode	Sample	Percentage recovery	Average	Standard deviation
BDD	1	101.10	98.81	2.21
	2	98.63		
	3	96.69		
Glassy carbon	1	86.52	102.96	14.72
	2	114.94		
	3	107.43		

Both the BDD electrode and the glassy carbon electrode responses were linear in the concentration range measured. The linear regression (R-square) value for the diamond electrode (0.999) was found to be higher than that of the glassy carbon electrode (0.993). It is evident from **Table 7.2** that the percentage recovery values for the BDD electrode is much closer to 100% than the glassy carbon electrode.

The low R-square and high variation in percentage recovery values for the glassy carbon electrode may be attributed to the fouling of the electrode surface by dopamine. According to **Equation 7.1**, the product from the electro-oxidation of dopamine is dopamine ortho-quinone. Quinones have a tendency to adsorb onto surfaces that have a high degree of oxygen-carbonyl functionalities, and these may be expected to form on glassy carbon during the anodic stage of the voltammetry cycle. **Equation 7.2** [27] illustrates a possible mechanism for dopamine ortho-quinone chemisorption at a glassy carbon electrode surface. This mechanism could explain why the glassy carbon electrode had to be polished after every dopamine determination during the dopamine calibration.

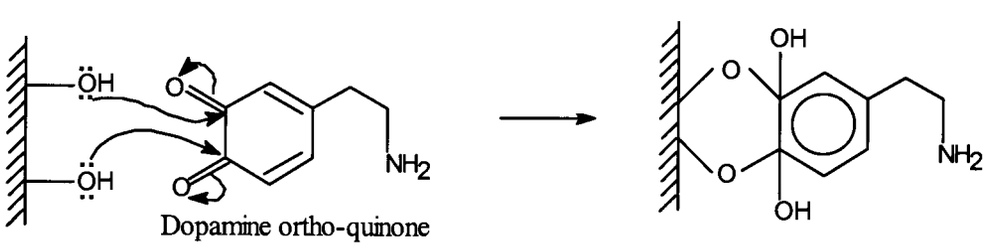

(7.2)

From the calibration graphs and the percentage recovery values, it can be deduced that BDD is a better electrode material for the determination of dopamine than the glassy

carbon electrode. This is accredited to the lack of adsorption of dopamine or its electro-oxidation product on the BDD electrode surface. It must be noted that, although BDD electrodes are preferred in the determination of dopamine, the rate of electron transfer at the electrode surface is slow.

In the determination of dopamine, the BDD electrode was found to be stable over a three month period. During this period, the electrode was stored in contact with air. Using chronoamperometry, the detection limit for dopamine at the BDD electrode was determined to be 0.56 μmol/L. Fujishima et. al. [9] reported a dopamine detection limit of 50 nmol/L, which is among the lowest values ever reported. The resistivity of the BDD electrode used by Fujishima et. al. was of the order of 10^{-3} Ω.cm, whilst the resistivity of the CVDBD4 electrode employed for the detection of dopamine was calculated to be approximately 17 Ω.cm. This indicates that the BDD diamond electrode used by Fujishima et. al. must have been "heavily doped". Therefore, in order to decrease the observed detection limit for dopamine, a higher level of boron dopant (probably in the order of 10^{21} boron atoms.cm^{-3}) is necessary.

Dopamine coexists in the ECF in the brain with ascorbic acid. The concentration of ascorbic acid and other acidic metabolites in the ECF is much greater than that of the catechols and catecholamines [4]. It is therefore essential that a biosensor should be capable of detecting low concentrations of dopamine in the presence of much larger concentrations of ascorbic acid.

7.3.2 Asorbic acid

Ascorbic acid (AA) normally occurs in the extracellular fluid (ECF) in the brain. With its high concentration and ease of oxidation, AA is probably the simplest molecule to detect in the brain ECF. The structure of AA is found in **Figure 6.4**. Using voltammetry techniques, the oxidation of ascorbic acid was investigated at a glassy carbon electrode as well as at a boron-doped diamond electrode.

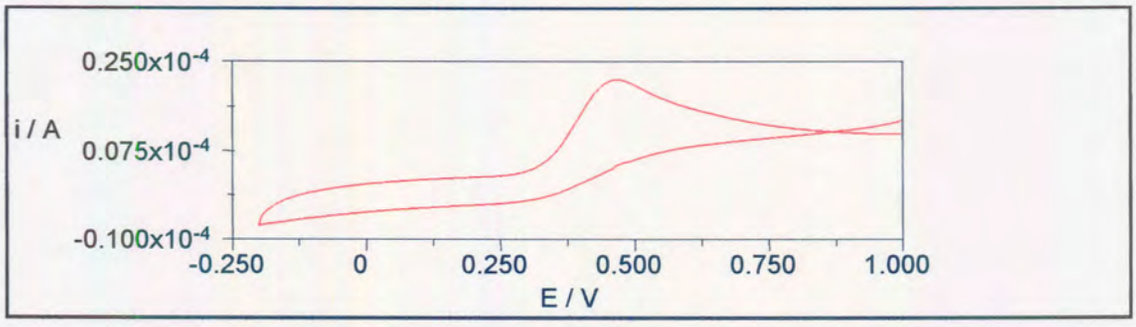

Figure 7.9 : Cyclic voltammogram for 2 mmol/L AA in 0.1 mol/L $HClO_4$ at a glassy carbon electrode - scan rate is 50 mV/s. E_i = -0.2 V, scan direction = positive

Figure 7.9 shows the cyclic voltammogram for 2 mmol/L AA in 0.1 mol/L $HClO_4$ obtained at a glassy carbon electrode. The oxidation peak of AA is seen at a potential of approximately 0.46 V. It must be noted that there is no reduction peak on the reverse scan, that is the cyclic voltammogram for AA is totally irreversible. This implies that the product of the electron transfer reaction for AA is stable, i.e. not electroactive.

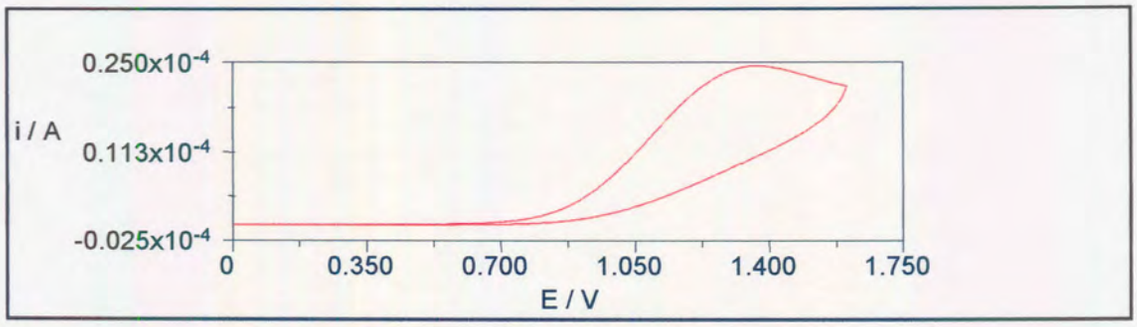

Figure 7.10 : Cyclic voltammogram for 2 mmol/L AA in 0.1 mol/L $HClO_4$ at a BDD electrode - scan rate is 50 mV/s. E_i = 0 V, scan direction = positive

The cyclic voltammogram representing the oxidation of 2 mmol/L AA in 0.1 mol/L $HClO_4$ at a BDD electrode is shown in **Figure 7.10.** If the surface of the BDD electrode was very hydrophobic, the oxidation peak potential of AA would have occurred at approximately 0.8 V, according to Fujishima et. al. [9]. However, since CVDBD4 is partially hydrophobic, a well-defined AA oxidation peak is evident at approximately 1.3 V. The cyclic voltammogram for AA at a BDD electrode is again entirely irreversible. The reproducibility of the BDD electrode in the AA system was investigated (**Figure 7.11).** It can be deduced from **Figure 7.11** that the BDD electrode is fairly reproducible in the AA system.

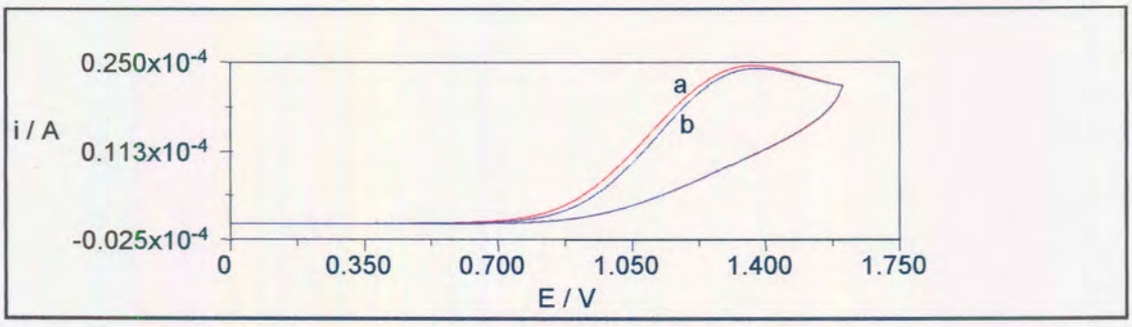

Figure 7.11 : Cyclic voltammogram illustrating the reproducibility of the BDD electrode for 2 mmol/L AA in 0.1 mol/L HClO4; (a) first scan, (b) second scan - scan rate is 50 mV/s. E_i = 0 V, scan direction = positive

Figure 7.12 and **Figure 7.13** illustrate the calibration plot for AA at a BDD electrode and at a glassy carbon electrode respectively. Percentage recoveries and the relative standard deviation of the samples measured are found in **Table 7.3**. The glassy carbon electrode had to be polished between measurements during the calibration in order to remove any adsorbed species present on the electrode surface.

The BDD electrode and the glassy carbon electrode calibration curves were found to be linear in the concentration range measured. The R-square value for the diamond electrode (1) was again found to be higher than that of the glassy carbon electrode (0.998). Also, the percentage recovery values for AA at the BDD electrode were much closer to 100% than at the glassy carbon electrode. These positive results for the BDD electrode can be attributed to the lack of adsorption of AA on the electrode surface.

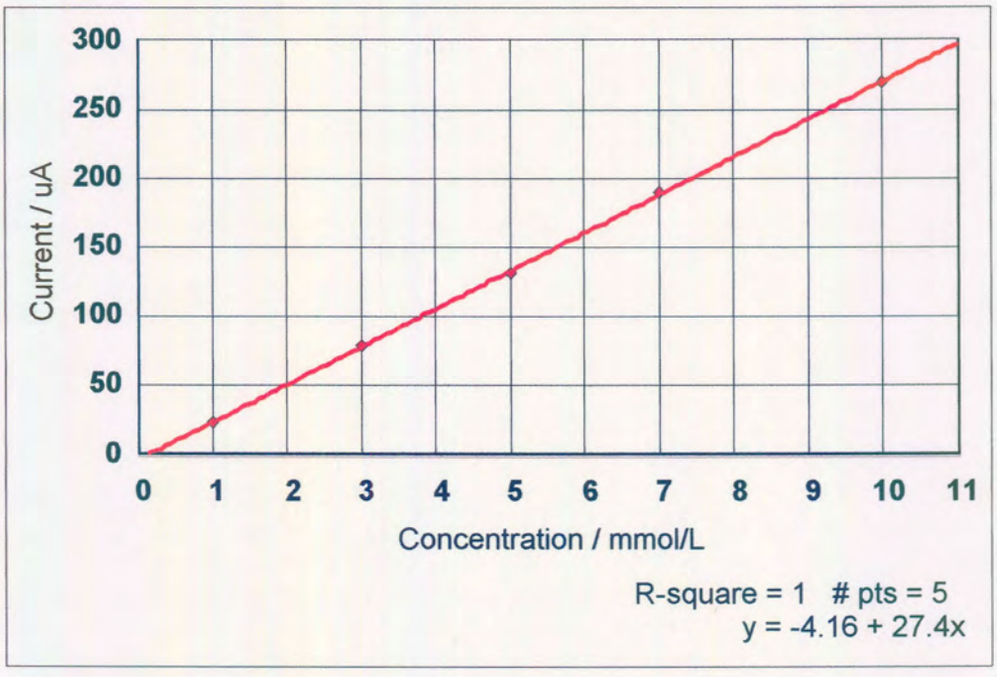

Figure 7.12 : Calibration plot for AA at a BDD electrode

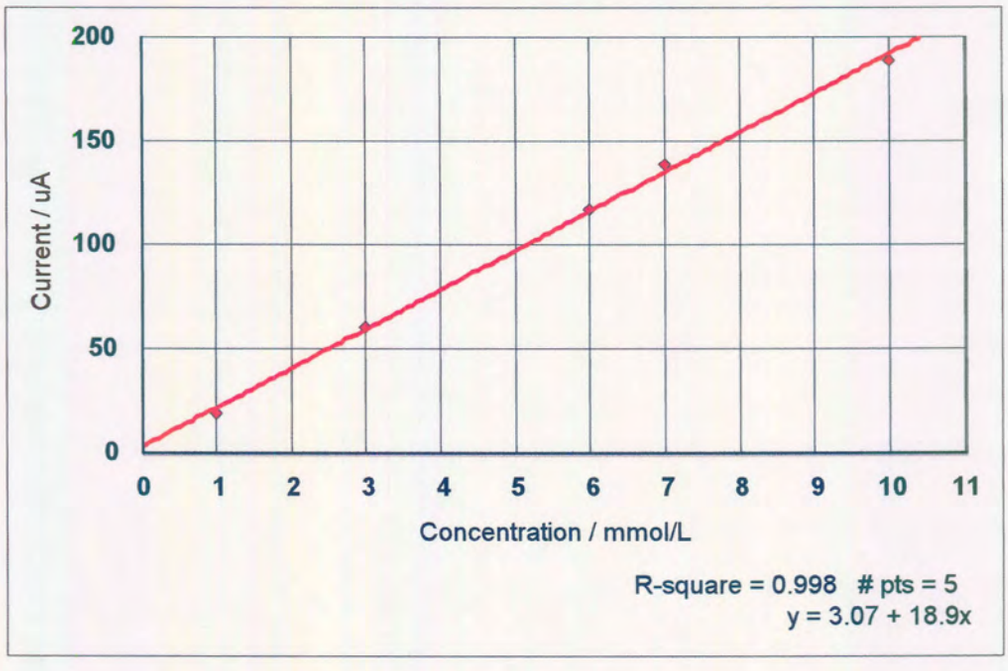

Figure 7.13 : Calibration plot for AA at a glassy carbon electrode

Table 7.3 : Percentage recoveries and the relative standard deviation of the samples measured

Electrode	Sample	Percentage recovery	Average	Standard deviation
BDD	1	100.53	100.36	0.49
	2	100.75		
	3	99.82		
Glassy carbon	1	111.27	107.14	3.88
	2	103.56		
	3	106.59		

The BDD electrode was also found to be stable over a three month period when used for the detection of AA. During this period, the electrode was exposed to a laboratory environment. The detection limit for AA at the BDD electrode was determined to be 20 nmol/L.

In the *in vivo* determination of dopamine, ascorbic acid is a major interferent. It is therefore essential to achieve good resolution between the responses for AA and dopamine. This may be accomplished using two well known techniques [4] :

(a) By using an anionic Nafion membrane at the electrode surface, and a pH above that of the pKa for AA, the negatively charged ascorbic acid should be repelled from the surface while the neutral dopamine molecule passes through the membrane and is

detected at the electrode surface. The drawback of using such a membrane is a decrease in the response time of the electrode. This is a disadvantage if the electrode is to be used as an implantable biosensor giving fast feedback on fluctuating dopamine levels.

(b) The surface of the electrode can be anodically pretreated such that the oxidation peak of the ascorbic acid is shifted towards more positive potentials, and away from the peak potential of dopamine. On anodisation of the BDD electrode, oxygen functionalities (which replace the surface hydrogen atoms) are adsorbed onto the electrode surface. Fujishima et. al. [9] believe that these oxygen functionalities are highly oriented. They proposed that this highly oriented oxygen layer exerts a dipolar field. This field might be effective in repelling a molecule such as AA, which has four OH groups and one >C=O group on its periphery. Thus, the AA anodic peak position is expected to shift from its original position. The net effect is a dopamine and AA peak separation.

7.3.3 Dopamine in the presence of ascorbic acid

Figure 7.14 and **Figure 7.15** represents the cyclic voltammograms for a mixture of 0.2 mmol/L dopamine and 2 mmol/L ascorbic acid in 0.1 mol/L $HClO_4$ at a glassy carbon electrode and at a BDD electrode respectively. The concentration of the ascorbic acid was 10 times higher than that of dopamine.

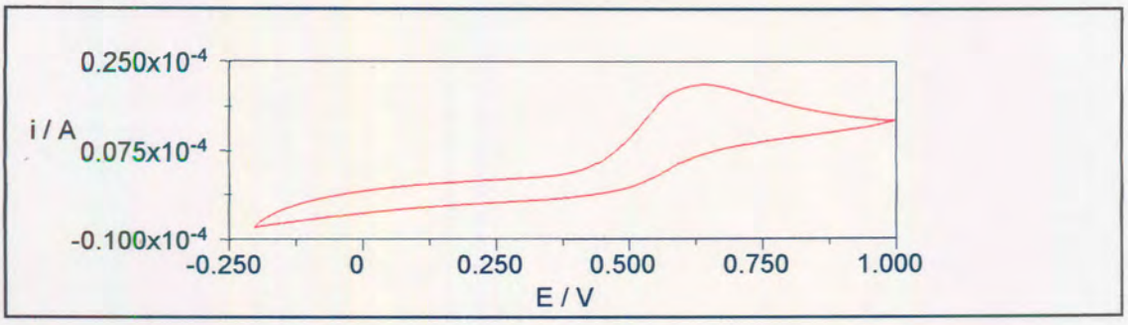

Figure 7.14 : Cyclic voltammogram for 0.2 mmol/L dopamine and 2 mmol/L ascorbic acid in 0.1 mol/L $HClO_4$ at a glassy carbon electrode - scan rate is 50 mV/s. E_i = -0.2 V, scan direction = positive.

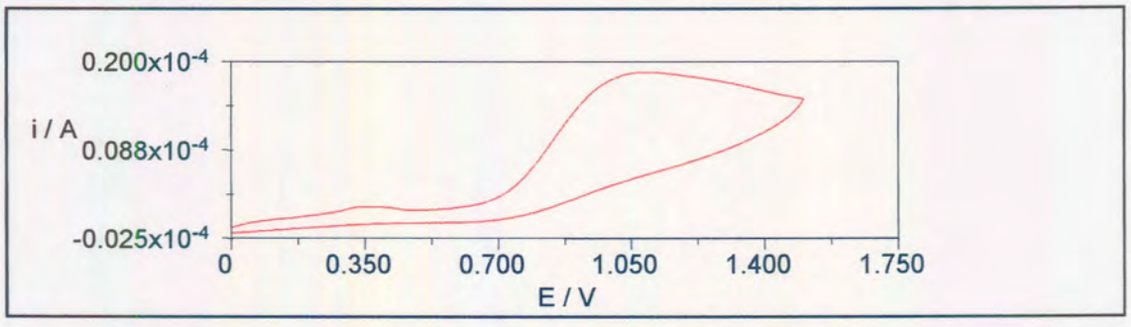

Figure 7.15 : Cyclic voltammogram for 0.2 mmol/L dopamine and 2 mmol/L ascorbic acid in 0.1 mol/L $HClO_4$ at a BDD electrode - scan rate is 50 mV/s. E_i = 0 V, scan direction = positive.

It is evident from the voltammograms shown in **Figures 7.14** and **7.15** that no separation of the AA and dopamine peaks was achieved. Voltammograms with a single broad peak were obtained due to the overlap of the individual peaks. The accumulative AA and dopamine oxidation peak is seen at approximately 0.62 V for the glassy carbon electrode and at approximately 1 V for the BDD electrode.

To detect dopamine in the presence of ascorbic acid, the method of anodic pretreatment was adopted. The BDD electrode was anodically treated at 2.7 V for 90 minutes in a strong base (KOH). The method for anodisation is described in **Section 5.3.2**. This method attaches oxygen functionalities to the diamond surface, thereby converting the surface from hydrophobic or partially hydrophobic to hydrophilic. By employing this method, the AA peak potential is shifted more positive, whilst the shift in the dopamine peak potential is negligible.

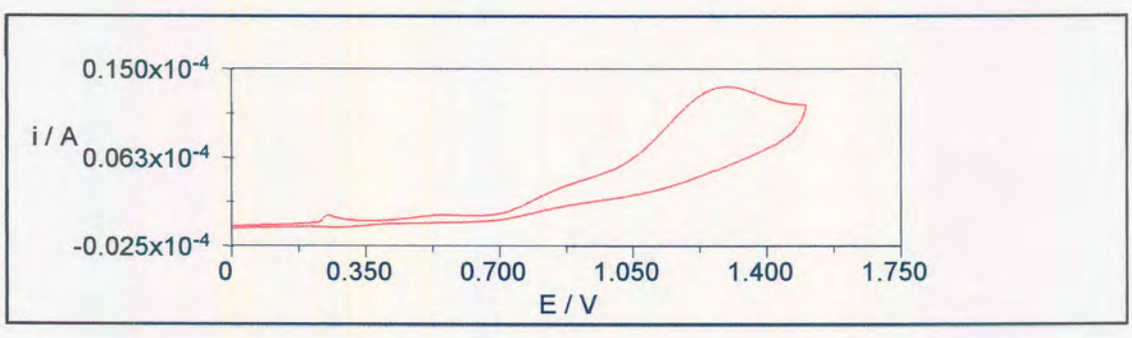

Figure 7.16 : Cyclic voltammogram for 0.2 mmol/L dopamine and 2 mmol/L AA in 0.1 mol/L $HClO_4$ at an anodised BDD electrode - scan rate is 50 mV/s. E_i = 0 V, scan direction = positive.

Figure 7.16 illustrates the cyclic voltammogram for 0.2 mmol/L dopamine and 2 mmol/L AA in 0.1 mol/L $HClO_4$ at an anodised BDD electrode. A distinct shoulder is observed at approximately 0.87 V. This shoulder can be attributed to the oxidation of dopamine. A well-defined oxidation peak occurs at approximately 1.3 V. This peak is most likely due to the oxidation of AA, and may be explained by the presence of highly oriented oxygen functionalities as proposed by Fujishima. et. al. [9] (see **Section 7.3.2**).

The boron concentration of the BDD electrode used in this investigation was 543 mg/L. According to the work undertaken by Fujishima et. al. [9], a BDD diamond electrode having a film resistivity in the order of 10^{-3} Ω.cm, was used to obtain an effective dopamine and AA peak separation. This led to the belief that in order to convert the observed dopamine shoulder (**Figure 7.16**) to a more prominent peak, a BDD electrode having a higher boron concentration (probably in the order of 10^{21} boron atoms.cm^{-3}) is necessary. BDD electrodes containing this amount of boron are referred to as being "heavily doped". A number of attempts were made to source "heavily doped" BDD electrodes from De Beers, but these are currently unavailable.

Unlike the glassy carbon electrode, the anodically pretreated BDD electrode is able to electrochemically distinguish between the dopamine and AA oxidation peaks without the use of a membrane, which is known to decrease the response time of an electrode. There is thus potential for a BDD electrode to be transformed into a microelectrode having a diameter similar to that of the common carbon fibre electrode (approximately 10 μm) developed by Gonon and his colleagues [7] in 1978. This microelectrode, after the anodisation pretreatment, can be inserted into the ECF in the brain for online *in vivo* monitoring of dopamine.

A proposed method [28] for a microelectrode fabrication to be used for the *in vivo* monitoring of dopamine could be the chemical vapour deposition of boron-doped diamond onto the tip of a microscopic substrate that resembles a needle-like structure. This needle could contain a tiny reference electrode as well as a counter electrode.

Electrical contact can be made using silver wire and/or silver paste. Silver is chosen since it is less harmful to the body than most other common electrical contacts such as copper.

7.4 Conclusion

The BDD electrode was found to be superior to the glassy carbon electrode in the detection of dopamine and AA. This is evidenced by the excellent R-square and percentage recovery values obtained for the BDD electrode as compared to the values obtained for the glassy carbon electrode. However, in comparison to glassy carbon, the rate of electron transfer at the BDD electrode surface was found to be slow.

The BDD electrode also appeared to be reproducible in both the dopamine and the AA systems. On comparison of the electrochemical behaviour of the De Beers BDD electrode to that of literature in the dopamine as well as the AA system, no significant difference was observed. The BDD electrode was found to be stable over a three month period in both the dopamine and AA systems. The detection limits for dopamine and AA at a BDD electrode surface were found to be 0.56 µmol/L and 20 nmol/L respectively. The expected concentrations of dopamine in tissue are 0.1 – 0.01 µmol/L (10 – 100 nmol/L) [29]. In order to achieve these detection limits, it is suggested that "heavily boron-doped" (10^{21} boron atoms.cm^{-3}) diamond electrodes be used.

In order to detect dopamine in the presence of AA, the BDD electrode may be anodically pretreated in 0.1 mol/L KOH solution. This pretreatment shifts the AA peak position

more positive and in so doing, the dopamine and AA peaks may be resolved. It appears therefore that an anodically pretreated BDD electrode would make an ideal biosensor for the detection of dopamine in the presence of ascorbic acid, since it is accurate, reproducible, resistant to fouling, reliable and most importantly biocompatible. However, further work needs to be done to improve the sensitivity of the BDD electrode to be used for dopamine detection. One possible method is to use a "heavily boron-doped" diamond sample as the electrode material. This is expected to increase the size of the dopamine peak. A prolonged electrode lifetime and stability study on the anodically pretreated BDD electrode is also essential in order for the eventual design and fabrication of an implantable microelectrode.

7.5 References

[1] http://www.onu.edu/user/FS/tfaulkner/Dopamine.htm

[2] P Capella, B Ghasemzadeh, K Mitchell and R N Adams, **Electroanalysis, 2** (1990) 175.

[3] J M Zen and I L Chen, **Electroanalysis, 7** (1997) 537.

[4] J A Stamford and J B Justice Jr., **Analytical Chemistry News & Features,** (1996) 359A.

[5] http://www.csuchico.edu/psy/BioPsych/neurotransmission.html

[6] http://www.utexas.edu/research/asrec/dopamine.html

[7] http://www.qmc.ac.uk/~physiol/aboutFCV.html

[8] P T Kissinger, J B Hart and R N Adams, **Brain Res., 55** (1973) 209.

[9] A Fujishima, T N Roa, E Popa, B V Sarada, I Yagi and D A Tryk, **J. Electroanalytical Chemistry, 473** (1999) 179.

[10] G A Gerhardt, A F Oke, G Nagy, B Moghaddam and R N Adams, **Brain Res., 290** (1984) 390.

[11] De Beers internal report by De Montfort University, Leicester, United Kingdom, 2000.

[12] G Heinrich, T Grögler, S M Rosiwal, R F Singer, **Surface and Coatings Technology, 94-95** (1997) 514.

[13] http://www.biosensor.com/bio/intro.htm

[14] http://www.biosensor.com/lead.htm

[15] http://www.cranfield.ac.uk/biotech/chinap.htm

[16] http://userpages.umbc.edu/~jshull/ench772/development

[17] http://www.hitl.washington.edu/scivw/EVE/I.D.1.c.Biosensors.html

[18] http://userpages.umbc.edu/~jshull1/ench772/intro

[19] http://userpages.umbc.edu/~jshull1/ench772/commercial

[20] http://www.cranfield.ac.uk/biotech/biosen_1.htm

[21] http://www.ibeweb.org/IBE2/news/news1.1/biotech.htm

[22] http://www.biosd.com/Biosensors.html

[23] M C Granger, M Witek, J Xu, J Wang, M Hupert, A Hanks, M D Koppang, J E Butler, G Lucazeau, M Mermoux, J W Strojek and G M Swain, **Anal. Chem., 72** (2000) 3793.

[24] S Hunt-Du Vall and R L McCreery, **Anal. Chem., 71** (1999) 4594.

[25] H Jaegfeldt, **J. Electroanal. Chem., 110** (1980) 295.

[26] J W Strojek, M C Granger and G M Swain, **Anal. Chem, 68** (1996) 2031.

[27] T W G Solomons, Organic Chemistry, 2nd Edition, John Wiley & Sons Limited, (1976) 707.

[28] S P J Higson and P M Vadgama, **Medical & Biological Engineering & Computing,** (1994) 601.

[29] Personal communication, Ms Jill van Veen, Neuroscience Laboratory and EEG unit, Johannesburg General Hospital, May (2001).

CHAPTER 8

Electroanalysis of organic systems via a bio-recognition element – thyroid hormones (L-T_3 and L-T_4)

8.1 Introduction

Thyroid hormones (iodinated amino acids), which are produced by the thyroid gland, are essential for adequate growth, development and energy metabolism [1]. In the foetus, they affect growth and differentiation, and in the mature human, they regulate metabolism. These hormones are secreted directly into the blood stream where they are transported to various cells and tissues in the body.

The two principal thyroid hormones are L-thyroxine (L-T_4) and L-triiodothyronine (L-T_3). The structures of these hormones are found in **Figures 8.1 and 8.2** respectively. L-T_4 has four iodine atoms attached to its aromatic rings, whereas L-T_3 contains three iodine atoms. These hormones are transported to various cells in the body via two plasma proteins, namely the thyroid hormone-binding globulin (TBG) and the thyroid hormone-binding prealbumin (TBPA). Only a small fraction (<0.3 %) of the total hormones in circulation is free. L-T_4, a prohormone, is converted into the more active L-T_3 by tissue deiodinases in the body. Approximately 90% of the L-T_3 in the body is formed by the

deiodination of L-T_4 [3]. The secretion of L-T_3 and L-T_4 by the thyroid gland is regulated by a complex system that originates in the central nervous system (CNS). Normal thyroid function yields about 28 – 50 µg of L-T_3 daily [3].

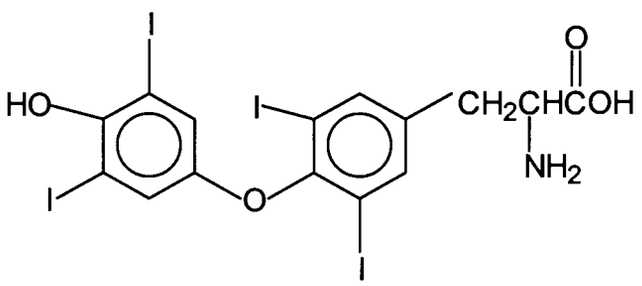

Figure 8.1 : Chemical structure of L-thyroxine (L-T_4) [2]

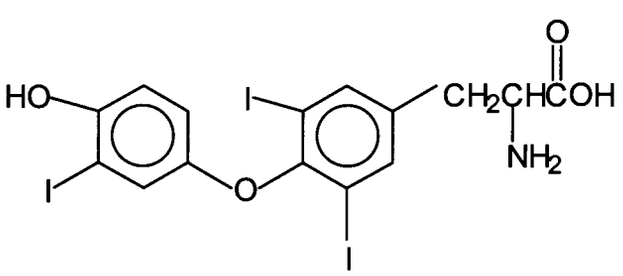

Figure 8.2 : Chemical structure of L-triiodothyronine (L-T_3) [2]

Since the L-T_3 and L-T_4 thyroid hormones affect growth in the foetus and regulate the metabolism of a mature human, the presence and equilibrium balance of these hormones are very important. It is common for humans in later life to develop thyroid hormone imbalances, and it is therefore necessary to be able to monitor these hormone levels in order to correct these imbalances by means of medication.

Classical methods of L-T_3 and L-T_4 analysis are very time consuming and more importantly, very expensive. An alternative technique that may be employed for the detection of L-T_3 and L-T_4, is voltammetry. In order to use this technique, the working electrode must be an immunosensor, which is very similar to a biosensor, except that it involves an antibody-antigen reaction [4].

Antibodies are proteins produced by B cells, which are designed to control the immune response in extracellular fluids. They are diverse, with more than 10^{10} possible variations, yet each antibody is designed to recognise only a specific antigen [5]. Antigens are foreign substances that enter the body, and are often proteins on the surface of bacteria and viruses [6]. Because of the ability of the antibody to recognise a specific antigen, an immunosensor is capable of selectively analysing for a biological compound in a complex matrix such as blood or ECF. An immunosensor is therefore said to function via a so-called bio-recognition system.

8.1.1 Bio-recognition system

A bio-recognition system (**Figure 8.3**) consists of bio-recognition elements (enzymes or antibodies) that are attached to an electrode surface [4,7-9]. Examples of potential electrode materials are diamond, glassy carbon, carbon paste, gold and platinum.

Once the bio-recognition element is immobilised on the electrode surface, the electrode is inserted into the sample matrix. The specific analyte of interest then combines with the

bio-recognition element in a "lock and key" [10] type mechanism. During this interaction, electrons are either released or consumed, depending on whether the reaction is an oxidation or reduction. The flow of electrons occurs via the electrode, and is recorded as a voltammogram.

For the thyroid hormone system, the mouse monoclonal anti-thyroxine (anti-T_4) combines with the L-T_4, thereby releasing electrons and hence producing an electrochemical signal. Likewise, the mouse monoclonal anti-triiodothyronine (anti-T_3) combines with the L-T_3 hormone to produce an electrochemical signal.

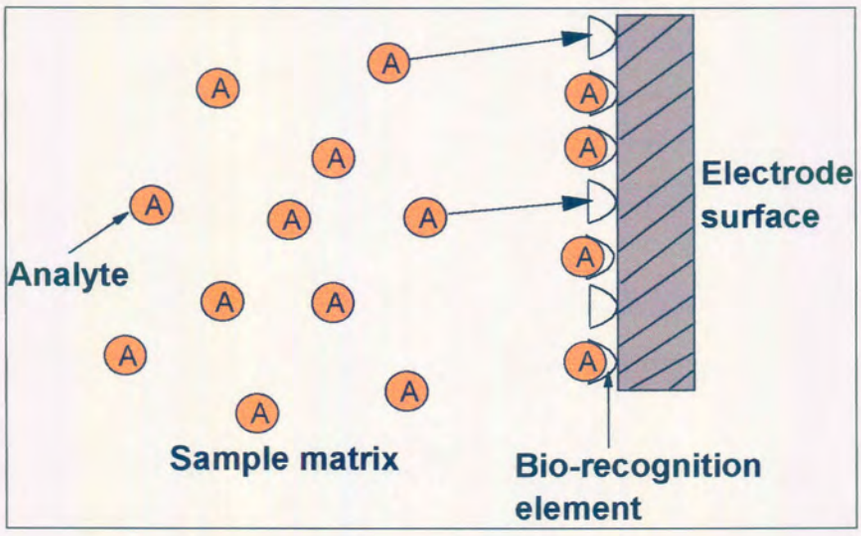

Figure 8.3 : Diagram illustrating a bio-recognition system

A bio-recognition element can be immobilised on an electrode surface using various techniques :

(a) The element can be chemically or physically adsorbed onto the electrode surface

(b) The electrode surface can be anodically treated such that the surface is terminated by oxygen functionalities. The bio-recognition element can then be chemically bound to these functionalities.

(c) Chemical attachment and entrapment of bio-recognition elements in conductive polymer matrixes, which are in contact with the electrode surface, can also be used.

(d) The bio-recognition element can be immobilised in a membrane, for example cellulose acetate. This membrane can then be attached to the electrode surface.

Bourdillon et. al. [11] attached a glucose oxidase conjugated antibody (antimouse IgG) to the surface of a glassy carbon electrode by soaking the electrode in the glucose oxidase solution overnight. Stefan et. al. [3] successfully impregnated graphite paste with mouse monoclonal anti-T_3. By using a chronoamperometric technique, the immunosensor was used for the L-T_3 assay at µg/L-ng/L concentration levels. There are as yet no reports in the literature describing the detection of thyroid hormones at diamond electrodes.

A number of methods may be used to attach anti-T_3 and anti-T_4 to a BDD electrode surface. If the anti-T_3 and anti-T_4 are to be entrapped in a membrane or a polymer, the construction of the immunosensor has to be reproducible, and it is known that there are inherent problems with reproducibility in this approach [12]. For this reason, an alternative novel method for the attachment of the anti-T_3 and anti-T_4 to the electrode surface was developed. This technique involves the absorption of the anti-thyroid hormones into the pores of a boron-doped porous diamond electrode.

8.1.2 Porous diamond electrode

The manufacture of boron-doped porous diamond may be accomplished by the high temperature, high pressure sintering of crushed boron-doped CVD diamond. According to the shape and size of the crushed diamond particles, as well as the sintering conditions, various pore shapes are possible : cylindrical pores (circular in cross-section), ink-bottle pores having a narrow neck and wide body, and slit-shaped pores with parallel plates [13]. As this is a new electrode material, no data regarding the pore structure of porous diamond electrodes exists yet. The pore volume and pore size distribution may be measured using mercury porosimetry or low temperature gas adsorption–desorption (BET method) [14]. However, the research work detailed below was an initial feasibility study of the use of porous diamond electrodes as thyroid immunosensors, and detailed measurements of the pore structure lay outside the scope of this work.

For the electrochemical detection of the thyroid hormones (L-T_3 and L-T_4), the anti-thyroid hormones (anti-T_3 and anti-T_4) must be incorporated in the pores of the BDD electrode. One method of accomplishing this is to allow the anti-thyroid hormones to diffuse into the pores of the electrode by soaking the electrode in the anti-thyroid solution, and to rely on capillary forces to retain the solution within the pores. It is vital that the anti-thyroid hormone remains in the pores when the electrode is subsequently immersed in the thyroid hormone solution: if the anti-thyroid hormone diffuses out of the pores, no antibody-antigen reaction will be recorded, and the electrochemical signal will be lost.

Figure 8.4 illustrates a schematic diagram of a porous diamond substrate containing the anti-thyroid hormones and the formation of an antibody-antigen complex. When an antibody encounters an antigen, the two establish a bond which stays intact indefinitely or for a time of the order of hours [15]. The mean time until the molecules dissociate again depends on the antibody. This implies that the immunosensor (porous diamond electrode/antibody system) will become inactive after a measurement, and will have to be regenerated in some way, or be discarded, i.e. a disposable immunosensor.

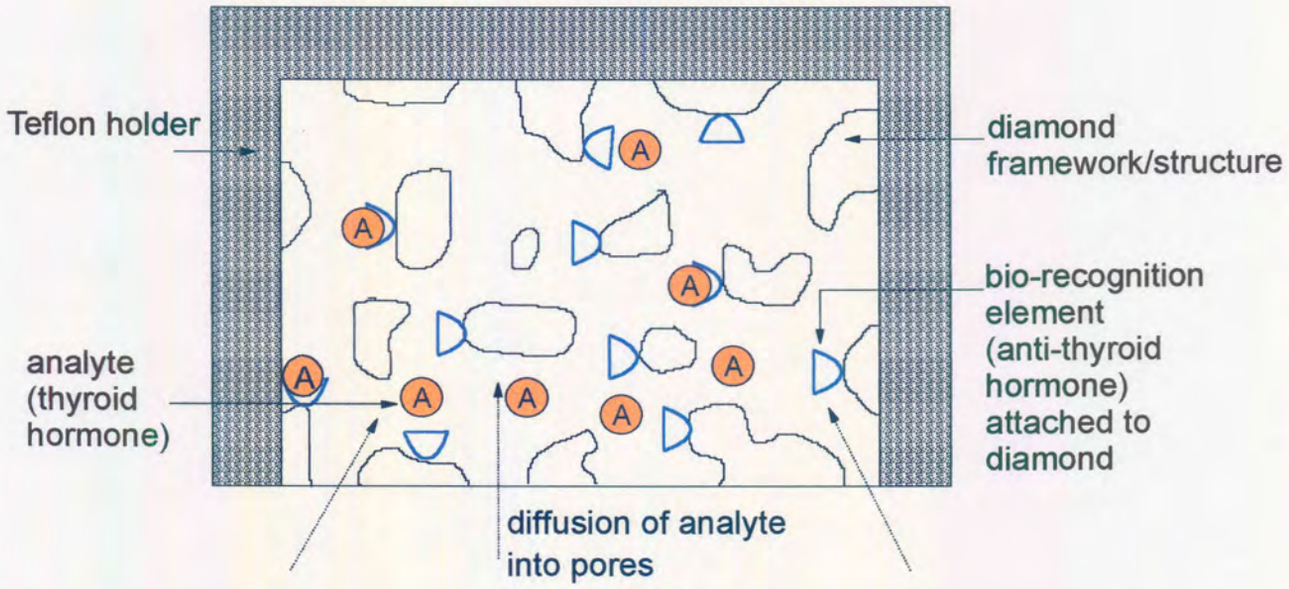

Figure 8.4 : Schematic diagram of a porous diamond substrate containing the anti-thyroid hormones and the formation of the antibody-antigen complex

8.2 Experimental

8.2.1 Crushing and sintering

Boron-doped CVD diamond webbing was crushed (to smaller size fractions) using iron rings in a ring crusher. Two size fractions were investigated: 49/57 US mesh (ca. 310 – 330 μm diameter) and 75/90 US mesh (ca. 180 – 200 μm diameter). During ring crushing of the CVD diamond, the diamond was inevitably contaminated with trace amounts of iron. Since iron is soluble in hydrochloric acid (HCl), the crushed CVD diamond was boiled in HCl to remove the iron impurity. The diamond particles were then compacted and sintered under high pressure and high temperature conditions. Afterwards, the sintered porous compact was lapped in order to produce discs of approximately 1 mm thickness and 20 mm diameter.

At this stage, the porosity of the two size fractions (49/57 US mesh and 75/90 US mesh) was determined by calculating the volume (π x radius^2 x height) of the circular lapped substrate. The theoretical mass of the substrate was then calculated (volume x density of diamond (3.51 g/cm^3)). Thereafter, the substrate was weighed and the percentage ratio of the actual mass over the theoretical mass was taken as a measurement of the porosity of the porous diamond. The porosity of the two size fractions was calculated to be 14% in each case. The porous diamond compact was then laser cut to size and inserted into a Teflon electrode holder as decribed previously in **Section 5.3.2**, to give a projected surface area of 0.15 cm^2.

8.2.2 Characterisation

Characterisation of the boron-doped porous diamond electrode was done using SEM, XPS and contact angle measurements.

One of the important milestones for the detection of the thyroid hormones using an immunosensor is the attachment of the antiserum in the pores of the BDD electrode. As mentioned previously, the antiserum may be absorbed into the pores by allowing the electrode to soak in the antiserum solution for a certain period of time. To determine the absorption kinetics, linear sweep voltammograms for the 75/90 US mesh porous BDD electrode were generated as a function of time in an ascorbic acid (AA) solution. Ascorbic acid was chosen since the solution is very stable, and the cyclic voltammograms that were generated thus far using the CVDBD electrodes were found to be very reproducible.

The surface chemistry of the porous BDD electrode was also manipulated in order to assess its effect on the electrochemical behaviour of the electrode.

8.2.3 Detection of thyroid hormones (L-T_3 and L-T_4)

The L-T_4 stock solution (12.51 mmol/L) was prepared by dissolving 0.064 g of solid L-T_4 in a mixture of 0.5886 g analytical grade sodium hydroxide (NaOH) and 4.738 g analytical grade ethanol. Similarly, L-T_3 stock solution (14.27 mmol/L) was prepared by

dissolving 0.0641 g of solid L-T_3 in a mixture of 0.6 g analytical grade NaOH and 4.8 g analytical grade ethanol. Both the thyroid hormones (L-T_3 and L-T_4) were obtained from Sigma Aldrich. The NaOH and ethanol were obtained from Saarchem.

The anti-T_3 was diluted to a working dilution of 1:70 in 0.01 mol/L phosphate buffered saline, pH = 7.4, containing 0.1% sodium azide, whilst the anti-T_4 was diluted to a working dilution of 1:40 in 0.01 mol/L phosphate buffered saline, pH = 7.4, containing 0.1% sodium azide. The 0.01 mol/L phosphate buffered saline solution was prepared using ultrapure water from a Millipore purification system (18 μΩ.cm). After preparation, both the antiserum solutions were stored at 0°C. The antiserums (anti-T_3 and anti-T_4) were obtained from Sigma Adrich.

To speed up the process of impregnating the porous electrode with antiserum, a vacuum dessicator was used. Basically, the porous BDD was inserted into the antiserum solution and the solution together with the porous BDD was placed in a dessicator. A vacuum pump was connected to the dessicator and switched on. The vacuum thus created in the pores caused the liquid antiserum to be drawn quickly and efficiently into the pores of the electrode. The duration of the vacuum treatment was 10 minutes. After this period, the porous BDD electrode was removed from the antiserum solution and inserted into the Teflon electrode holder using carbon paste.

Electrochemical experiments were performed using an AutoLab PGStat 100 with the AutoLab GPES software. A porous BDD electrode, Ag/AgCl electrode and a platinum

electrode served as the working, reference and counter electrodes in the cell respectively. Cyclic voltammetry scans were initially performed in a phosphate buffered saline solution, pH = 7.4, containing 0.1% sodium azide, before and after the addition of L-T_3 and L-T_4, in order to optimise the working conditions for the chronoamperometry technique. Chronoamperometry techniques were used to obtain the detection limits of both L-T_3 and L-T_4.

After each voltammetric measurement, the surface of the porous BDD electrode was cleaned by boiling it in HCl. All measurements were carried out at room temperature (25°C) and at a pH = 7.4 in a deaerated, stationary analyte solution. The projected surface area of the 75/90 US mesh porous BDD electrode used in the experiments was 0.15 cm^2.

8.3 Results and discussion

8.3.1 Characterisation of the porous BDD electrode

8.3.1.1 Surface morphology

The morphology of the two porous BDD electrodes (made from 49/57 US mesh and 75/90 US mesh size fractions) was viewed under the SEM. **Figure 8.5** and **Figure 8.6** represents the SEM image of the 49/57 US mesh and 75/90 US mesh electrodes respectively. Randomly oriented facets can be seen in both the SEM images. The surface of the diamond is very rough and the presence of pores can be clearly seen. The pores appear to be randomly distributed, with a variation in the pore size.

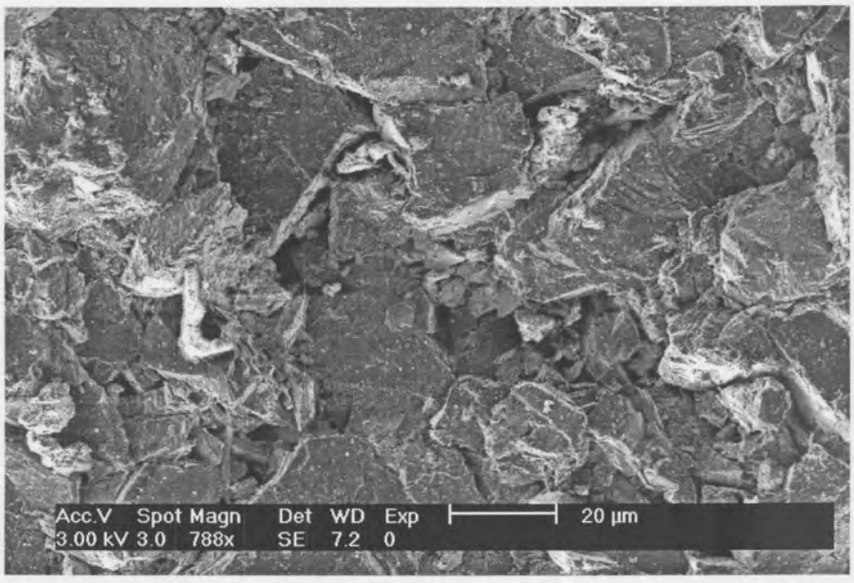

Figure 8.5 : SEM image depicting the surface of the 49/57 US mesh porous BDD size fraction

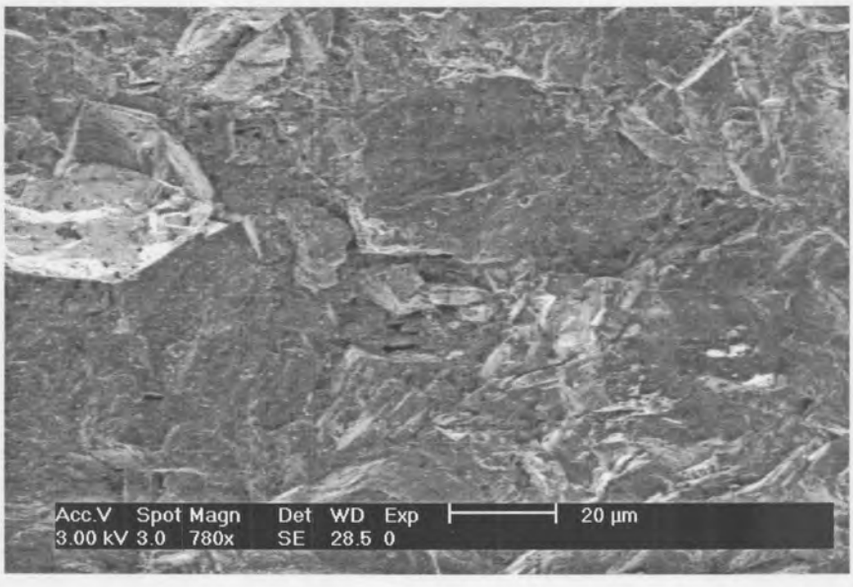

Figure 8.6 : SEM image depicting the surface of the 75/90 US mesh porous BDD size fraction

The surface of the 75/90 US mesh electrode was analysed using energy dispersive spectroscopy (EDS). The presence of trace amounts of iron was again detected in the EDS spectrum. It is assumed that this contaminant was introduced during ring crushing of the boron-doped CVD webbing using iron rings, and was not entirely removed by treating the crushed diamond powder with HCl, prior to sintering. Subsequent treatment of the sintered porous diamond with HCl effectively removed these traces of iron.

8.3.1.2 Surface chemistry

The contact angles (**Table 8.1**) of the two electrodes were measured to determine their surface state. The surfaces were found to be only partially hydrophobic, with the 49/57 US mesh electrode slightly more hydrophobic than the 75/90 US mesh electrode. This indicates that the surface of the diamond contains oxygen functionalities.

Table 8.1 : Contact angle measurements for the two porous BDD electrodes

Size fraction	Contact angle		
	Range / °	Average/ °	Std Deviation
49/57 US mesh	58 - 71	64.70	6.29
75/90 US mesh	43 - 57	52.55	5.02

The oxygen content of the 75/90 US mesh porous BDD electrode was determined using XPS (**Figure 8.7**). The oxygen content of the porous diamond was found to be 2.69 x 10^{15} atoms/cm^2 and the surface oxygen coverage was found to be 1.4 monolayers.

UNIVERSITEIT VAN PRETORIA
UNIVERSITY OF PRETORIA
YUNIBESITHI YA PRETORIA

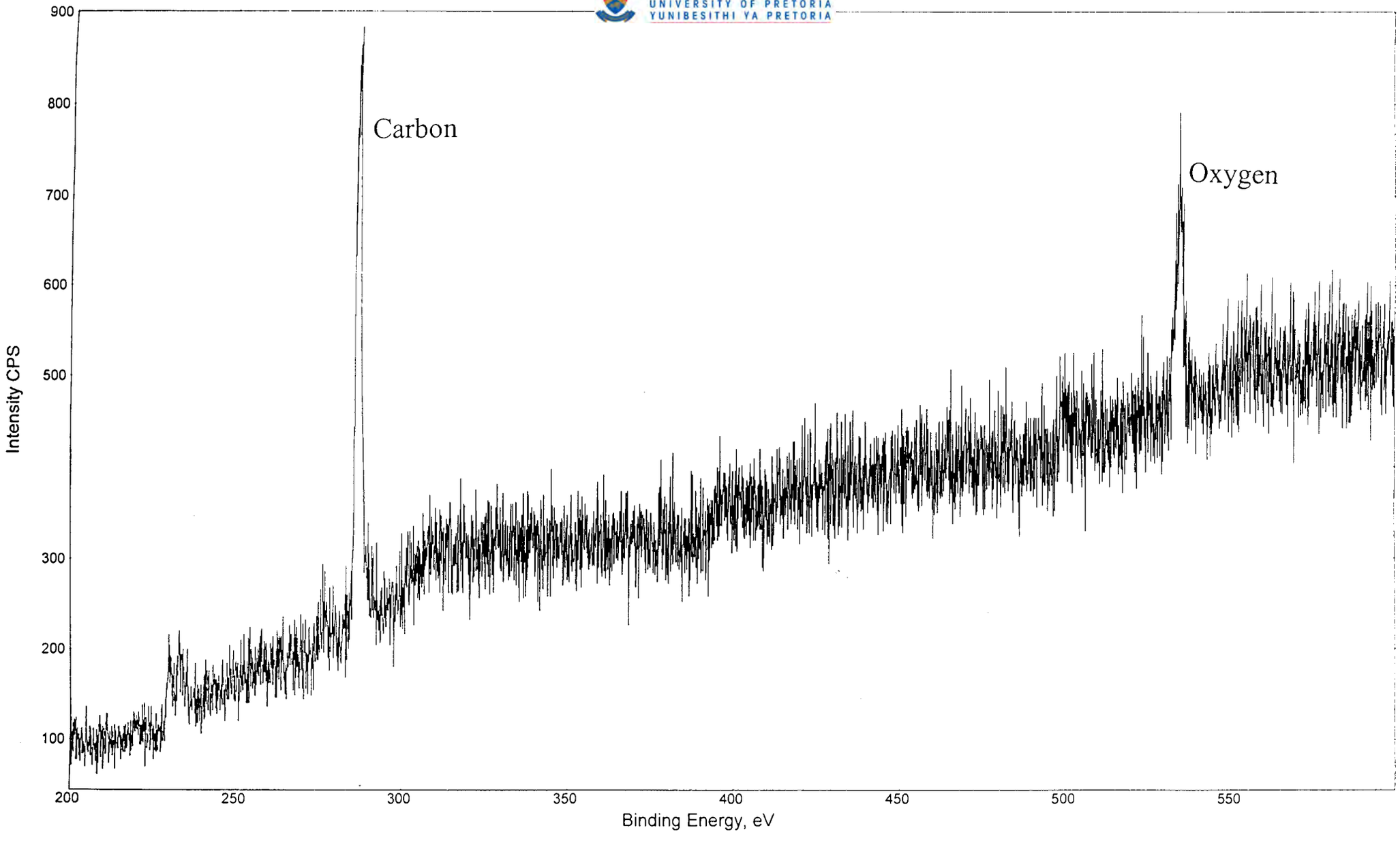

Figure 8.7 : XPS spectrum for the 75/90 US mesh porous BDD electrode

Contact angle measurements taken after treatment of the porous electrodes to remove trace iron impurities revealed that the hydrophilic/hydrophobic nature of the surface was not significantly changed.

8.3.1.3 Electrochemical behaviour of porous BDD electrodes

Figure 8.8 illustrates the cyclic voltammograms for 0.1 mol/L $HClO_4$ before and after HCl treatment at a 75/90 US mesh porous BDD electrode. A large baseline current is observed in the porous BDD electrode before treatment in HCl. This may be due to the presence of oxygen functionalities on the electrode surface and/or trace amounts of iron. A redox couple, probably the Fe^{2+}/Fe^{3+} couple, is also evident. Subsequent treatment in HCl may have caused some of the surface functionalities to become hydrogen terminated, thus decreasing the observed baseline current. The redox couple was also absent.

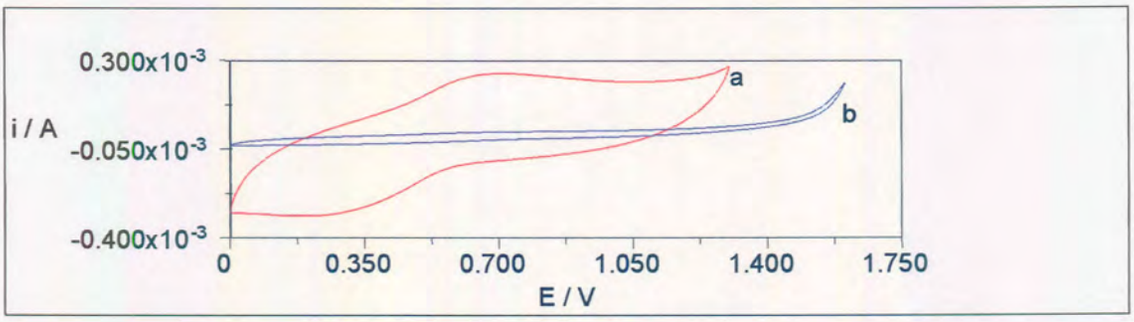

Figure 8.8 : Cyclic voltammograms for 0.1 mol/L $HClO_4$ at a 75/90 US mesh porous BDD electrode, (a) before HCl treatment, (b) after HCl treatment - scan rate is 50 mV/s. E_i = 0 V, scan direction = positive

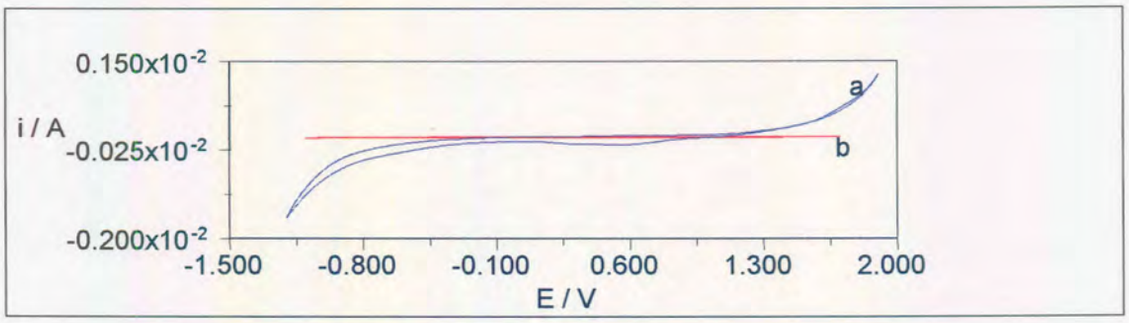

Figure 8.9 : Cyclic voltammograms for 0.5 mol/L $HClO_4$ at a 75/90 US mesh porous BDD electrode as well as at a CVDBD4 electrode : (a) 75/90 US mesh porous BDD electrode, (b) CVDBD4 electrode – scan rate is 50 mV/s.

Figure 8.9 represents the cyclic voltammograms for 0.5 mol/L $HClO_4$ at a 75/90 US mesh porous BDD electrode as well as at a CVDBD4 electrode. The baseline current for the 75/90 US mesh porous BDD electrode is much larger than that of the CVDBD4 electrode. This could be attributed to the increased surface area of the 75/90 US mesh diamond caused by an increase in the porosity, or the hydrophilic nature of the 75/90 US mesh diamond caused by oxygen functionalities on the electrode surface : the presence of these functionalities are known to make the diamond electrode more electroactive.

A further cause of the increased baseline current for the 75/90 US mesh porous BDD electrode could be the presence of non-diamond carbon on the electrode surface. This non-diamond carbon could have formed during the high pressure, high temperature sintering of the crushed CVD diamond. In order for diamond to convert to graphite, the presence of solvent metal catalysts (for example iron) is necessary. The EDS spectrum (discussed earlier) shows that trace amounts of iron were present on the electrode surface

after the sintering process. Iron could have therefore catalysed the conversion of diamond to graphite.

It is also evident from the cyclic voltammogram shown in **Figure 8.9**, that the potential window for water electrolysis for the 75/90 US mesh porous BDD electrode has decreased when compared with the CVDBD4 electrode. Oxygen evolution begins at approximately 1.4 V, whilst hydrogen evolution starts at about –0.8 V.

Figure 8.10 shows the cyclic voltammogram for 0.1 mol/L $HClO_4$ at a 75/90 US mesh and at a 49/57 US mesh porous BDD electrode respectively. It is apparent that the baseline current for the 49/57 US mesh electrode is greater than the baseline current for the 75/90 US mesh electrode. This could be due to surface area effects or the presence of non-diamond carbon on the surface of the 49/57 US mesh electrode.

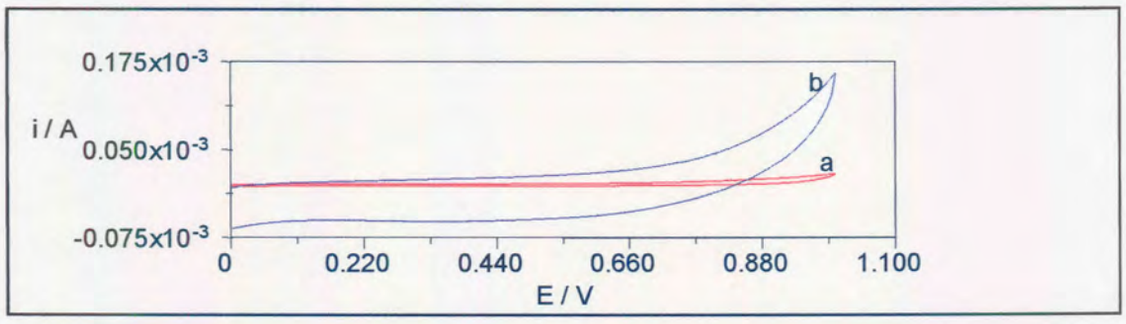

Figure 8.10 : Cyclic voltammogram for 0.1 mol/L $HClO_4$ at a 75/90 US mesh (a) and at a 49/57 US mesh (b) porous BDD electrode – scan rate is 50 mV/s. E_i = 0 V, scan direction = positive

The surface chemistry of the 49/57 US mesh porous BDD electrode was modified by boiling the electrode in chromic acid (0.5 g potassium dichromate in 100 ml sulphuric acid) in order to oxidise the surface of the electrode. This surface manipulation was performed in order to observe the effect of the surface state of the electrode on its electrochemical behaviour.

Figure 8.11 illustrates the cyclic voltammogram for 0.1 mol/L $HClO_4$ at a 49/57 US mesh porous BDD electrode before and after treatment. After the chromic acid treatment, the baseline current had increased tremendously with the additional occurrence of a redox couple which could be due to the presence of chromium. The oxidation potential of the redox couple occurs approximately 0.5 V and the reduction potential occurs at about 0.3 V. **Equations 8.1** and **8.2** depict the reduction of two chromium species [16]. The relevant reduction potentials of the chromium species versus a hydrogen reference electrode as well as a Ag/AgCl reference electrode are shown in **Table 8.3** [16].

$$Cr_2O_7^{2-} + 14H^+ + 6e^- \leftrightarrow 2Cr^{3+} + 7H_2O \qquad (8.1)$$

$$Cr^{6+} + 3e^- \leftrightarrow Cr^{3+} \qquad (8.2)$$

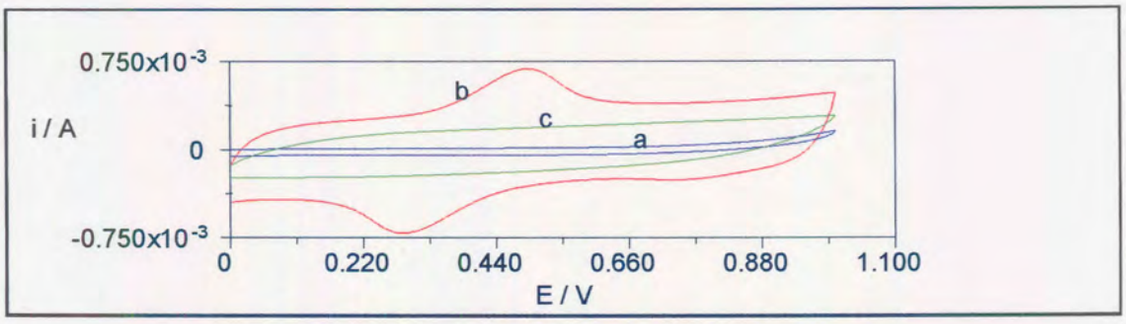

Figure 8.11 : Cyclic voltammogram for 0.1 mol/L $HClO_4$ at a 49/57 US mesh porous BDD electrode before and after treatment : (a) HCl treated 49/57 US mesh electrode, (b) 49/57 US mesh electrode after treatment in chromic acid, (c) 49/57 US mesh electrode after treatment in chromic acid, then boiled in HCl – scan rate is 50 mV/s. E_i = 0 V, scan direction = positive

It is apparent that the oxidation and reduction potentials of the redox couple shown in **Figure 8.11** are higher than the standard reduction potentials of the chromium species indicated in **Table 8.3**. However, this shift in peak potentials could be ascribed to the electrode material being used.

Table 8.3 : Reduction potentials of chromium species

Reduction reaction	Potential / V	
	Hydrogen reference electrode	Ag/AgCl reference electrode
$Cr_2O_7^{2-} + 14H^+ + 6e^- \leftrightarrow 2Cr^{3+} + 7H_2O$	1.33	1.11
$Cr^{6+} + 3e^- \leftrightarrow Cr^{3+}$	1.10	0.88

The contact angle of the 49/57 US mesh porous BDD electrode was measured after the chromic acid treatment and was found to be 0°. This implies the surface of the electrode to be extremely hydrophilic with numerous oxygen functionalities attached to the electrode surface. The hydrophilic nature of the electrode surface could explain the observed increase in the baseline current.

Interestingly, when the 49/57 US mesh porous BDD electrode was subsequently boiled in HCl, the assumed chromium redox couple was absent (**Figure 8.11**). In addition, the baseline current was also reduced in magnitude. It appears that the HCl removed the chromium from the surface of the electrode and partially terminated the electrode surface with hydrogen atoms, possibly making the electrode surface more hydrophobic. This would explain the observed decrease in the baseline current.

8.3.2 Absorption kinetics

Figure 8.12 illustrates the absorption curve for 2 mmol/L AA in 0.1 mol/L $HClO_4$ at a 75/90 US mesh porous BDD electrode. Linear sweep voltammograms (background corrected) were generated every hour for the period that the electrode was in contact with the stationary AA solution.

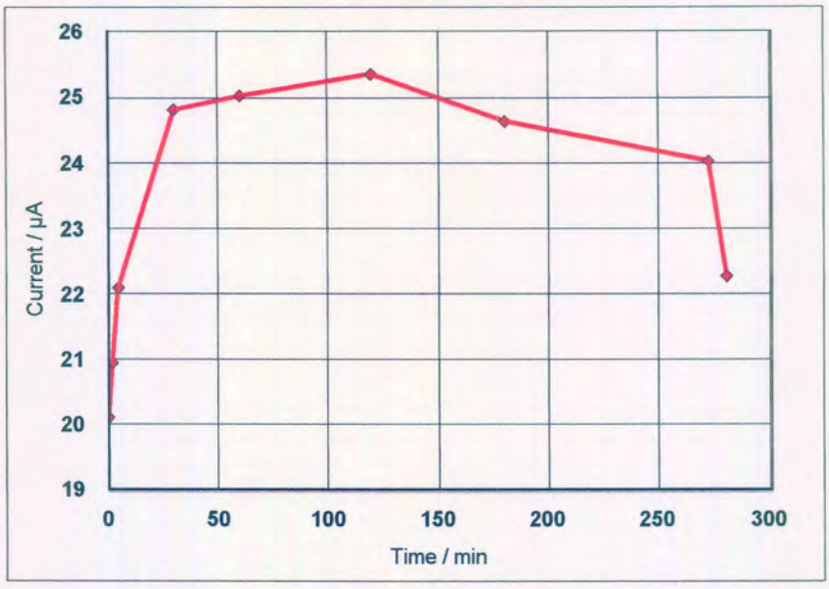

Figure 8.12 : Absorption curve for 0.6 mmol/L AA in 0.1 mol/L $HClO_4$ at a 75/90 US mesh porous BDD electrode

It can be seen from **Figure 8.12** that the current increased steeply for the first 30 minutes, then gradually increased for the next 100 minutes. Afterwards, the current began to slowly decrease. The increase in current is thought to be due to the diffusion of the AA into the pores of the BDD electrode, which effectively increased the electrode surface area in contact with the solution. The decrease in current after 120 minutes is ascribed to the depletion of AA in the pores during the periods when the potential was applied. Replenishment of AA in these pores, especially those deepest inside the electrode, would be retarded by diffusion, and by the fact that the capillary interaction which initially would have helped the pores to fill relatively quickly with AA, would no longer play a role once the pores were filled with liquid.

In all, it can be inferred from **Figure 8.12** that in order for the antiserum to absorb into the pores of the BDD electrode, the electrode will have to be soaked in the antiserum solution for a period of no less than two hours.

8.3.3 Detection of thyroid hormones (L-T_3 and L-T_4)

8.3.3.1 Detection of L-T_4

The antiserum (anti-T_3 or anti-T_4) was intially absorbed into the pores of the 75/90 US mesh BDD electrode by allowing the electrode to soak in the antiserum solution for a period of two hours. A linear sweep voltammogram (background current for 0.01 mol/L phosphate buffered saline, containing 0.1% sodium azide subtracted) for 0.44 mmol/L L-T_4 in 0.01 mol/L phosphate buffered saline was generated (**Figure 8.13**).

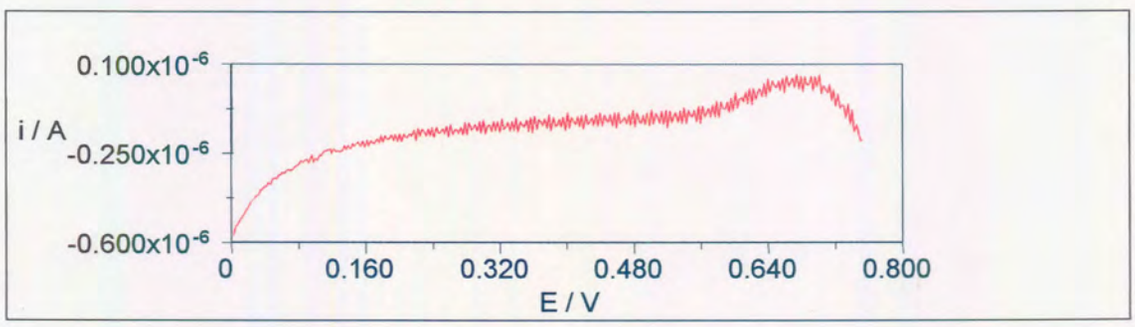

Figure 8.13 : Linear sweep voltammogram for 0.44 mmol/L L-T_4 in 0.01 mol/L phosphate buffered saline containing 0.1% sodium azide, pH = 7.4 – scan rate is 50 mV/s. E_i = 0 V, scan direction = positive.

An oxidation peak, which probably occurs as a result of the formation of the antigen-antibody complex, is seen at approximately 680 mV. Considering the potential at which this peak occurred, the chronoamperometric technique was performed at an optimum potential of 780 mV vs the Ag/AgCl electrode. The potential, however, was applied in two stages. The initial applied potential was 100 mV with a duration of 5 seconds. The potential was then stepped up to 780 mV.

During the course of the chronoamperometry measurements, it was found that the immunosensor was only able to detect the presence of L-T_4 on the first voltammetric scan. The subsequent scans did not yield an increase in the observed current. It was thought that the antiserum may be diffusing out of the diamond electrode pores, thereby resulting in a decrease in the observed signal.

The antiserum was thus drawn into the electrode pores using a vacuum dessicator technique. This technique proved to be quite effective in that the subsequent scans also showed an increase in the observed current. **Figure 8.14** shows a chronoamperometric scan for 0.01 mol/L phosphate buffered saline before and after the addition of 17.51 µmol/L L-T_4.

A definite increase in the current is observed on addition of 17.51 µmol/L L-T_4. This increase in the current was initially thought to be due to the presence of NaOH and ethanol in the solution. However, subsequent scans carried out in 0.01 mol/L phosphate buffered saline containing small quantities of NaOH and ethanol, failed to yield an

increase in the current. Thus, the increase in the observed current (**Figure 8.14**) is definitely due to the presence of L-T_4. According to **Figure 8.14**, a plateau was reached after approximately 16 seconds. The lower detection limit for L-T_4 was found to be 12.51 µmol/L. At the other end of the scale, L-T_4 concentrations above 37.53 µmol/L could not be detected, due to the precipitation of L-T_4 in solution.

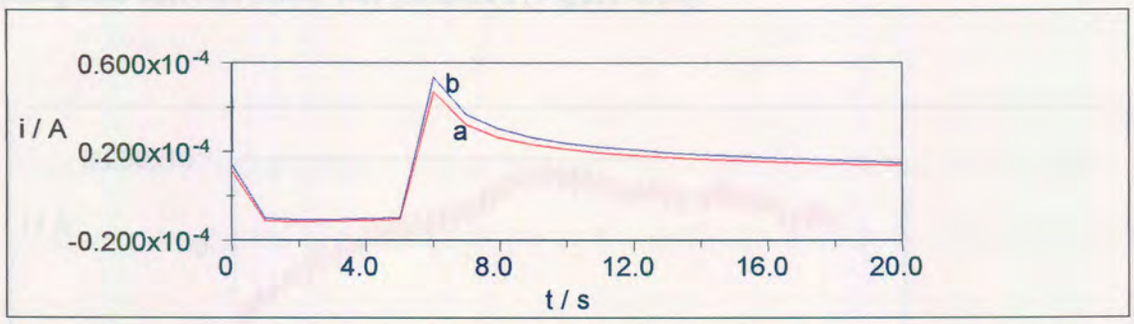

Figure 8.14 : Chronoamperometric scan for 0.01 mol/L phosphate buffered saline before (a) and after (b) the addition of 17.51 µmol/L L-T_4

Although the porous BDD electrode was successful in the detection of L-T_4, the immunosensor response was found to be very irreproducible. Thus a calibration plot for the L-T_4 assay could not be generated. The irreproduciblity of the porous BDD electrode could be due to the questionable reproducibility of the vacuum dessicator technique in impregnating the diamond pores with the antiserum or it may be due to differences in the diffusion rate of the phosphate buffer and L-T_4 solution into the electrode pores.

The immobilisation of the antiserum in the diamond electrode pores may be improved by blending the antiserum in a gel and then impregnating the pores with this gel containing antiserum. The gel should ideally not hinder the electrochemical detection of L-T_4.

Another method for the attachment of the antiserum onto the electrode surface is through the use of a membrane. However, both these methods are expected to further decrease the response time of the electrode.

The diffusion rate of the phosphate buffer and L-T_4 solution could be increased by oxygen terminating the surface of the porous BDD electrode, thereby making the surface hydrophilic. In this way, the electrolyte would wet the electrode surface more easily and diffuse into the electrode pores at a much faster rate. The response of the porous BDD electrode may be made more consistent by integrating the area under the chronoamperometric peak as a function of time, so that small differences in diffusion rates and response times would be eliminated. In this way, a calibration curve may be drawn.

A further improvement on the detection limit and sensitivity of the porous BDD electrode in the L-T_4 assay would be to decrease the baseline current obtained. This can be achieved by hydrogen terminating the electrode surface. However, a hydrogen terminated electrode surface may decrease the diffusion rate of the analyte into the electrode pores, due to poor wetting of the electrode surface by the solution. The baseline current can also be decreased by the removal of any non-diamond carbon present on the electrode surface. It is suspected that the surface of the 75/90 US mesh porous BDD electrode contained non-diamond carbon (as discussed previously under **Section 8.3.1.3**). The presence of this graphitic carbon may have resulted in the increased baseline current observed which would have negatively affected the detection limit of L-T_4.

8.3.3.2 Detection of L-T_3

For the detection of L-T_3, the corresponding antiserum was impregnated in the pores of the 75/90 US mesh BDD electrode using the vacuum dessicator technique. A background current corrected linear sweep voltammogram for 51 µmol/L L-T_3 in 0.01 mol/L phosphate buffered saline was generated (**Figure 8.15**).

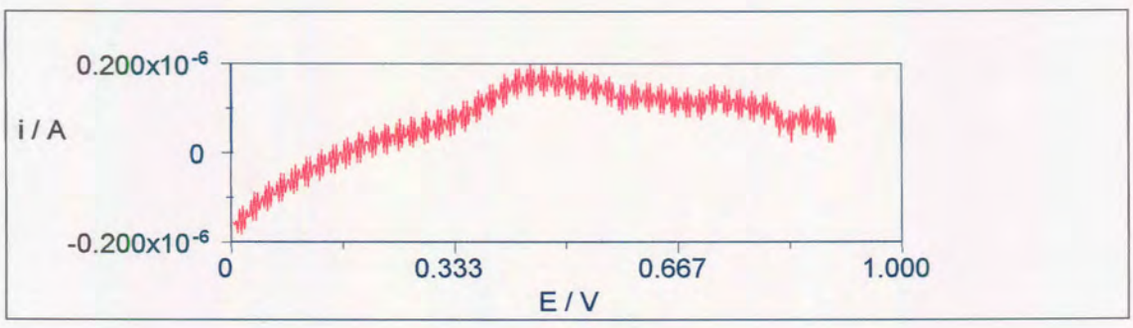

Figure 8.15 : A background current corrected linear sweep voltammogram for 51 µmol/L L-T_3 in 0.01 mol/L phosphate buffered saline – scan rate is 50 mV/s. E_i = 0 V, scan direction = positive

An oxidation peak is evident at approximately 500 mV. This peak is most probably due to the formation of the antigen-antibody complex. In view of the oxidation peak potential, the chronoamperometric technique was performed at an optimum potential of 780 mV vs the Ag/AgCl electrode. The potential was again applied in two stages : the initial applied potential was 100 mV and the subsequent applied potential was increased to 780 mV.

Figure 8.16 illustrates a chronoamperometric scan for 0.01 mol/L phosphate buffered saline solution before and after the addition of 14.27 µmol/L L-T_3 at a 75/90 US mesh

porous BDD electrode. A plateau was reached after 18 seconds. The lower limit of detection for L-T_3 was found to be 856 nmol/L.

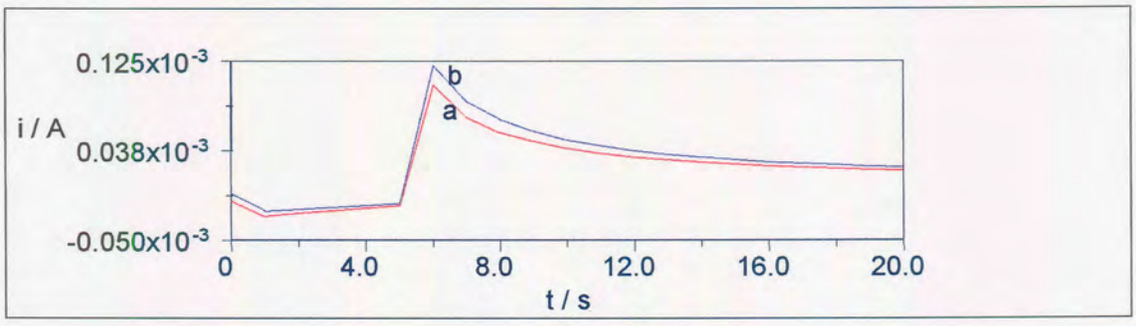

Figure 8.16 : Chronoamperometric scan for 0.01 mol/L phosphate buffered saline solution, pH = 7.4, (a) before addition of 14.27 µmol/L T_3, (b) after addition of 14.27 µmol/L L-T_3.

Due to the irreproducible nature of the 75/90 US mesh porous BDD electrode in the L-T_3 system (for the reasons mentioned previously), a calibration plot could not be generated.

8.4 Conclusion

Porous BDD electrodes were successfully used to analyse for L-T_3 and L-T_4 in synthetic samples, by impregnating the electrode with antiserum using a vacuum technique. The lower limit of detection for L-T_3 was found to be 856 nmol/L, while that of L-T_4 was 12.5 µmol/L. As the respective concentrations of free L-T_3 and L-T_4 in the blood are 0.89 pmol/L and 0.031 nmol/L (2.97 nmol/L and 0.103 µmol/L respectively protein-bound)[1], further work is necessary to improve the sensitivity of this immunosensor.

The response of the porous BDD electrode was found to be highly dependent on its surface state, with a hydrophobic surface giving a lower baseline than that of a hydrophilic surface.

Problems were experienced with reproducibility in both the L-T_3 and L-T_4 cases, and were thought to be related to the electrode surface state, and/or the impregnation and retention of the antiserum in the pores.

In conclusion, the feasibility of using porous BDD electrodes for the detection of thyroid hormones has been demonstrated. In order to develop a commercial diamond biosensor for thyroid hormone detection based on this material, further work is required to improve the sensitivity and reproducibility of the electrode.

Generally, the porous BDD electrode offers a significant advantage over a CVD BDD electrode, as it is much cheaper to manufacture, and may be manufactured to have a vastly increased surface area, which opens up possibilities of future application in systems where the analyte is present in very low concentrations. These systems vary from biological or medical to wastewater applications.

8.5 References

[1] Kirk-Othmer, **Encyclopaedia of Chemical Technology,** 3rd Edition, Wiley-Interscience, Vol 23, (1984) 1.

[2] J C Creager, **Human Anatomy and Physiology,** 2nd Edition, Wm.C. Brown Publishers, (1992).

[3] H Y Aboul-Enein, R I Stefan, G L Radu and G E Baiulescu, **Analytical Letters, 32**, (1999), 447.

[4] http://userpages.umbc.edu/~jshull1/ench772/construction

[5] http://wilson-squier.ucsd.edu/research/sb/ve/immunology/molecules1.html

[6] http://www.hon.ch/Library/Theme/Allergy/Glossary/ig.html

[7] http://www.devicelink.com/ivdt/archive/97/07/010.html

[8] http://www.ibeweb.org/IBE2/news/news1.1/biotech.htm

[9] http://bioinfo.weizmann.ac.il/_1s/meir_wilchek/meir_wilchek.html

[10] R I Stefan, J F van Staden and H Y Aboul-Enein, **Fresenius J. Anal. Chem., 366** (2000) 659.

[11] C Bourdillon, C Demaille, J Moiroux and J M Savéant, **J. Am. Chem. Soc., 117,** (1995), 11499.

[12] Private communication , R I Stefan, University of Pretoria, August (2000).

[13] http://hplc.chem.shu.edu/NEW/HPLC_Book/Adsorbents/ads_pore.html

[14] S J Gregg, K S W Sing and H F Stoeckli, **Characterisation of porous solids,** London: Society of Chemical Industry, (1979) 369.

[15] http://www2.uni-linz.ac.at/fak/TNF/theophys/group/kat/da/da.html

[16] R C Weast, **CRC Handbook of Chemistry and Physics,** 54th Edition, (1973).

CHAPTER 9

Conclusions

The as-received samples were characterised using various techniques, namely SEM, LA-ICP-MS, Raman spectroscopy and XPS. Contact angle and resistance measurements were also performed. SEM analysis showed the surface of the boron-doped samples to have randomly oriented facets, whilst LA-ICP-MS measurements indicated that CVDBD2 contained the lowest boron concentration and CVDBD6 contained the highest boron concentration. It was inferred from the Raman spectroscopy analysis, that the presence of boron in the boron-doped CVD samples seems to suppress the formation of sp^2 carbon.

Using XPS, the oxygen content of the as-received CVDBD4 sample was found to be 2.37 x 10^{15} atoms/cm^2, with a surface oxygen coverage of 1.26 monolayers. The contact angle measurements revealed CVDBD1 and CVDBD2 to be hydrophobic, CVDBD3 and CVDBD4 to be partially hydrophobic and CVDBD5 and CVDBD6 to be more hydrophilic. The resistance measurements showed CVDBD2 and CVDBD3 to have a low conductivity, whilst CVDBD4 – CVDBD6 were found to have a high conductivity. Thus, the minimum level of boron required to make diamond a suitable electrode material was found to be 500 mg/L.

Various hydrogenation (tube furnace, TGA and hydrogen plasma) and oxygenation (tube furnace, TGA, chromic acid and anodisation) techniques were employed to modify the surface state of the boron-doped diamond electrodes. This investigation was deemed necessary since literature reports that the surface state of the electrode may significantly affect its electrochemical behaviour. The most effective hydrogenation technique was found to be the hydrogen plasma treatment (yielding a very hydrophobic surface), whilst all of the oxygenation techniques investigated were successful in producing a very hydrophilic electrode surface.

However, one of the drawbacks in producing an oxygen terminated electrode surface is the formation of boron oxide on the surface. Boron oxide could drastically affect the observed electrochemical signal. It is therefore proposed that in order to minimise the formation of boron oxide, mild oxygenation methods should be used, for example heat treating the boron-doped diamond sample in air at temperatures below 250°C for a short peroid of time or boiling the diamond sample in hydrogen peroxide for short intervals.

On investigating the electrochemical behaviour of various boron-doped CVD diamond electrodes, it was found that, as the boron concentration of the electrode increases, the potential window decreases. However, it was also found that the potential window for the highest boron-doped diamond electrode (CVDBD6) was still wider than that of the glassy carbon electrode, thereby confirming the advantage that the BDD electrode has over glassy carbon when investigating aqueous systems.

The electrochemical behaviour of two redox systems was investigated, namely potassium iron (III) cyanide and cerium (III) sulphate. It was found that the electrochemical behaviour of the potassium iron (III) cyanide redox couple was very complex when a boron-doped diamond electrode was used. The peak separation of the $[Fe(CN)_6]^{3-}$ /$[Fe(CN)_6]^{4-}$ redox couple (690 mV) was found to be an order of magnitude larger than that of the glassy carbon electrode (61 mV). It is suggested that oxygen termination of the BDD electrode surface inhibits the electron transfer of the $[Fe(CN)_6]^{3-}$/$[Fe(CN)_6]^{4-}$ redox couple. It can thus be assumed that in order to reduce the peak separation, the surface of the electrode will have to be made hydrophobic.

The BDD electrode proved to be more effective (wider potential window, therefore better peak resolution) for the quantitative analysis of cerium (III) sulphate, than the glassy carbon electrode. This is evidenced by the BDD electrode producing a better quality calibration plot and percentage recovery values than the glassy carbon electrode.

The electrochemical behaviour of two biological systems, dopamine and ascorbic acid, were also investigated. Dopamine co-exists with ascorbic acid (a major electrochemical interferent) in the extracellular fluid in the brain. The boron-doped diamond electrode was found to be superior to the glassy carbon electrode in the detection of dopamine and ascorbic acid, as evidenced by the excellent R-square and percentage recovery values obtained for the boron-doped diamond electrode.

The detection limits for dopamine and ascorbic acid at a boron-doped diamond electrode surface were found to be 0.56 µmol/L and 20 nmol/L respectively. The expected concentrations of dopamine in tissue are 0.1 – 0.01 µmol/L (10 – 100 nmol/L). In order to achieve these detection limits, it is suggested that "heavily boron doped" (10^{21} boron atoms.cm^{-3}) diamond electrodes be used. Finally, the BDD electrode was found to be stable over a three month period in both the dopamine and ascorbic acid investigations.

In order to detect dopamine in the presence of ascorbic acid, the boron-doped diamond electrode may be anodically pretreated in potassium hydroxide. This pretreatment shifts the ascorbic acid peak position more positive and in so doing, the dopamine and ascorbic acid peaks may be resolved. It appears therefore that an anodically pretreated boron-doped diamond electrode would make an ideal biosensor for the detection of dopamine in the presence of ascorbic acid, since it is accurate, reproducible, resistant to fouling, reliable and most importantly biocompatible.

However, further work needs to be done to improve the sensitivity of the BDD electrode to be used for dopamine detection. One possible method is to use a "heavily" boron-doped diamond sample as the electrode material. This is expected to increase the size of the dopamine peak. A prolonged electrode lifetime and stability study on the anodically pretreated boron-doped diamond electrode is also essential in order for the eventual design and fabrication of an implantable microelectrode.

For the first time, the electrochemical detection of thyroid hormones was investigated at diamond electrodes, as detailed in this study. Also documented for the first time is the use of porous boron-doped diamond electrodes. This electrode material was successfully used to analyse for the thyroid hormones (L-T_3 and L-T_4) in synthetic samples, by impregnating the electrode with antiserum using a vacuum technique. Since the electrochemical determination of the thyroid hormones using porous boron-doped diamond electrodes is novel, the results obtained could not be compared to that of literature. The lower limit of detection for L-T_3 was found to be 856 nmol/L, while that of L-T_4 was 12.5 µmol/L. As the respective concentrations in blood are 0.89 pmol/L and 0.031 nmol/L (2.97 nmol/L and 0.103 µmol/L respectively protein-bound), further work is necessary to improve the sensitivity of this immunosensor.

The response of the porous boron-doped diamond electrode was found to be highly dependent on its surface state, with a hydrophobic surface giving a lower baseline than that of a hydrophilic surface. Problems were experienced with reproducibility in both the L-T_3 and L-T_4 cases, and were thought to be related to the electrode surface state, and/or the retention of the antiserum in the pores.

The feasibility of using porous boron-doped diamond electrodes for the detection of thyroid hormones has been demonstrated. In order to develop a commercial diamond biosensor for thyroid hormone detection based on this material, further work is required to improve the sensitivity and reproducibility of the electrode.

Generally, the porous boron-doped diamond electrode offers a significant advantage over a CVD boron-doped diamond electrode, as it is much cheaper to manufacture, and may be manufactured to have a vastly increased surface area, which opens up possibilities of future application in systems where the analyte is present in very low concentrations. These systems vary from biological or medical to wastewater applications.

In conclusion, the De Beers boron-doped diamond electrode has been shown to possess definite advantages over the conventional glassy carbon electrode, in that it has a wide potential window for water stability (as confirmed using the cerium (III) sulphate system), low baseline current, and is chemically inert and resistant to fouling (as evidenced by the results obtained for both the biological systems, dopamine and ascorbic acid). The electrochemical behaviour of the De Beers boron-doped diamond electrode was also found to be very similar to that reported in literature, for the various electrochemical systems investigated (except for the novel thyroid hormone system, where no literature is available).

In all, the boron-doped diamond electrode is an excellent candidate for the analysis of various electrochemical compounds or species and would therefore have wide commercial electrochemical applications, especially for the detection of low levels of dopamine in the presence of ascorbic acid, and the detection of the thyroid hormones. It is, however, recommended that further work be done in order to improve the electrochemical behaviour of the boron-doped diamond electrodes for use in these systems.